UNIVERSIDAD DE CHILE
FACULTAD DE MEDICINA
ESCUELA DE POSTGRADO

ROLE OF Ca^{2+} SIGNALING IN MITOCHONDRIAL DYSFUNCTION AS A BASIS OF NEURODEGENERATION IN EARLY-ONSET FAMILIAL ALZHEIMER'S DISEASE

MARIOLY ANNELIESE MÜLLER SOBARZO

TESIS PARA OPTAR AL GRADO DE DOCTOR EN CIENCIAS BIOMEDICAS

Directores de Tesis: Prof. Dr. J. César Cárdenas
Dr. J. Kevin Foskett

2021

UNIVERSIDAD DE CHILE
FACULTAD DE MEDICINA
ESCUELA DE POSTGRADO

INFORME DE APROBACIÓN TESIS DE DOCTORADO EN CIENCIAS BIOMÉDICAS

Se informa a la Comisión de Grados Académicos de la Facultad de Medicina, que la Tesis de Doctorado en Ciencias Biomédicas presentada por la candidata

MARIOLY ANNELIESE MÜLLER SOBARZO

ha sido aprobada por la Comisión Informante de Tesis como requisito para optar al Grado de **Doctor en Ciencias Biomédicas** en Examen de Defensa de Tesis rendido el día 7 de abril de 2021.

Prof. Dr. J. César Cárdenas
Director de Tesis
Depto. de Biología, Facultad de Ciencias, Universidad Mayor

COMISION INFORMANTE DE TESIS

PROF. DR. DIEGO VARELA
Presidente Comisión de Examen

PROF. DR. JORGE BEVILACQUA

PROF. DRA. ANDREA PAULA LIMA

PROF. DRA. URSULA WINECKEN

DEDICATION

Dedicated to the memory of my beloved mother, who passed away two days before I restarted my doctoral studies and taught me that it is never too late to reach our dreams and to pursue your true passion. I hope you are proud of me.

To my Dad, for his support and encouragement to complete this challenge in this stage of my life despite all the adversities.

To my family, my children César and Rafael. I could never have done this without your love, support, patience and understanding through all these years. To my husband Rodrigo, without your company, containment and challenge me day after day to never give up.

DEDICATORIA

Dedicado a la memoria de mi querida madre, quien falleció dos días antes de que reiniciara mis estudios de doctorado y me enseñó que nunca es tarde para alcanzar nuestros sueños y perseguir tu verdadera pasión. Espero que estés orgullosa de mí.

A mi padre, por su apoyo y aliento para completar este desafío en esta etapa de mi vida a pesar de todas las adversidades.

A mi familia, mis hijos César y Rafael, nunca podría haber hecho esto sin su amor, apoyo, paciencia y comprensión durante todos estos años. Y a mi esposo Rodrigo que, sin su compañía y contención, me alentó día a día a no rendirme.

ACKNOWLEDGMENTS

It is a genuine pleasure to express my deep sense of thanks and gratitude to my mentor Dr. J. Kevin Foskett, Chair of the Department of Physiology School of Medicine, University of Pennsylvania. Thanks to his timely advice, meticulous scrutiny, scholarly advice and scientific approach have helped me to a very great extent to accomplish this task. I owe a deep gratitude to Dr. Riley Payne for his interest on my research at every stage of my research. Thanks for his time for training me, time, suggestions and enthusiasm during hard days of work in Foskett-Lab that have enabled me to complete my thesis.

I thank Dr. J. César Cárdenas for his kind help, support and collaboration throughout my study period providing relevant assistant and help to complete this thesis.

I extend my gratitude and thank my thesis advisory committee members for their guidance, corrections, constructive criticism and patience to make a better work.

My special appreciation to my colleagues at the Medical Technology School of the University of Chile for helping me survive all the stress, for their constant encouragement and kind help with my teaching hours. I am extremely thankful of Esteban Órdenes, Isabel Castro, Mayarling Troncoso and especially Ignacio Maureira, my unconditional friend and partner during happy and difficult times.

I would also like to thank the authorities of my Institution for allowing me to achieve this goal, the Department of Medical Technology and School of Medical Technology with special emphasis to my former Directors, Cecilia Leyton and Denisse Karl.

Nobody has been more important to me in the pursuit of this project than all the members of my family, especially my parents, kids and husband who took care of them for long periods of time while I was out of the country performing experiments.

Special thanks to all the people who along the way believed in me.

1. INDEX

2. TABLE OF FIGURES

3. ABBREVIATIONS

α-KGDH	α-ketoglutarate dehydrogenase
AD	Alzheimer's disease
ANOVA	One-way analysis of variance
APP	Amyloid precursor protein
Aβ	β-amyloid
ATCC	American Type Culture Collection
ATP	Adenosine triphosphate
BK	Bradykinin
CCCP	Carbonilcianuro-m-clorofenilhidrazona
CFP	Cyan fluorescent protein
CGP	CGP37157 (inhibitor of the Na^+/Ca^{2+} exchanger)
CO_2	Carbon dioxide
$\Delta\Psi_m$	Mitochondrial membrane potential
Dg	Digitonin
DMEM	Dulbecco's modified eagle's medium
EGFP	Enhanced green fluorescent protein
EMEM	Eagle's minimum essential medium
EMRE	Essential MCU regulator
ER	Endoplasmic reticulum
ETC	Electron transport chain
FAD	Familial Alzheimer's disease
FBS	Fetal bovine serum
FCCP	Carbonylcyanide p-trifluoromethoxyphenylhydrazone
FRET	Fluorescence resonance energy transfer
G418	Geneticin
HRP	Horseradish peroxidase
ICM	Intracellular medium
IDH	Isocitrate dehydrogenase
IP_3	Inositol trisphosphate

kDa	Kilo daltons
LAR-GECO1	Low affinity R-GECO1
IMM	Inner mitochondrial membrane
$InsP_3R$	Inositol 1,4,5-trisphosphate receptor
mCG1	mitoCAR-GECO1
MAMs	Mitochondria-associated membranes
MCU	Mitochondrial Ca^{2+} uniporter
MCUb	MCU regulator subunit b
MCUR1	MCU regulator 1
MICU1	Mitochondrial Ca^{2+} uptake protein 1
MICU2	Mitochondrial Ca^{2+} uptake protein 2
NCLX	Na^+/Ca^{2+} Li^+- permeable exchanger
NCX	Na^+/Ca^{2+} exchanger
NCKX	K^+ dependent Na^+/Ca^{2+} exchanger
O_2	Oxygen
OCR	Oxygen consumption rate
OXPHOS	Mitochondrial oxidative phosphorylation system
PDH	Pyruvate dehydrogenase
PLC	Phospholipase-C
PS1	Presenilin-1
PS2	Presenilin-2
PTP	Permeability transition pore
H^+	Proton
ROS	Reactive oxygen species
RT	Room temperature
RyR	Ryanodine receptor
SAD	Sporadic Alzheimer's disease
SERCA	Sarcoplasmic Endoplasmic Reticulum Ca^{2+} ATPase
TCA	Tricarboxylic acid cycle
TMRE	Tetramethylrhodamine ethyl
Tg	Thapsigargin

WB	Western blot
XeB	Xestospongin B
YFP	Yellow fluorescent protein

4. ABSTRACT

Familial Alzheimer's disease (FAD) is characterized by autosomal-dominant heritability and early onset. Mutations in the gene encoding presenilin-1 (PS1) are found in approximately 80% of cases of FAD. The etiology of AD is currently unknown, however exaggerated intracellular Ca^{2+} signaling may be a major contributing factor in early and late stages of the disease. Many PS1 mutations affect intracellular Ca^{2+} homeostasis, although the molecular details are still debated. Altered Ca^{2+} signaling is observed early in the development of the disease, long before the onset of measurable histopathology or cognitive deficits. One proposed molecular mechanism underlying exaggerated Ca^{2+} signaling is mediated by Ca^{2+} release from the endoplasmic reticulum (ER) through inositol 1,4,5-trisphosphate receptors ($InsP_3R$). In FAD, the higher open probability of the $InsP_3R$ caused by PS mutations is predicted to lead to a significant increase in the Ca^{2+} microdomain concentration near the Ca^{2+} release channels and its spatial extent. To date, the involvement of exaggerated Ca^{2+} signaling in FAD on mitochondrial function has been evaluated only theoretically. Therefore, we proposed to investigate the role of $InsP_3R$-mediated exaggerated Ca^{2+} signals on mitochondrial function in the context of FAD. **Hypothesis: *FAD-PS1 mutations enhance Ca^{2+} transfer between the ER and mitochondria inducing mitochondrial malfunction that leads to impaired cell function and death*.**

We determined the role of Ca^{2+} dysregulation mediated by $InsP_3R$-PS1 mutant interaction on mitochondrial function using two different *in vitro* cell models of FAD. Our findings, support our working hypothesis that cells expressing mutant PS1 are

subjected to elevated mitochondrial Ca^{2+} levels, due to an exaggerated ER Ca^{2+} leak through the $InsP_3R$, a decrease of mitochondrial Ca^{2+} extrusion capacity by the Na^+/Ca^{2+} exchanger as a result of decreased expression of NCLX and an increase in reactive oxygen species (ROS) production. These features may explain the increased vulnerability and eventual death of these cells due to progressive mitochondrial dysfunction, promoting a pathological cycle essential to disease progression.

5. INTRODUCTION

5.1 Alzheimer´s disease, an overview

Alzheimer's disease (AD) is a progressive neurodegenerative disorder and the most frequent cause of dementia, affecting millions of people worldwide and still incurable (Cornejo and Hetz 2013). It is characterized clinically as a decline of intellectual and cognitive functions and irreversible memory loss as major features. Aging is the major risk factor to develop this disease. In Chile, AD prevalence is near 1-2% in the population between 60 and 75 years old, increases significantly in the group between 75 and 84 years old, and is near 50% in the population over 85 years old (Slachevsky, Budinich et al. 2013). Most cases of AD are sporadic and characterized by a late onset of the classical symptoms. However, nearly 10% of the cases are dominantly inherited familial AD (FAD) and develop early as a result of mutations in presenilin-1 (PS1), presenilin-2 (PS2) or amyloid precursor protein (APP) (Cutler, Kelly et al. 2004). The etiologies of sporadic AD (SAD) and FAD are widely assumed to be similar. They share the features of accumulated extra- and intra-cellular β-amyloid (Aβ) plaques, intracellular neurofibrillary tangles, selective neuronal and synaptic death in multiple brain regions, with FAD presenting earlier in life and with a more aggressive progression (Hardy and Selkoe 2002). However, to date, the exact pathogenic mechanisms of the disease remain unknown and there is no effective treatment for AD.

Presenilins (PSs) are transmembrane proteins that are part of the catalytic core of the γ-secretase complex that is responsible for APP processing. Mutant PSs contribute to the amiloidogenic pathway that leads to production of toxic Aβ species (Francis, McGrath et al. 2002). Whether FAD mutations cause a gain of function or loss

of γ-secretase function is still a subject of debate (Popugaeva, Pchitskaya et al. 2018). Extensive studies support the notion that soluble Aβ oligomers represent toxic species that affect multiple early molecular mechanisms leading to synaptic dysfunction in AD (Cleary, Walsh et al. 2005). While excessive production of Aβ peptides is observed early in patients that developed AD and is essential for AD pathology, it is not sufficient. Some aged individuals have significant Aβ load, but do not develop cognitive impairment (Iacono, Resnick et al. 2014). Of note, the amiloidogenic pathway, the basis of the "amyloid cascade" hypothesis, has so far failed to yield disease-modifying therapies (Mullane and Williams 2013) and does not address other central questions about the disease pathogenesis.

5.2 The Calcium Hypothesis of AD

Ca^{2+} is a critical second messenger that regulates many physiological and pathological processes at multiple levels, ranging from gene transcription to membrane potential and excitability, synaptic plasticity and memory. Disruptions of Ca^{2+} homeostasis can result in alterations of cell functions (Greer and Greenberg 2008). Intracellular Ca^{2+} dynamics are tightly associated with cognitive and memory-related neuronal functions, so any Ca^{2+} dysregulation in the major intracellular store, the endoplasmic reticulum (ER), could contribute to persistent alterations of cytoplasmic Ca^{2+} concentration ($[Ca^{2+}]_i$), which in turn could affect synaptic functions (Berridge 2014). A significant body of research suggests that AD-causing PS mutations are associated with Ca^{2+} signaling dysregulation independently of their γ-secretase function and Aβ accumulation. Dysregulation of Ca^{2+} homeostasis in cells from AD patients has

been observed for more than two decades (Peterson, Gibson et al. 1985). Compelling evidence suggests that FAD PS mutations result in changes in $[Ca^{2+}]_i$ signaling in the absence of and prior to the appearance of Aβ plaques, indicating that it is an early event that could be involved in disease pathogenesis (Stutzmann, Smith et al. 2007) (Cheung, Shineman et al. 2008) (Gillardon, Rist et al. 2007) (Su, Wang et al. 2010) (Berridge 2013) (Chakroborty, Kim et al. 2012). The "calcium hypothesis" suggests that sustained intracellular Ca^{2+} disturbances are a proximal cause of AD (Khachaturian 1987). In this hypothesis, neurons affected by dysregulated Ca^{2+} homeostasis during aging become compromised, leading to excessive $[Ca^{2+}]_i$ and reactive oxygen species (ROS) generation, mitochondrial dysfunction and eventually apoptosis. One hypothesis is that PS mutations result in increased Ca^{2+} release from the ER (Mattson 2004), possibly due to increased ER Ca^{2+} loading by SERCA (Sarcoplasmic endoplasmic reticulum Ca^{2+} ATPase) (Green, Demuro et al. 2008), over-expression of the ryanodine receptor (RyR) (Chakroborty, Kim et al. 2012) or sensitization of the $InsP_3R$ (Cheung, Shineman et al. 2008) (Cheung, Mei et al. 2010). Interesting, increases in $[Ca^{2+}]_i$ can stimulate the metabolism of APP (Hardy and Selkoe 2002, LaFerla 2002), raising the question as to which one of these processes may be part of the primary cause of AD. In addition to effects of mutant PS, Aβ generated from APP processing can disrupt $[Ca^{2+}]_i$ homeostasis by triggering Ca^{2+} flux into the cytoplasm from both extracellular and intracellular sources (Demuro and Parker 2013). In particular, intracellular Ca^{2+} release evoked by Aβ42 oligomers involves the opening of the $InsP_3R$ as a result of stimulated production of inositol trisphosphate (IP_3) via G-protein mediated activation of phospholipase-C (PLC), resulting in cytotoxicity. It has

been proposed that depletion of ER Ca^{2+} stores by Aβ oligomers may activate store-operated Ca^{2+} entry, leading to a further increases in $[Ca^{2+}]_i$ via the STIM/Orai pathway (Cahalan 2009). Recently, however, it was demonstrated that store-operated Ca^{2+} entry was attenuated by PS1-associated γ-secretase cleavage of STIM1 in PS1 mutant-expressing cells (Tong, Lee et al. 2016). Together, the precise mechanisms of how Aβ contributes to Ca^{2+} signaling require further investigation. For FAD, the loss of Ca^{2+} homeostasis due to several causes such as the combination of risk factor genes plus the progressive oxidative damage that accumulates with age may be the cause of disease pathology. In this work we propose to evaluate a potential role of altered $[Ca^{2+}]_i$ homeostasis independent of Aβ deposition, considering Ca^{2+} dysregulation and the loss of mitochondrial function as a root cause of AD.

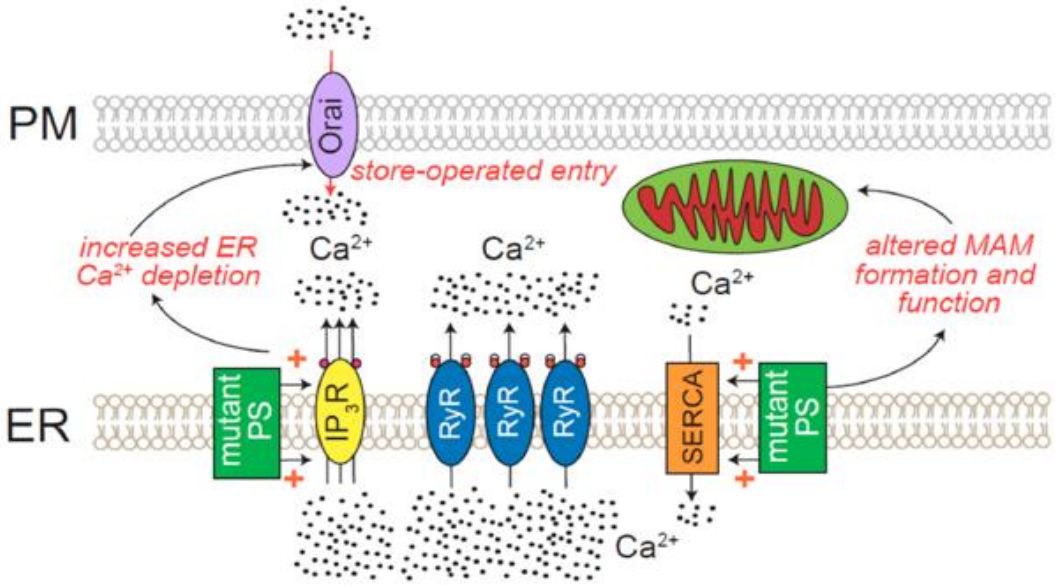

Figure 1i: Mechanisms of ER Ca^{2+} dyshomeostasis in Alzheimer's disease (AD). Mutated presenilin (PS) increases ER Ca^{2+} release. Various models of AD display increased expression of RyR, which can also produce elevated Ca^{2+} release from the ER. Additionally, mutated PS stimulates sarco/endoplasmic reticulum Ca^{2+}-ATPase (SERCA), which can fuel further release through ER Ca^{2+} channels. Increased ER Ca^{2+} store depletion can activate store operated Ca^{2+} entry. Function of mitochondria associated membranes (MAMs) are also altered by mutated PS. *Taken from Karagas NE and Venkatachalam K, 2019.*

5.3 Mitochondrial Ca^{2+}

Mitochondria play a major role in Ca^{2+} signaling and homeostasis through its uptake, sequestration and release (De Stefani, Rizzuto et al. 2016). While this role is ubiquitous, it is particularly critical in neurons because their function is almost exclusively dependent on mitochondrial oxidative phosphorylation (OXPHOS) as a major source of ATP (Herrero-Mendez, Almeida et al. 2009). Mitochondrial Ca^{2+} in these cells is a key to guarantee activity-dependent regulation of cellular energy metabolism.

Ca^{2+} is accumulated into the mitochondrial matrix at the expense of energy, provided by the oxidation of substrates fueling OXPHOS (Deluca and Engstrom 1961). Thanks to the large electrical gradient across its inner membrane, mitochondria can import large amounts of Ca^{2+} through the mitochondrial Ca^{2+} uniporter (MCU) Ca^{2+} channel complex, serving to fuel OXPHOS and to provide a potent buffer in periods of high cytoplasmic [Ca^{2+}], such as during neuronal excitation (Qiu, Tan et al. 2013). Nevertheless, mitochondrial-matrix Ca^{2+} concentration ($[Ca^{2+}]_m$) must be tightly controlled to maintain a balance between optimal energy production and toxic effects, including inner mitochondrial membrane (IMM) depolarization and activation of the permeability transition pore (PTP), reflecting the key role of mitochondrial Ca^{2+} in cell death.

The molecular identity of the MCU Ca^{2+} ion channel complex was only recently unveiled (Baughman, Perocchi et al. 2011) (De Stefani, Raffaello et al. 2011). MCU is the pore-forming subunit of a complex that includes mitochondrial Ca^{2+} uptake protein1 (MICU1) (Plovanich, Bogorad et al. 2013), MICU2, MCU regulator subunit b (MCUb)

(Raffaello, De Stefani et al. 2013), the essential MCU regulator (EMRE), a small membrane-spanning protein essential for the mitochondrial Ca^{2+} uptake (Chaudhuri, Sancak et al. 2013) and MCUR1 (Mallilankaraman, Cardenas et al. 2012) (Figure 1i, De Stefani D, et al 2016). The composition of the MCU channel complex may vary depending on the cell type and different epigenetic control mechanisms.

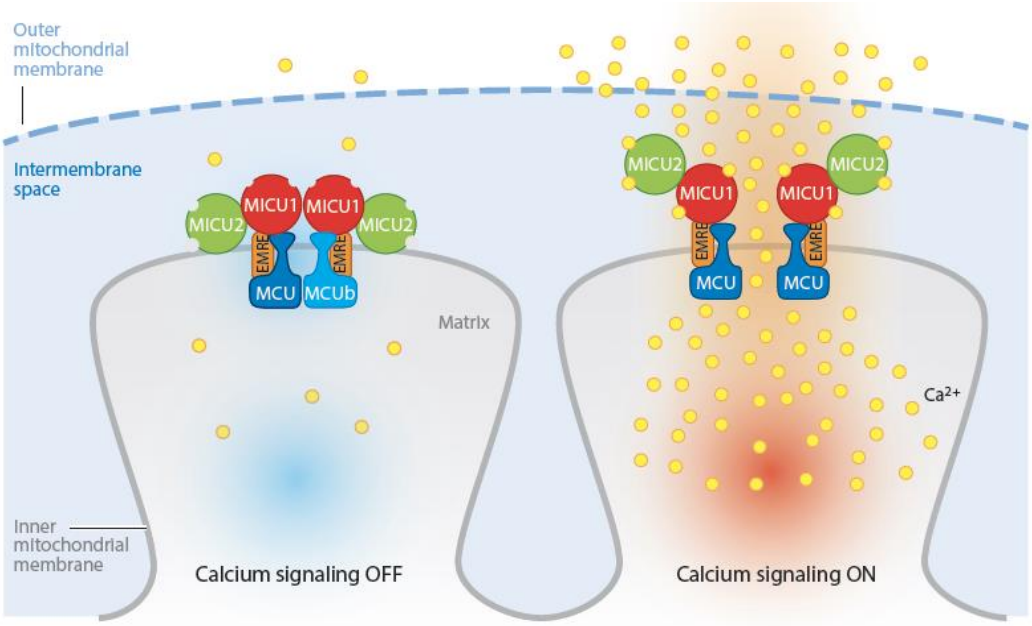

Figure 2i: Schematic representation of the Mitochondrial Calcium Uniporter (MCU) complex in resting condition and under mitochondrial Ca^{2+} uptake controlled by a multiprotein complex that can consist of MCU and MCUb together with EMRE, MICU1 and MICU2. MICU1/MICU2 heterodimers act as MCU gatekeepers and prevent vicious Ca^{2+} cycle and energy sinks. (De Stefani D, et al, 2016).

Ca^{2+} that enters into mitochondria can be extruded by the Na^+/Ca^{2+} exchanger NCLX (Palty, Silverman et al. 2010). NCLX is capable of exchanging Ca^{2+} not only with Na^+ but also with Li^+, a typical feature of the mitochondrial Na^+/Ca^{2+} exchanger but not of the classical plasma membrane transporters NCX or NCKX (Sekler 2015). Several studies have shown that mitochondrial Na^+ is lower than cytosolic Na^+ and this Na^+

gradient may be used as a driving force to extrude Ca^{2+} from the matrix via NCLX. There is some evidence suggesting that the NCLX is electrogenic, exchanging 3 Na^{+} ions for 1Ca^{2+} ion (Boyman, Williams et al. 2013), suggesting that the mitochondrial membrane potential can also regulate the rate of NCLX-mediated Ca^{2+} extrusion. Ca^{2+} efflux mechanisms (including Letm1, a $2H^{+}/Ca^{2+}$ exchanger) is essential for the maintenance of mitochondrial function and cell survival and any dysregulation of $[Ca^{2+}]_m$ would lead to mitochondrial Ca^{2+} overload and cell death (Luongo, Lambert et al. 2017). Because it is crucial to maintain mitochondrial Ca^{2+} homeostasis, mechanisms are necessary to ensure that in the steady-state the rate of Ca^{2+} influx does not exceed extrusion capacity and cause Ca^{2+} overload. It is well known that mitochondrial Ca^{2+} accumulation is a key component in the control of cellular bioenergetics by regulating several pyruvate dehydrogenase (PDH) and rate-limiting tricarboxylic acid cycle (TCA) dehydrogenases (α-ketoglutarate- and isocitrate-dehydrogenases), and possibly components of the respiratory chain and the ATP synthase. The three dehydrogenases are activated by matrix Ca^{2+} through different mechanisms. PDH activation depends on the dephosphorylation of the catalytic subunit by a Ca^{2+}-dependent phosphatase (Denton, Randle et al. 1972), whereas α-ketoglutarate dehydrogenase (α-KGDH) and isocitrate dehydrogenase (IDH) are directly activated by Ca^{2+} binding (Rutter and Denton 1988). Increases in $[Ca^{2+}]_m$ results in activation of these three enzymes to fuel ATP synthesis, coupling bioenergetics to neuronal excitation/activity (Llorente-Folch, Rueda et al. 2015).

The existence of Ca^{2+} nanodomains at sites of close apposition of mitochondria to ER or plasma membrane Ca^{2+} channels can account for the very rapid and large

Ca^{2+} uptake by mitochondria in cells. The ER and mitochondria couple at specific sites termed mitochondria-associated membranes (MAMs), which are believed to integrate and coordinate several cellular functions, including synthesis and exchange of phospholipids, apoptosis, mitochondrial dynamics and Ca^{2+} signaling (Liu and Zhu 2017). Notably, all these processes are affected early during AD pathogenesis and other neurodegenerative conditions, suggesting a role for MAMs in the pathogenesis of these diseases (Area-Gomez, de Groof et al. 2018). Furthermore, excessive mitochondrial Ca^{2+} uptake can be toxic, contributing to increased ROS production, activation of the PTP and neuronal death (Rasola and Bernardi 2011). Mitochondrial Ca^{2+} overload and subsequent dysfunction have been implicated in neurodegeneration.

5.4 Mitochondrial dysfunction in AD

The role of mitochondria in cellular bioenergetics and survival is well known. It has been suggested that mitochondrial deficits are an early event in AD pathogenesis and other neurodegenerative disorders (Itoh, Nakamura et al. 2013). Several mitochondrial functions mentioned above have been shown to be affected in AD, including diminished glucose metabolism, mitochondrial enzymatic failure, and increased ROS production, before Aβ and tau tangles have begun forming (Swerdlow and Khan 2004). Mitochondrial dynamics are also dysfunctional in early-stage AD, including disruption in the balance between mitochondrial fusion and fission, and decreased axonal transport of mitochondria, among others (Lin and Beal 2006). There is also a disruption of glycolytic processes, impairments to the enzymatic activity of the protein complexes of the electron transport chain (ETC), and negative alterations in

antioxidant enzymatic activity. However, the relationship between exaggerated Ca^{2+} signaling and altered mitochondrial physiology is unclear. Mitochondria serve as high-capacity Ca^{2+} sinks, which allow cells to respond to changes in cytosolic Ca^{2+} loads and aids in maintaining cellular Ca^{2+} homeostasis that is required for normal neuronal function (Rizzuto, Bernardi et al. 2000). In general, transfer of Ca^{2+} from ER to mitochondria is necessary to maintain mitochondrial function and cellular bioenergetics (Cardenas, Miller et al. 2010), which in neurons, given their limited glycolytic capacity, is essential. The communication between ER and mitochondria is supported by the presence of MAMs. Zampese *et al.* showed that overexpression or down regulation of PS2 modulates Ca^{2+} shuttling between ER and mitochondria through regulating interaction between the two organelles and potentially increasing mitochondrial Ca^{2+} uptake (Zampese, Fasolato et al. 2011). Nevertheless, the relationship between exaggerated ER Ca^{2+} signaling by gain-of-function of ER Ca^{2+} release activity by the $InsP_3R$ or RyR and mitochondrial bioenergetics and dysregulation in AD remains to be elucidated.

Mitochondrial Ca^{2+} regulates NADH production and ATP synthesis. Increases and decreases of $[Ca^{2+}]_m$ during cell activity is translated into parallel changes in the activities of Ca^{2+}-sensitive dehydrogenases that are part of the TCA cycle (Fernandez-Morales, Arranz-Tagarro et al. 2012). Several studies have demonstrated down-regulation of the PDH complex and α-KGDH in postmortem analyses of human AD brains (Bubber, Haroutunian et al. 2005). These are key rate-limiting enzymes of the TCA cycle, suggested to be therapeutic targets in age-related neurodegenerative diseases (Volgyi, Juhasz et al. 2015). In addition, in brain samples of a mouse model

of AD, decreased mitochondrial respiration and decreased PDH protein levels and activity were observed as early as 3 months of age (Yao, Irwin et al. 2009).

Inappropriate levels of mitochondrial Ca^{2+} uptake can lead to irreversible deleterious cellular changes. Whether MCU mediates excitotoxicity was recently evaluated using gain- and loss-of function experiments that demonstrated that MCU plays a central role in the cell death observed followed an excitotoxic insult (Qiu, Tan et al. 2013). However, the impact of altered MCU activity in AD is unknown and further investigation is required.

In addition, alterations in mitochondrial Ca^{2+} efflux may also play a role. For example, heart failure has been shown to lead to an increase in cytoplasmic $[Na^{+}]$, which is suggested to reduce $[Ca^{2+}]_m$ by enhancing Ca^{2+} efflux via NCLX (Liu, Takimoto et al. 2014). Although reduced $[Ca^{2+}]_m$ associated with increased efflux or reduced Ca^{2+} uptake can have detrimental effects, it is likely that overexpression of MCU or total loss of NCLX and the resultant accumulation of matrix Ca^{2+} would also be detrimental.

Although several studies have proposed that mitochondrial dysfunction is a primary cause for AD development, to date no causal studies have directly implicated alterations in mitochondrial Ca^{2+} exchange with AD, or examined the direct contribution of mitochondrial Ca^{2+} dynamics and signaling with disease progression (Du, Guo et al. 2008) (Luongo, Lambert et al. 2015). However, recently, it was reported that dysregulation of mitochondrial Ca^{2+} efflux through NCLX precedes neuropathology and memory decline in AD, providing a possible missing link between the Ca^{2+} dysregulation and mitochondrial dysfunction, both phenomena widely described in the AD literature (Jadiya, Kolmetzky et al. 2019).

5.5 Summary of antecedents

Our laboratory previously revealed the involvement of the $InsP_3R$ in exaggerated $[Ca^{2+}]_i$ signaling observed in many FAD experimental models (Cheung KH 2008) (Cardenas, Miller et al. 2010) (Muller, Cardenas et al. 2011) (Shilling, Muller et al. 2014). Although the mechanisms are still controversial, these observations indicate that increased ER Ca^{2+} release caused by FAD PS is an early phenotype and could accordingly contribute to disease pathogenesis (Honarnejad and Herms 2012). We have linked this Ca^{2+} dysregulation caused by PS mutations with exaggerated production of ROS (Muller, Cardenas et al. 2011) and with activation of downstream Ca^{2+}-dependent pathways, including mis-regulation of the transcription of important neuronal genes (Müller, Cardenas et al. 2011). More recently, we described a genetic approach in which the Ca^{2+} hypothesis of FAD was confirmed (Shilling, Muller et al. 2014). Decreasing $InsP_3R$ protein expression by 50% normalized FAD PS-associated exaggerated neuronal Ca^{2+} signaling. Moreover, this $InsP_3R$ reduction rescued the biochemical, electrophysiological and behavioral phenotypes observed in two different PS1-FAD animal models, suggesting an important contribution in AD pathogenesis as an early event involved in the disease.

During this study, we demonstrated clear evidence of intracellular Ca^{2+} dysregulation, suggesting that cells expressing mutant PS1 may be subjected to elevated mitochondrial Ca^{2+} levels, triggering a Ca^{2+} overload which is linked to exacerbated by impaired mitochondrial Ca^{2+} efflux capacity which results in metabolic dysfunction.

6. HYPOTHESIS

"FAD-PS1 mutations enhance Ca^{2+} transfer between the ER and mitochondria inducing mitochondrial malfunction that leads to impaired cell function and death."

7. General goal

Determine how FAD-associated *PS1* mutations affect Ca^{2+} transfer through the $InsP_3R$-MCU axis and mitochondrial function in human cell culture models.

8. Specific Aims

Aim 1. Determine the role of the FAD-mutant PS1-M146L disruptions of intracellular Ca^{2+} homeostasis on MCU-mediated mitochondrial Ca^{2+} uptake, extrusion and $\Delta\Psi m$ under basal and $InsP_3R$ agonist stimulation in human neuronal culture cell lines and FAD-patient fibroblasts.

Aim 2. Explore the effects of the FAD-mutant PS1-M146L on mitochondrial metabolism by determining the role of Ca^{2+} transfer through the $InsP_3R$-MCU axis in regulating oxygen consumption rates (OCR) and expression levels of PDH, αKGDH and IDH in neuronal culture cell lines and FAD-patient fibroblasts.

9. MATERIALS AND METHODS

9.1 Cell culture and transfection, SH-SY5Y cells

We used the human neuroblastoma SH-SY5Y cell line purchased from ATCC (American Type Culture Collection, Rockville, MD, USA). SH-SY5Y cells were maintained in a 1:1 mixture of ATCC-formulated Eagle's Minimum Essential medium (EMEM) and F12 medium supplemented with fetal bovine serum (FBS) to a final concentration of 10% (Hyclone), 100 U/ml penicillin, 100 μg/ml streptomycin and 0.25 μg/ml fungizone (Gibco). The atmosphere was 95% air; 5% CO_2 and temperature 37°C. Human wild-type (WT) PS1 and mutant PS1-M146L cDNAs were subcloned into pIRES2-EGFP (Clontech) and transfected into SH-SY5Y cells through electroporation using a Nucleofector™ Technology device and the Cell Line Nucelofector™ Kit V (Lonza, catalog# VCA-1003). To select stable SH-SY5Y polyclonal lines, transfected cells were drug-selected in 2 mg /ml Geneticin (G418) (Invitrogen). PS expression was confirmed by western blot (WB) using a primary antibody against PS1 (CST catalog#3622). For live cell imaging of $[Ca^{2+}]_m$, cells were transiently transfected through electroporation with either mitoCAR-GECO1 (mCG1; K_D= 490 nM), a genetically encoded Ca^{2+} indicator targeted to the mitochondrial matrix, or the 4mtD3cpv, a second-generation chameleon Ca^{2+} indicator (FRET sensor; K_D= 0,6 μM), and immediately seeded onto glass coverslips.

9.2 Cell culture, human patient fibroblasts

Human skin fibroblasts derived from FAD and SAD patients and normal individuals were purchased from the Coriell Institute (Table 1). They were maintained at 37°C (95% air and 5% CO_2) and cultured with EMEM with Earle's salts and 15% FBS (Hyclone), 100 U/ml penicillin, 100 μg/ml streptomycin and 0.25 μg/ml fungizone (Gibco), following provider instructions.

ID	Affected	Gene	Mutation	Sex	Age
AG06840	Yes	PSEN1	ALA246GLU	Male	56 YR
AG06848	Yes	PSEN1	ALA246GLU	Female	56 YR
AG08711	N/I	PSEN1	ALA246GLU	Female	34 YR
AG07559	NO	NO	NO	Female	45 YR
AG07621	NO	NO	NO	Male	57 YR
AG08179	NO	NO	NO	Male	54 YR
AG08243	Yes	NO	NO	Male	72 YR
AG07374	Yes	NO	NO	Male	73 YR
AG09908	Yes	PSEN2	ASN141ILE	Female	81 YR
AG0246E	Yes	PSEN1	M146V	Male	78 YR

Table 1: List of human skin fibroblasts isolated from FAD and control patients obtained from the Coriell Institute (Camden, NJ).

For live cell imaging of $[Ca^{2+}]_m$, human patients fibroblast were transiently transfected either with the mCG1 Ca^{2+} indicator using Effectene transfection reagent (Qiagen), optimal for primary cells due to its low cytotoxicity, or with the FRET sensor 4mtD3cpv, or with the low affinity R-GECO1 (LAR-GECO1;K_D ~20 μM) that has ~10-fold increase

in fluorescence intensity upon binding of Ca^{2+}, and immediately seeded onto glass coverslips.

9.3 Simultaneous measurements of mitochondrial Ca^{2+} uptake and membrane potential in permeabilized cells.

Human *wild-type* (*wt*) PS1 (PS1wt)-, empty vector pIRES2-EGFP- (EGFP) (Clontech), and FAD-mutant PS1-M146L SH-SY5Y cells were grown in 10 cm tissue-culture coated dishes and detached with Versene Solution (EDTA, non-enzymatic cell dissociation reagent) (ThermoFisher, catalog# 15040066). Then, cells were counted (6 X 10^6), and washed in an extracellular-like Ca^{2+}-free buffer (in mM: 120 NaCl, 5 KCl, 1 KH_2PO_4, 0.2 $MgCl_2$, 0.1 EGTA, and 20 HEPES-NaOH pH 7.4). Following centrifugation, cells were transferred to an intracellular-like medium [ICM; permeabilization buffer: 120 mM KCl; 10 mM NaCl; 1 mM KH_2PO_4; 20 mM HEPES-Tris, pH 7.2; protease inhibitors (EDTA-free complete tablets; Roche Applied Science, Minneapolis, MN, USA)] that had been treated with BT Chelex® 100 resin (Bio-Rad, 143-2832) prior to use to attain an initial free [Ca^{2+}] of ~20 nM and transferred to a cuvette. The cell suspension in the cuvette was supplemented with 5 mM succinate and placed in a temperature-controlled (37°C) experimental compartment of a multi-wavelength-excitation dual wavelength-emission high-speed spectrofluorometer (Delta RAM, Photon Technology International). Membrane-impermeable Fura-2 K^+ salt (K_D = 140 nM) or Fura-2FF K^+ salt (K_D = 5.5 μM) (final concentration 1 μM) and tetramethylrhodamine ethyl (TMRE, final concentration 50 nM) were added at 25 sec to measure bath $[Ca^{2+}]_c$ and mitochondrial inner membrane potential ($\Delta\Psi m$) concurrently. Fluorescence at 340 nm

excitation/535 nm emission and 380 nm excitation/535 nm emission for the Ca^{2+}-bound and Ca^{2+}-free Fura-2/Fura-2FF species, along with 560 nm excitation/595 nm emission for TMRE, respectively was measured at 5 – 2 Hz. 40 μg/ml digitonin was added at 50 sec to permeabilize the cells and allow the cytoplasm to equilibrate with the bath solution such that the TMRE fluorescence reports the relative ΔΨm. Fura-2/Fura-2FF fluorescence under these conditions is related to the cytoplasmic $[Ca^{2+}]$ ($[Ca^{2+}]_c$) per the equation below, where R is the measured fluorescence ratio (340/380 nm) and Sf_2 and Sb_2 are the absolute 380 nm excitation/535 nm emission fluorescence under 0-$[Ca^{2+}]$ and saturating $[Ca^{2+}]$, respectively.

$$[Ca^{2+}] = \left(\frac{R - R_{min}}{R_{max} - R}\right)\left(\frac{Sf_2}{Sb_2}\right) * K_D$$

Thapsigargin (Tg; 2 μM) was added at 100 sec to inhibit Ca^{2+} uptake into the ER and CGP37157 was added at 400 sec to inhibit NCLX-mediated mitochondrial-Ca^{2+} extrusion. After $[Ca^{2+}]_c$ reached a steady state at 700 sec, MCU-mediated Ca^{2+} uptake was initiated by adding a bolus of 5 μl of 5 mM $CaCl_2$ (final concentration 5 μM $CaCl_2$) to the cuvette to achieve an increase in $[Ca^{2+}]_c$. After $[Ca^{2+}]_c$ was monitored for 300 sec following addition of the $CaCl_2$ bolus, 2 μM CCCP was added to uncouple ΔΨm and allow unimpeded Ca^{2+} efflux from mitochondria as a measure of the total extent of uptake. Under these conditions, the Ca^{2+} bolus added to initiate mitochondrial Ca^{2+} uptake caused a transient depolarization as measured with TMRE that revered after ~ 50-60 sec (Payne, Hoff et al. 2017). To confirm that this Ca^{2+} transient was MCU-

mediated, we performed some experiments in the presence of 1 μM Ru360, an inhibitor of MCU, which blocked the Ca^{2+} uptake (Mallilankaraman, Cardenas et al. 2012).

9.4 Quantitative measurement of basal $[Ca^{2+}]_m$

SH-SY5Y cells were grown in 10 cm tissue-culture coated dishes and trypsinized, counted and transiently transfected with a plasmid encoding mCG1 using electroporation (Nucleofector™ Technology device) and the Cell Line Nucelofector™ Kit V (Lonza, catalog# VCA-1003). mCG1 exhibits an increase in fluorescence emission at ~610 nm upon Ca^{2+} binding with a K_D of ~490 nM. To verify localization of the probe in mitochondria, cells were imaged 48-hr post-transfection using confocal microscopy with a 40x-oil objective at 37°C.

Fluorescence images of mCG1 (560-nm excitation/600-nm emission) and EGFP (488 nm excitation/510-550 nm emission) and MitoTracker Red (581 nm excitation/644 nm emission) and a transmitted-light image of each individual field, were collected within 30 sec. To qualitatively estimate basal $[Ca^{2+}]_m$, cells grown in 6 well plates over 12 mm coverslips were transfected transiently with mCG1 and imaged 48 hr post-transfection using a epifluorescence microscope with a 20X objective at RT. Images of live cells in complete medium in resting conditions were obtained at 545-nm excitation/620-nm emission with identical gain- and exposure- settings among experiments. Ionomycin was added to promote Ca^{2+} influx into mitochondria to saturate the probe (F_{max}), which was followed by the addition of EGTA to chelate Ca^{2+} to determine F_{min}. Fluorescence measurements were transformed to $[Ca^{2+}]_m$ using the equation.

$$[Ca^{2+}] = \left(\frac{F - F_{min}}{F_{max} - F}\right) * K_D$$

Initial Ca^{2+} uptake rates in permeabilized cells were determined for each experiment using single-exponential fits from the time of Ca^{2+} addition to achievement of a new steady state to obtain parameters **A** (extent of uptake) and τ (time constant) (IGOR Pro; RRID:SCR_000325).

To determine the contribution of the Ca^{2+} release by $InsP_3R$, we used a specific inhibitor, Xestospongin B (XeB) at 5 μm. Previous studies demonstrated that XeB blocks $InsP_3R$-mediated Ca^{2+} signaling more effectively than Xestospongin C specifically without affecting the Ca^{2+} pump *(Jaimovich, Mattei et al. 2005)*.

9.5 Simultaneous measurement of cytoplasmic and mitochondrial [Ca^{2+}] in response to bradykinin stimulation.

SH-SY5Y cells (EGFP, PS1wt and M146L) were grown in 10 cm tissue-culture coated dishes and detached with Versene, counted and transiently transfected with mCG1 using the Nucleofector™ Technology device and the Cell Line Nucelofector™ Kit V. After 48 hrs transfection, cells were loaded with 1 μM Fura-2 AM, in Tyrode's solution (in mM: 140 NaCl, 5 KCl, 2 $CaCl_2$, 1 $MgCl_2$, 10 glucose, 10 Hepes-NaOH, 5 sodium pyruvate, pH 7.4) with 0.01% (wt/vol) pluronic F127 for 15 min at RT, to report $[Ca^{2+}]_c$. After loading, ~$3x10^6$ cells were transferred to a cuvette in the temperature-controlled (37°C) experimental compartment of a multi-wavelength-excitation dual-wavelength-emission high-speed spectrofluorometer (Delta RAM, Photon Technology

International). Fluorescence at 560-nm excitation/610-nm (long-pass) emission for mCG1, along with 340 nm excitation/535 nm emission and 380 nm excitation/535 nm emission for the Ca^{2+} bound and Ca^{2+}-free Fura-2 species, respectively was measured at 5 Hz. 100 nM Bradykinin (BK) was added at 200 sec to induce $InsP_3R$-mediated ER Ca^{2+} release. The mCG1 fluorescence was calibrated as described above.

9.6 Live cell imaging of cytoplasmic and mitochondrial [Ca^{2+}].

All imaging experiments were carried out in an extracellular-like medium with 2 mM $CaCl_2$ Tyrode´s solution. For $[Ca^{2+}]_c$ determinations, cells were loaded with Fura-2AM (2 µM) with 0.01% (wt/vol) pluronic F127 for 20 min at RT followed by washing. For $[Ca^{2+}]_m$ determinations, cells were loaded with Rhod-2 (0.5 µM) for 15 min at RT. For both [Ca^{2+}] determinations, cells were imaged with a 20x objective at RT using an epifluorescence Olympus IX-83 microscope equipped with a xenon lamp (Sutter Lambda LS, Sutter Instruments, Novato, CA), excitation and emission filter wheels (Sutter Instruments) and a 16-bit Hamamatsu Orca Flash 4.0 sCMOS camera. Images of live cells under resting conditions and upon stimulation were obtained at 545-nm excitation/620-nm emission with identical gain- and exposure-settings between experiments along with 340nm excitation/535 nm emission and 380 nm excitation/535 nm emission for the Ca^{2+} bound and Ca^{2+} -free Fura-2 species respectively was measured.

To qualitatively estimate basal $[Ca^{2+}]_m$, cells were grown in 10-cm tissue-culture dishes and transfected with mCG1 or LAR-GECO1 or 4mtD3cpv (FRET sensor), and imaged 48-hr post-transfection using an epifluorescence microscope with a 20x

objective at RT. Calibrated measurements of $[Ca^{2+}]_m$ were determined by incubating cells in an extracellular-like medium with 2 mM $CaCl_2$ Tyrode´s solution. Measure of $[Ca^{2+}]_c$ was obtained when fluorescence of each sensor was stabilized. Bradykinin (BK; 100 nM) or ATP (10 μM) was added at 200 sec and after peaking and reaching a new steady-state, 3.75 μl of 2 mM CCCP was added (5 μM final). After a new steady was reached (350 sec), 1.5 μl of 10 mM ionomycin was added (10 μM final) to ensure that F_{max} was achieved for all probes tested, which was followed by the addition of 0 Ca^{2+} Tyrode´s solution plus EGTA to chelate Ca^{2+} to determine F_{min}.

To confirm mitochondrial localization of the various mitochondrial Ca^{2+} sensors, we used MitoTracker® Deep Red FM, a far red-fluorescent dye (absortion/emission ~644/665 nm) that stains mitochondria in live cells (ThermoFisher Scientific).

9.7 Western blotting.

SH-SY5Y cells (EGFP, PS1wt and M146L-expressing) and human skin fibroblasts were grown in 10 cm tissue-culture coated dishes, washed with PBS and lysed with RIPA buffer supplemented with protease inhibitors (cOmplete, Roche), and protein concentrations were calculated using Pierce BCA Protein Assay kit. Mini-Protean® TGX™ gel 4-15% or 10% precast gels (Bio-Rad) were transferred to iBlot™ Transferred Stack, PVDF membrane regular size (catalogue #IB401031 from Thermo Fisher Scientific), using iBlot™ 7-Minute Blotting System (Thermo Fisher Scientific). Transferred membranes were probed with various antibodies. Antibodies used were, anti-PS1 (Cell Signaling #3622), anti-MICU1 (Cell Signaling #12524), anti-MCU (Sigma, #HPA016480) and anti-MCU (Cell Signaling #14997s), anti-MICU2 (Abcam,

#ab101465), anti-MCUR1 (Cell Signaling #13706), anti-α-actin (Cell Signaling #3700S), anti-phospho-PDH (Cell Signaling, #31866), anti-PDH (Cell Signaling, #2784), anti-IDH1 (Cell Signaling #3997), anti-αKGDH (Cell Signaling #28865), anti-β-tubulin (Invitrogen, #MAB1563) and anti-Hsp60 (Abcam, #ab46798). Membranes were blocked in 5% fat-free milk for 1 hr at RT, incubated overnight at 4°C with primary antibody, and then for 2 hrs at RT with anti-rabbit IgG-HRP (Cell Signaling, #7074S) or anti-mouse IgG-HRP (Cell Signaling, #7076S) secondary antibodies conjugated to horseradish peroxidase (HRP). Chemiluminescence detection was carried out using SuperSignal West Chemiluminescent Substrate (Thermo) and a series of timed exposures images were acquired with a FluorChem Q system (ProteinSimple) to ensure densitometric analysis were performed at exposures within the linear range. To ensure equal protein loading across gels, membranes were submerged in stripping buffer (Restore western blot stripping buffer; Pierce), incubated at 37°C for 20 min, and re-probed with a loading control antibody. All experiments were done at least in triplicate. The mean pixels densities of bands were quantified using Image J (NIH) for densitometric analysis.

9.8 Oxygen consumption measurements.

Oxygen (O_2) consumption is an excellent read-out for mitochondrial respiratory activity. Measurement of the O_2 consumption rate (OCR) is the current experiment of choice to determine underlying mitochondrial dysfunction (Brand and Nicholls 2011) With appropriate pharmacological manipulation, it is possible to isolate different respiratory parameters, including basal respiration, maximal respiration, proton (H^+)

leak and ATP production. Mitochondrial function was investigated in intact cells by measuring the OCR during sequential addition of mitochondrial respiratory inhibitors. The seeding density and concentrations of the injection compounds were optimized. Linear relationships between OCR and number of cells seeded were observed. Control (EGFP and PS1wt and mutant PS1-M146L SH-SY5Y cells and human fibroblasts were subjected to OCR measurements in real time at 37°C in an XF96 extracellular flux analyzer (Agilent). Cells ($3x10^4$) were plated and after 24 hr culture medium was switched to XF media, pH 7.4 supplemented with 25 mM glucose and 1 mM sodium pyruvate and 1 mM glutamine and further incubated in a CO_2-free incubator for 1 hr prior to measurements. In the basal state, mitochondrial OCR is predominantly driven by H^+ flux through F_1F_0 ATP synthase. Inhibition of the F_1F_0 ATP synthase with 1μM oligomycin reduces mitochondrial O_2 consumption, with the OCR in this phase predominantly driven by the H^+ leak (also by substrate oxidation). The uncoupler carbonylcyanide p-trifluoromethoxyphenylhydrazone (FCCP) was then added, causing an increase in the H^+ leak across the inner membrane, creating a H^+ short circuit and facilitating the measurement of maximal OCR. The optimal FCCP concentration to induce maximal respiration was determined for each cell type studied. Next, respiratory chain activity was inhibited with rotenone plus antimycin A at 1μM. OCR measured in this phase is due to non-mitochondrial O_2 consumption. After each injection, OCR was measured for 3 min, the medium was mixed and again measured for 3 min. Basal OCR was calculated as a difference of OCR before and after oligomycin. Maximum OCR was calculated as difference of OCR after FCCP and that measured after exposure to rotenone plus antimycin A. This allowed for an estimation of the contribution of

individual parameters for respiration, proton leak, spare respiratory capacity, non-mitochondrial respiration and ATP production. Data were normalized to protein concentrations by lysing samples after each experiment. The cell number was chosen to provide a nearly confluent uniform monolayer of cells. Before and after each experiment, uniformity and integrity of the monolayer was evaluated by DIC microscopy. Respiration rates are presented as the mean ± SEM of 3 or more independent experiments performed with 3 or more replicate wells in the Seahorse XF96 analyzer. Significance level was determined by performing ANOVA on the complete data set with Bonferroni post testing. The results were considered significant at $p < 0.05$. The general scheme of mitochondrial stress test is shown in figure 3i.

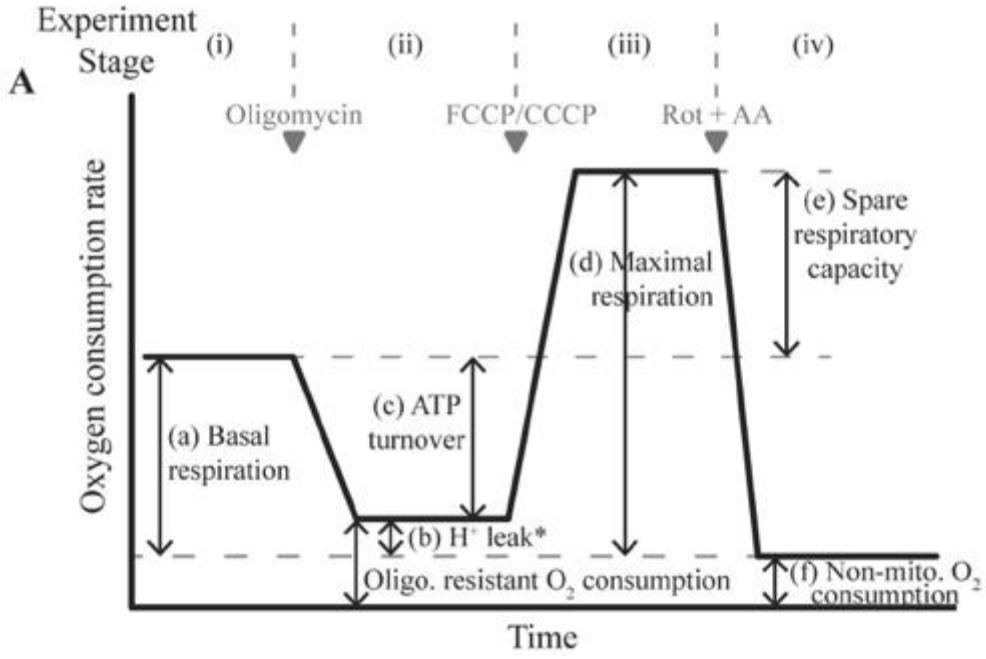

Figure 3i: Seahorse XF Cell Mito Stress Test profile of the key parameters of mitochondrial respiration. Sequential compound injections measure basal respiration, ATP production, proton leak, maximal respiration, spare respiratory capacity and non-mitochondrial respiration (Seahorse Bioscience, Agilent).

9.9 Data analysis and statistics.

Data were summarized as the mean ± SEM, and statistical significance of differences between means was assessed using unpaired Student's t test or one-way analysis of variance (ANOVA) for repeated measures. Statistical analyses were performed in Stata software with appropriate post-test as indicates, $p < 0.05$ was considered statistically significant. For comparisons of all samples within the data set, Tukey-Kramer post-test was used. For pre-selected pairwise comparisons, Bonferroni post-test was performed. All other data analysis was performed in Excel. For all figures, one asterisk indicates $p < 0.05$ and two asterisks indicate $p < 0.01$, respectively, *n.s*. indicates no statistical significance.

10. RESULTS

10.1 Expression of FAD mutant PS1-M146L causes excessive levels of mitochondrial Ca^{2+} in SH-SY5Y cells.

To explore whether the expression of mutant PS1-M146L plays a role in mitochondrial Ca^{2+} uptake and membrane potential in SH-SY5Y cell lines, we first used a permeabilized-cell assay. To measure MCU-mediated Ca^{2+} uptake activity, we made real-time measurements of bulk changes in bath (cytoplasmic) $[Ca^{2+}]$ ($[Ca^{2+}]_c$) in a suspension of 6-8x10^6 permeabilized SH-SY5Y cells stably transfected either with the empty vector EGFP, PS1wt or mutant PS1-M146L. The expression of the transfected PS1 proteins was evaluated periodically and confirmed by immunoblot (Figure 1A). PS1 levels in PS1wt and M146L lines were significantly higher than the endogenous levels in cells transfected with the empty vector or with EGFP as a control. First, we permeabilized cells in an intracellular-like medium lacking Ca^{2+} buffers (free $[Ca^{2+}]$ ~ 20 nM) with digitonin (Dg), added directly to the cell suspension, affecting the plasma membrane but leaving the inner mitochondrial membrane (IMM) intact (Payne, Hoff et al. 2017) (Mallilankaraman, Doonan et al. 2012). Then, we measured simultaneously the $[Ca^{2+}]_c$ using the low affinity ratiometric indicator Fura-2FF (K_D 5.5 μM) (Figure 1B) and the $\Delta\Psi_m$ using TMRE (Figure 3). Thapsigargin (Tg) was used to inhibit SERCA, preventing Ca^{2+} uptake into the ER and releasing the ER Ca^{2+} stores into the bath that resulted in a small increase in $[Ca^{2+}]_c$ that reached a steady-state ~300 sec (Figure 1B). Under these conditions, MCU-mediated mitochondrial Ca^{2+} uptake plays the dominant role in determining $[Ca^{2+}]_c$. CGP37157 (CGP) was then added to inhibit NCLX-

mediated Ca^{2+} efflux to isolate MCU as the only pathway for transport of Ca^{2+} between mitochondria and cytoplasm. Again, after reaching a steady-state $[Ca^{2+}]_c$, addition of 5 µL of 5 mM $CaCl_2$ at 700 sec to the bath, caused a rapid rise in $[Ca^{2+}]_c$ to ~5-7 µM followed by clearance of Ca^{2+} over 100-200 sec in all the cell lines analyzed, but not in cells in which MCU was pharmacologically blocked by Ru-360 (1 µM) (Figure 1B), indicating that uptake was mediated solely by MCU. Subsequent dissipation of $\Delta\Psi m$ with (2 µM) CCCP caused a rapid increase in $[Ca^{2+}]_c$ as the total matrix Ca^{2+} content was released, providing further evidence that mitochondria were responsible for clearance of cytoplasmic Ca^{2+}. In cells expressing mutant PS1-M146L, the increase in $[Ca^{2+}]_c$ upon CCCP addition was significantly higher than the control cells or overexpressing PS1*wt* (Figure 1A), suggesting that mitochondria from cells expressing PS1-M146L accumulated more Ca^{2+} compared with the control cells.

Calibration of Fura-2FF was carried out in each experiment to define the magnitude of the $[Ca^{2+}]_c$ signals (Figure 2). In these experiments, cells expressing PS1-M146L released more Ca^{2+} from the than the control cell lines (Figure 2A & 2B), consistent with previously reported FAD-PS1-induced exaggerated Ca^{2+} release from the ER. In contrast, no significant differences were found in the Ca^{2+} boluses added to the different cell lines (Figure 2C). We also estimated the total mitochondrial Ca^{2+} content. The initial mitochondrial Ca^{2+} taken up during the experiment. The initial mitochondrial Ca^{2+} content prior to Ca^{2+} addition was calculated by subtracting the peak value after the addition of 5 µM Ca^{2+} and the value of $[Ca^{2+}]_c$ before Tg addition from the $[Ca^{2+}]_c$ after CCCP addition. The average mitochondrial Ca^{2+} content (n = 5) is shown in Figure 2D. The results from these set of experiments show a greater

mitochondrial Ca^{2+} uptake in cells expressing the PS1-M146L. Because there were no significant differences in mitochondrial Ca^{2+} uptake rate among the cell lines (Figure 1C), this may indicate that Ca^{2+} release from the ER after Tg was taken up to a greater extent by the PS1-M146L-expressing cells.

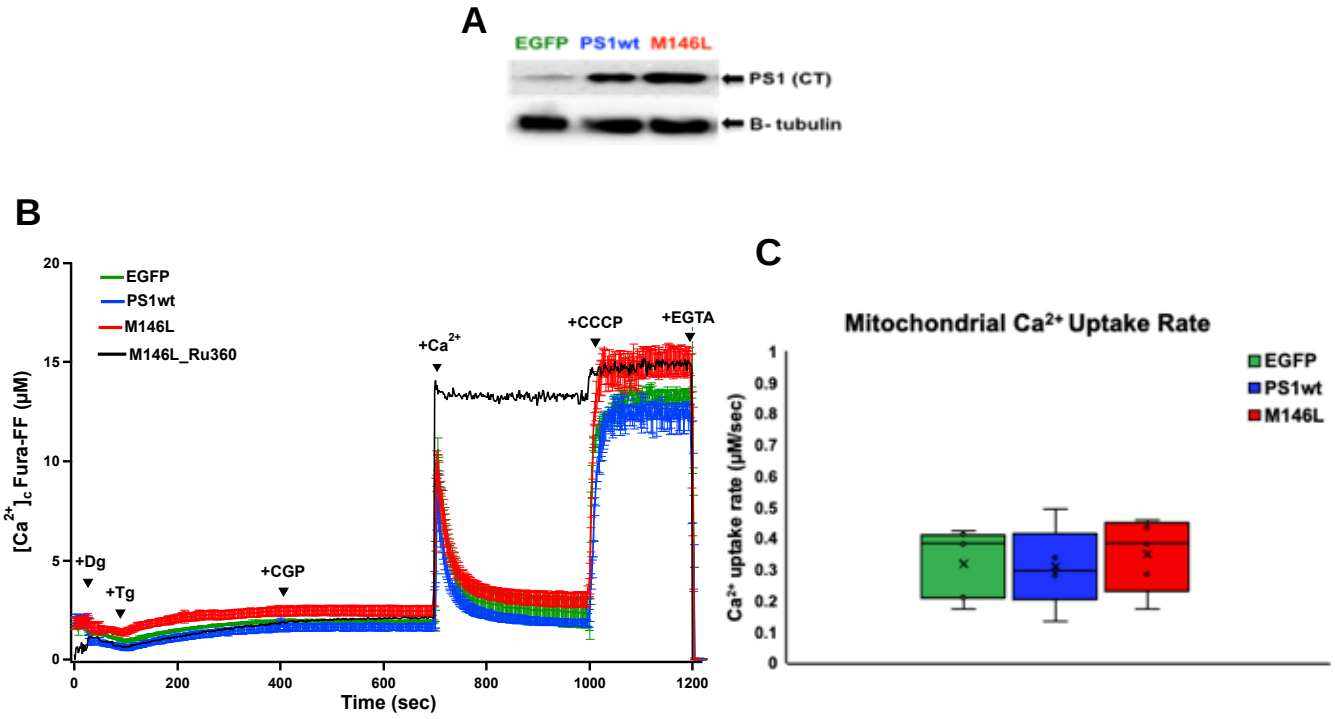

Figure 1: Mitochondrial Ca^{2+} uptake in mutant PS1-M146L is unaffected in SH-SY5Y cells. A) Representative immunoblot of PS1 expression in SH-SY5Y cells stably expressing EGFP, PS1wt or mutant PS1-M146L and normalized by β-tubulin. **B)** Calibrated mitochondrial Ca^{2+} uptake in permeabilized SH-SY5Y cells in response to 5 μM $CaCl_2$. Cells were treated with 0.004% digitonin (Dg) to permeabilize plasma membrane, 2 μM thapsigargin (Tg) to block ER Ca^{2+} uptake, and 20 μM CGP37157 (CGP) to inhibit mitochondrial Ca^{2+} efflux, added at t=50, 100 and 400s, respectively as indicated. races represent average from n=5 independent replicates for each cell line shown. **C)** Ca^{2+} uptake rates for control, PS1wt and M146L in response to 5 μM $CaCl_2$. Replicate measurements of 5 independent experiments. No significant differences unpaired test.

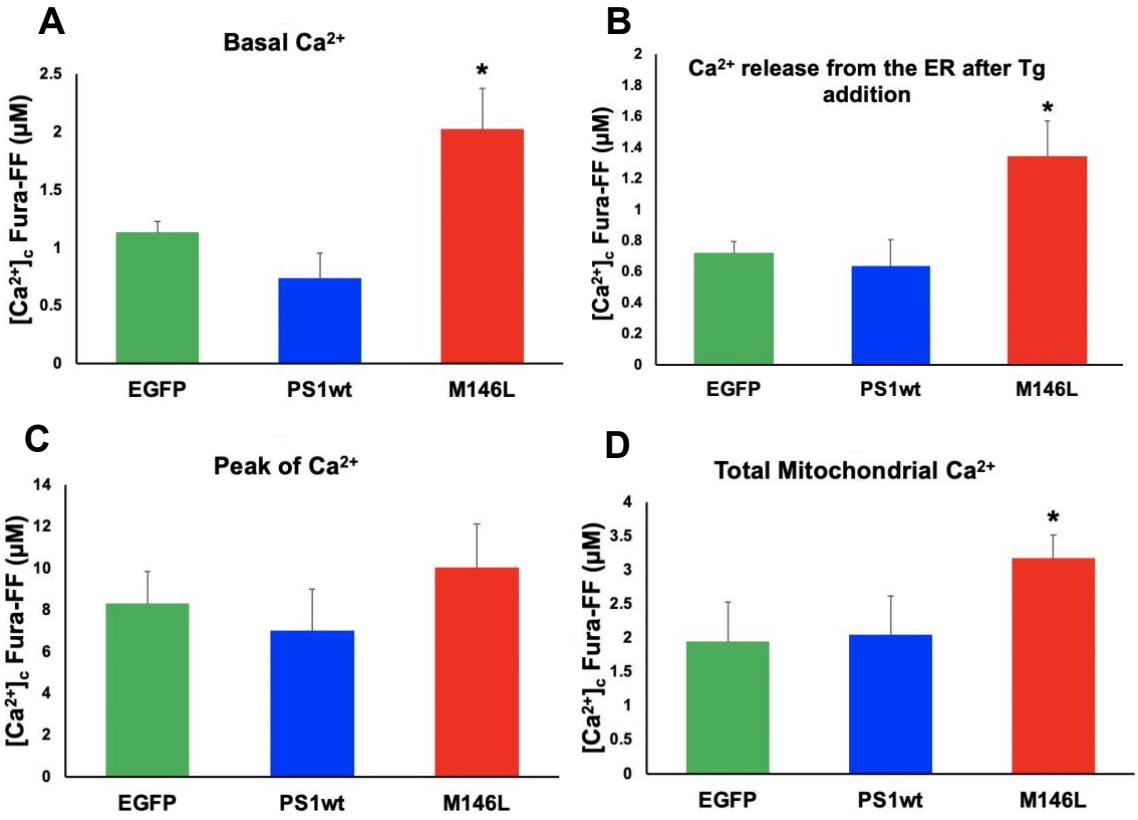

Figure 2: Summary of Quantitative Measurement of Mitochondrial Ca^{2+} levels in SH-SY5Y cells. A) Estimation of before Tg addition. PS1-M146L expressing cells shown higher compared with control cells. **B)** Estimation of total ER Ca^{2+} release from the ER after Tg addition was obtained subtracting the before CGP addition minus the before Tg. **C)** peak after addition of 5 µL of 5 mM $CaCl_2$ at 700 sec were no different among the cell lines. **D)** Estimation of total mitochondrial Ca^{2+} in SH-SY5Y cells. Values obtained by subtracting minus the peak value after the addition of 5 µM Ca^{2+} and the value of $[Ca^{2+}]_c$ before Tg addition. Bars represent average +/- SEM total mitochondrial Ca^{2+} content of 5 independent experiments. Significance was determined by one-way ANOVA with Dunnett's post-test using EGFP cells as control: *, $p < 0.05$.

10.2 Effects of PS1-M146L expression on mitochondrial membrane potential ($\Delta\Psi_m$).

The $\Delta\Psi_m$, defined as the electrical potential between the mitochondrial matrix and the cytoplasm, is an important mitochondrial parameter and a key indicator of cell health or injury as it relates to the capacity to generate ATP by OXPHOS. Perturbed

$\Delta\Psi_m$ can indicate disrupted respiration, ATP synthesis, or ionic fluxes across the mitochondrial membrane. The $\Delta\Psi_m$ provides the driving force for mitochondrial Ca^{2+} uptake and regulates ROS production. To assess this parameter, we used the lipophilic cationic compound TMRE, which accumulates within mitochondria in inverse proportion to $\Delta\Psi_m$. We used this probe in a quenching mode, which means that the dye accumulates within mitochondria at high concentration (50 nM) forming aggregates, which quench the fluorescent emission of the dye. Under these conditions, once the dye is loaded into mitochondria, a subsequent mitochondrial depolarization will result in release of dye, lowering its concentration, allowing the disassembly of the aggregates, unquenching the dye and increasing the fluorescent signal. In our experimental settings in permeabilized cells, we monitored in real-time the dynamic changes of $\Delta\Psi_m$. We observed a transient increase in TMRE fluorescence in response to addition of a bolus of Ca^{2+} as Ca^{2+} influx depolarized $\Delta\Psi$m, which recovered as $[Ca^{2+}]_c$ approached a steady state due to closure of MCU (Figure 3). Subsequent dissipation of $\Delta\Psi$m with 2 µM CCCP collapsed $\Delta\Psi$m. TMRE fluorescence in CCCP was used to normalize $\Delta\Psi$m between experiments. There was no significant difference in $\Delta\Psi_m$ between the control (EGFP) and PS1wt and PS1-M146L cells, under basal levels, after Ca^{2+} uptake or after CCCP addition (Figure 3).

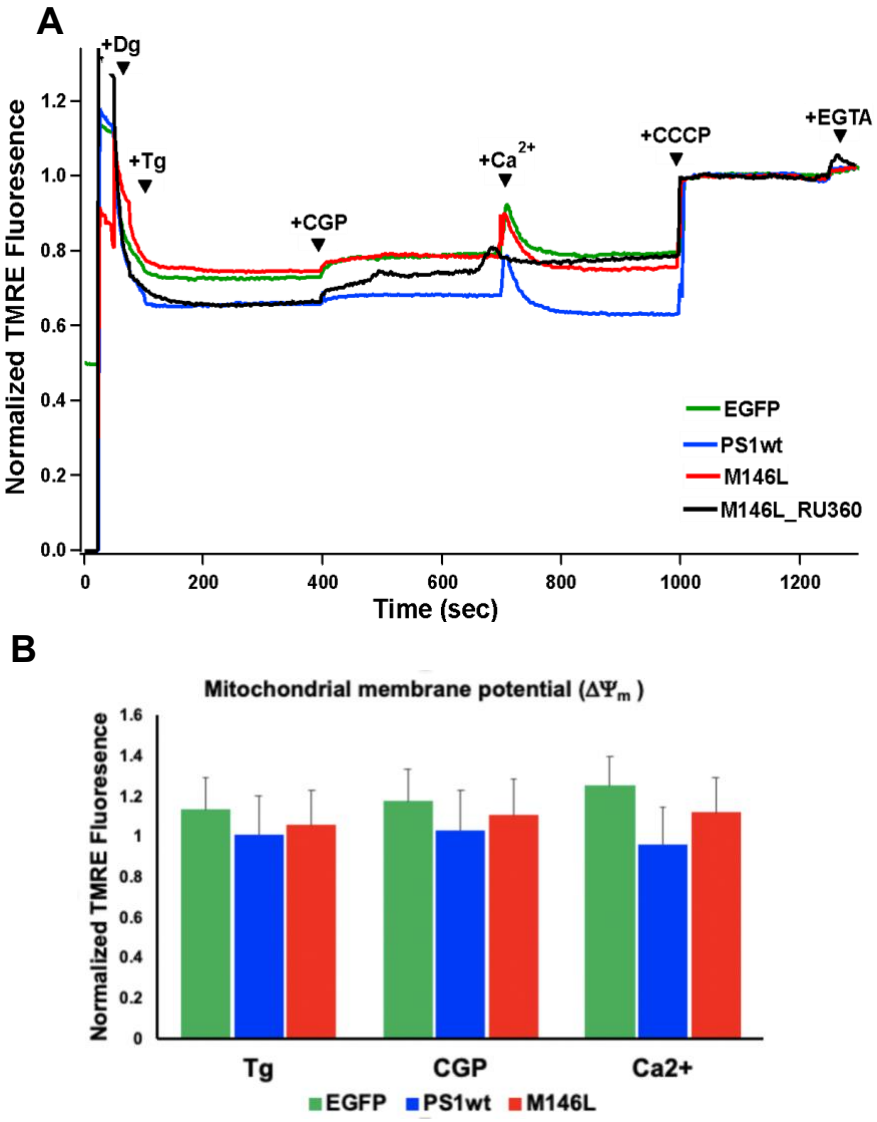

Figure 3: Expression of mutant PS1-M146L did not affect relative mitochondrial membrane potential ($\Delta\Psi_m$). A) Traces represent the average from 5 independent replicates for each cell line shown. $[Ca^{2+}]_c$ was measured simultaneously using the low affinity ratiometric indicator Fura-2FF (Figure 1A) and $\Delta\Psi_m$ using TMRE. SH-SY5Y cells were treated with 0.004% digitonin (Dg) to permeabilize plasma membrane, 2 μM thapsigargin (Tg) to block ER Ca^{2+} uptake, and 20 μM CGP37157 (CGP) to inhibit mitochondrial Ca^{2+} efflux, added at t=50, 100 and 400s, respectively as indicated. Transient depolarization was observed in response to Ca^{2+}, whereas addition of CCCP collapsed $\Delta\Psi_m$. **B)** Summary of relative $\Delta\Psi_m$ after Tg, CGP, and Ca^{2+} addition. No significant differences were observed between mutant PS1-M146L and control cells.

10.3 Simultaneous measurements of cytoplasmic and mitochondrial [Ca^{2+}] in intact cells in response to bradykinin.

To determine more directly and physiologically the role of PS1-M146L expression on mitochondrial Ca^{2+} dynamics, we performed experiments using intact SH-SY5Y cells stably transfected with EGFP, PS1wt or PS1-M146L, and transiently transfected with mitoCAR-GECO1 (mCG1; K_D= 490 nM), a genetically-encoded Ca^{2+} indicator targeted to the mitochondrial matrix. mCG1 exhibits an increase in fluorescence emission at >610 nm upon Ca^{2+} binding. 48 hours post transfection, 3 x 10^6 SH-SY5Y cells were loaded with the ratiometric dye Fura-2-AM (1 μM final) in a Tyrode's solution (140 nM NaCl, 5 mM KCl, 2 mM $CaCl_2$, 1mM $MgCl_2$, 10 mM glucose, 10 mM Hepes, 5 mM sodium pyruvate, pH 7.4) to report $[Ca^{2+}]_c$. Once Fura-2 and mCG fluorescence had stabilized, bradykinin (BK; 100 nM) was added at 200 sec to induce $InsP_3R$-mediated ER Ca^{2+} release. Basal $[Ca^{2+}]_c$ and $[Ca^{2+}]_m$ were significantly elevated in cells expressing mutant PS1-M146L (red traces in Figure 4; Figure 5C). Unexpectedly the responses of $[Ca^{2+}]_c$ and $[Ca^{2+}]_m$ to BK were significantly more robust in the control cells expressing the empty EGFP vector (green traces in Figure 4; Figure 6). When the $[Ca^{2+}]_c$ relaxed to a new elevated steady-state level due to opening of store-operated Ca^{2+} channels, addition of 5 μM CCCP dissipated $\Delta\Psi_m$ and caused a rapid $[Ca^{2+}]_c$ increase (Figure 4).

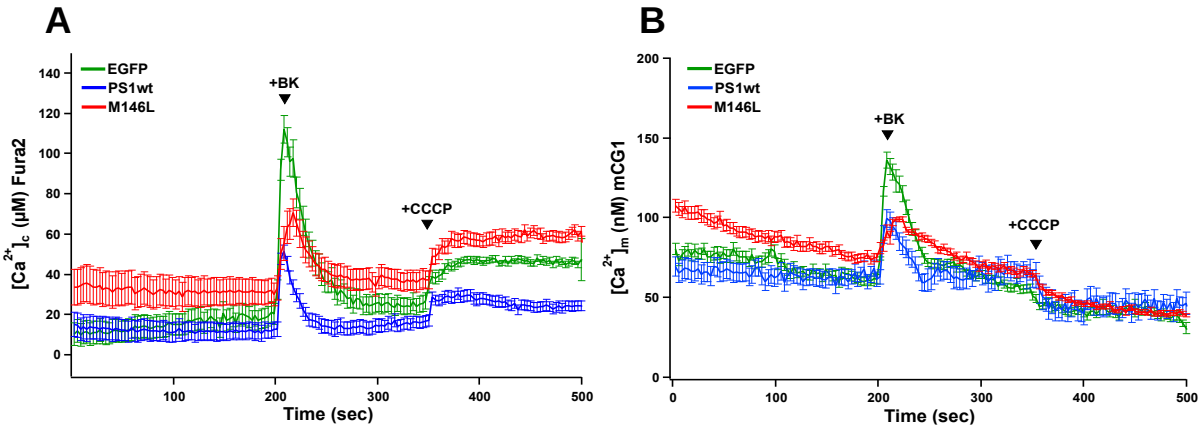

Figure 4: Simultaneous measurements of $[Ca^{2+}]_c$ and $[Ca^{2+}]_m$ in response to BK stimulation in SH-SY5Y cells. A) Average traces of cytoplasmic Ca^{2+} in intact cells stably expressing EGFP, PS1wt or PS1-M146L loaded with Fura-2. Cells were stimulated at 200 sec with BK (100 nM) to induce Ca^{2+} release from internal stores, and subsequently with CCCP to dissipate $\Delta\Psi_m$ and release the Ca^{2+} accumulated in the mitochondria. $[Ca^{2+}]_c$ was calibrated upon addition of ionomycin and EGTA in order to obtain the F_{max} and F_{min} respectively. **B)** Average traces of $[Ca^{2+}]_m$ from calibrated mCG fluorescence in cells transiently transfected with mCG.

These results demonstrated that the indicators were functional in each cellular compartment. They also indicate again that cells expressing the mutant PS1-M146L had higher levels of basal $[Ca^{2+}]_c$ and $[Ca^{2+}]_m$ compared to the EFGP and PS1*wt* controls. However, no significant differences were observed in the peak of Ca^{2+} reached in response of BK stimulation. Notably, after CCCP stimulation, mutant PS1-M146L cells exhibited a larger increase in cytoplasmic and mitochondrial Ca^{2+} compared with cells expressing EGFP or PS1*wt.*

To determine if elevated basal $[Ca^{2+}]_c$ observed in mutant PS1-M146L cells was due to constitutive Ca^{2+} release from the ER through the $InsP_3R$, cells were preincubated with 5 μM Xestospongin B (XeB), a specific $InsP_3R$ inhibitor. XeB

dramatically reduced the higher basal cytoplasmic and mitochondrial Ca^{2+} in PS1-M146L cells (Figure 5).

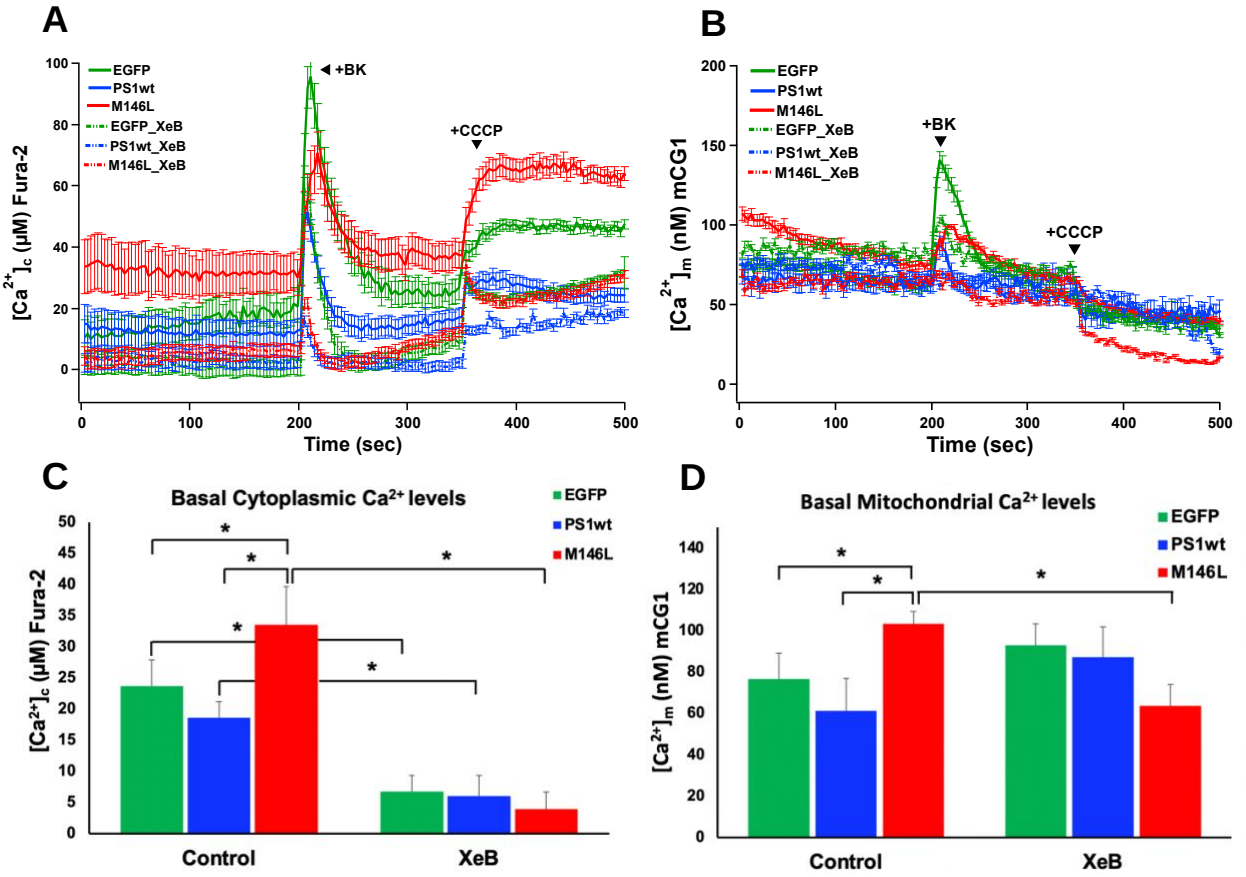

Figure 5: Effect of $InsP_3R$ inhibition on basal $[Ca^{2+}]_c$ and $[Ca^{2+}]_m$ in SH-SY5Y cells. A) Average traces of cytoplasmic Ca^{2+} in intact cells stably expressing EGFP only, PS1wt or PS1-M146L loaded with Fura-2. Cells were stimulated at 100 sec with BK (100 nM) to induce Ca^{2+} release from internal stores and CCCP to cause a subsequent dissipation of $\Delta\Psi_m$ and release Ca^{2+} accumulated in the mitochondria. **B)** Mitochondrial Ca^{2+} levels in cells transiently transfected with mCG. **C)** Comparison of calibrated Fura-2 340/380 measurements of cytoplasmic $[Ca^{2+}]$ in cells with (control) or without XeB preincubation. **D)** Comparison of calibrated mCG fluorescence as a measure of mitochondrial matrix $[Ca^{2+}]$ in cells with or without XeB preincubation. Bars represent the average +/- SEM total mitochondrial Ca^{2+} content of 3 independent experiments. Significance was determined by one-way ANOVA with Dunnett's post-test using EGFP cells as control: *, $p < 0.05$.

To improve the magnitude of the responses to BK, another set of experiments was performed using DMEM plus 1% of fetal bovine serum (FBS). Under these conditions the cytoplasmic Ca^{2+} peak obtained by BK stimulation in control cells expressing just the empty vector EGFP showed a significantly higher response compared to cells overexpressing either PS1wt or mutant PS1-M146L (Figure 6A). On the other hand, no significant differences in peak $[Ca^{2+}]$ upon BK stimulation were observed between control EGFP and mutant PS1-M146L cells (Figure 6B). In addition, in the presence of XeB, we observed that in control cells EGFP had just a slight decrease in cytoplasmic Ca^{2+} peak, but cells expressing PS1wt or M146L had a significant reduction in the peak response to BK in cytoplasmic and mitochondrial Ca^{2+} response elicited by BK compared to the EFGP only cells (Figure 6A&B).

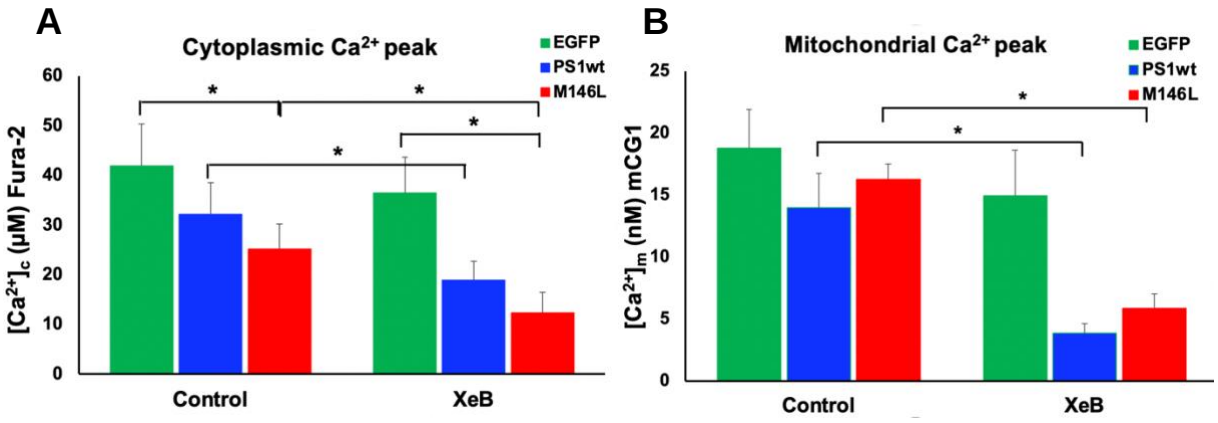

Figure 6. Inhibition of $InsP_3R$ decreases mitochondrial and cytoplasmic $[Ca^{2+}]$ in mutant PS1-M146L expressing cells. A) Comparison of normalized Fura-2 340/380 excitation ratio as a measure of relative cytoplasmic Ca^{2+} in cells with (control) or without XeB preincubation. **B)** Comparison of normalized mCG fluorescence as a measure of relative mitochondrial matrix Ca^{2+} in cells with or without XeB preincubation. Bars represent the average +/- SEM total mitochondrial Ca^{2+} content of 3 independent experiments. Significance was determined by one-way ANOVA with Dunnett's post-test using EGFP cells as control: *, $p < 0.05$.

10.4 Constitutively high basal $[Ca^{2+}]_m$ by imaging cells expressing mutant PS1-M146L.

To confirm that mutant PS1-M146L cells exhibited increased mitochondrial $[Ca^{2+}]_m$ responses compared to control cells, we qualitatively estimated $[Ca^{2+}]_m$ in cells grown in 10-cm tissue-culture dishes. Cells were loaded with Fura-2-AM and Rhod-2 and imaged using an epifluorescence microscope with a 20x objective at RT. Images of live cells in complete medium under resting conditions and upon stimulation were obtained at 545-nm excitation/620-nm emission with identical gain- and exposure-settings between experiments. Calibrated measurements of $[Ca^{2+}]_m$ were determined by suspending cells in a high Na^+/low K^+ extracellular-like medium with 2 mM $CaCl_2$ Tyrode's solution. In agreement with previous mitochondrial flux results obtained by the PTI assay (Figures 1 & 2), we observed a significantly higher basal Rhod-2 fluorescence intensity in cells expressing mutant PS1-M146L, suggesting again an increase in $[Ca^{2+}]_m$ in these cells compared to control cells (Figure 7). Nevertheless, because the positively charged fluorescent Ca^{2+} indicator Rhod-2 accumulates only incompletely in mitochondria (Connolly, Theurey et al. 2018), we also used another approach. We used a genetically-encoded fluorescent reporter mCG to determine the relative basal $[Ca^{2+}]_m$. Cells were transiently transfected using a Nucleofector device to obtain higher expression and efficiency levels of mCG1 in SH-SY5Y cells. To verify localization to mitochondria and transfection efficiency of mCG1 and qualitatively estimate basal $[Ca^{2+}]_m$, cells grown in 10-cm tissue-culture dishes were imaged using an epifluorescence microscope with a 20x objective at RT. Fluorescence images of mCG1 (560-nm excitation/600-750-nm emission) were all collected within 100 sec.

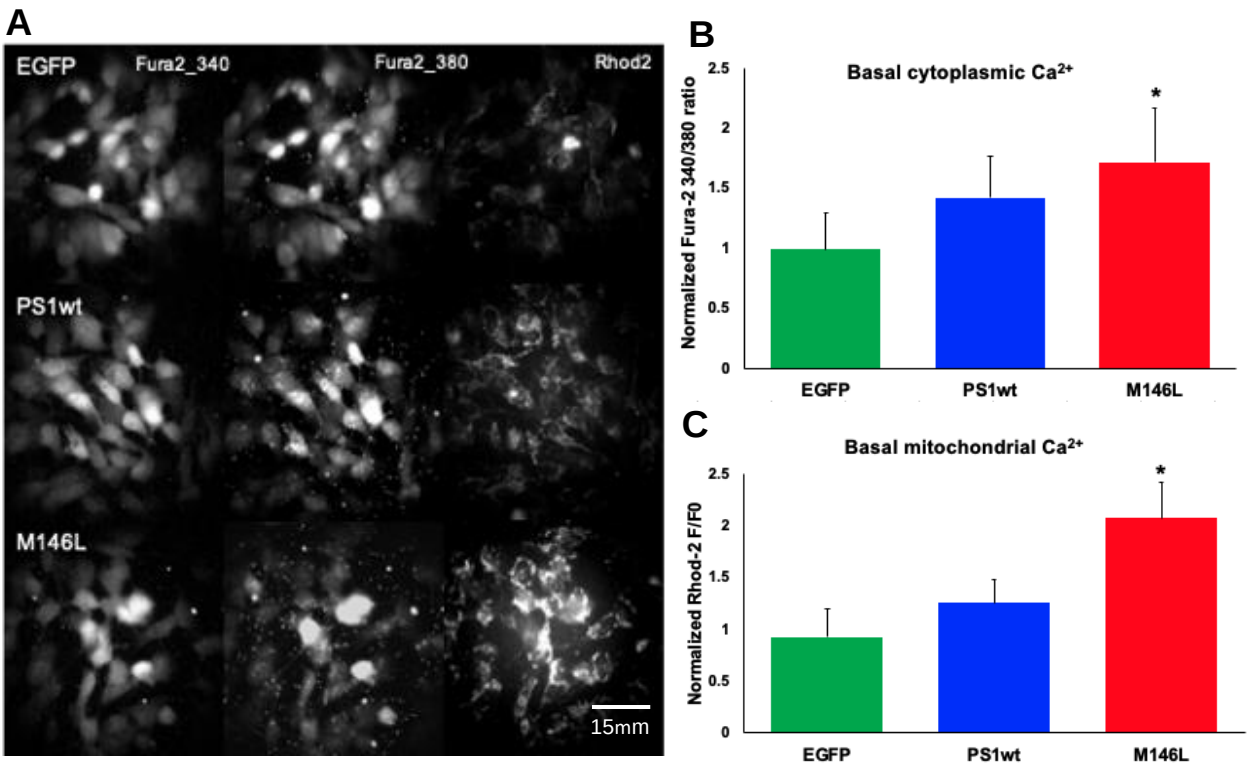

Figure 7. Increased basal mitochondrial [Ca^{2+}] in PS1-M146L expressing cells loaded with Fura-2 and Rhod-2. A) Representative images of cytoplasmic and mitochondrial Ca^{2+} in three different channels, 340 nm, 380 nm (Fura-2) and 581 nm (Rhod-2). Cells were incubated with Tyrod´s solution for 100 sec and then perfused with CCCP to cause a dissipation of $\Delta\Psi_m$ and release the Ca^{2+} accumulated in the mitochondria. **B) and C)** Normalized cytoplasmic and mitochondrial Ca^{2+} response was calculated as the relative ratio change (340/380nm; Fura-2) and relative change of Rhod-2 fluorescence (F/F0). Data represent means of three experiments from different cell preparations. Bars represent average +/- SEM total mitochondrial Ca^{2+} content of 3 independent experiments. Significance was determined by one-way ANOVA with Dunnett's post-test using EGFP cells as control: *, $p < 0.05$.

As shown in Figure 8, higher basal levels of both cytoplasmic (Fura-2) and mitochondrial (mCG1) [Ca^{2+}] were observed in PS1-M146L-expressing cells. The basal fluorescence intensity of mCG1 was constitutively higher in mutant cells as shown in lower panels of Figure 8A. To determine the basal differences among the cells in these experiments, Fura-2 ratios and mCG1 fluorescence of each experiment were

normalized using raw fluorescence values to compare experiments performed under identical conditions with identical microscope settings.

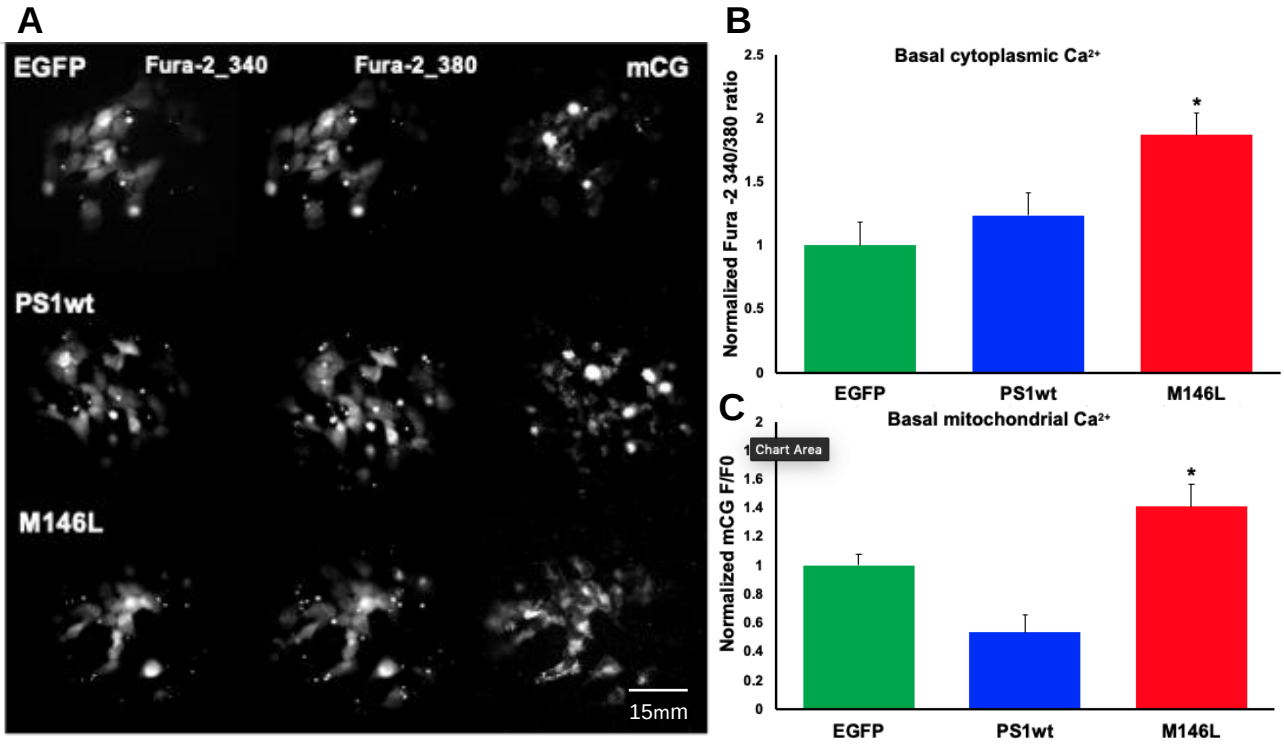

Figure 8. Increased basal mitochondrial [Ca^{2+}] in PS1-M146L expressing cells loaded with Fura-2- and transiently transfected with mCG. Expression of mito-CAR-GECO1 (mCG) transiently transfected in cell lines stably expressing either the empty pIRES vector EGFP, PS1wt or PS1-M146L, were imaged using an epifluorescence microscope with a 20x objective at RT (560-nm excitation/600-750-nm emission) and GFP expression (488-nm excitation/530-25-nm emission). **A)** Representative images in three different channels, 340 nm, 380 nm (Fura-2) and 581 nm (mCG). **B) and C)** Normalized responses calculated as the relative ratio change (340/380nm; Fura-2) and relative change of mCG fluorescence (F/F0). Data represent means of 3 experiments from different cell preparations. Bars represent the average +/- SEM total mitochondrial Ca^{2+} content of 3 independent experiments. Significance was determined by one-way ANOVA with Dunnett's post-test using EGFP cells as control: *, $p < 0.05$.

Cells expressing PS1-M146L presented higher basal levels of cytoplasmic and mitochondrial [Ca^{2+}] compared with the control cells stably transfected with EGFP only or PS1wt (Figure 8B) strongly suggesting a mitochondrial Ca^{2+} overload. However, when cells were treated with Tg, an increase in $[Ca^{2+}]_c$ and $[Ca^{2+}]_m$ was observed in all

cells, which was more pronounced in mutant PS1-M146L cells relative to control cells (Figure 9).

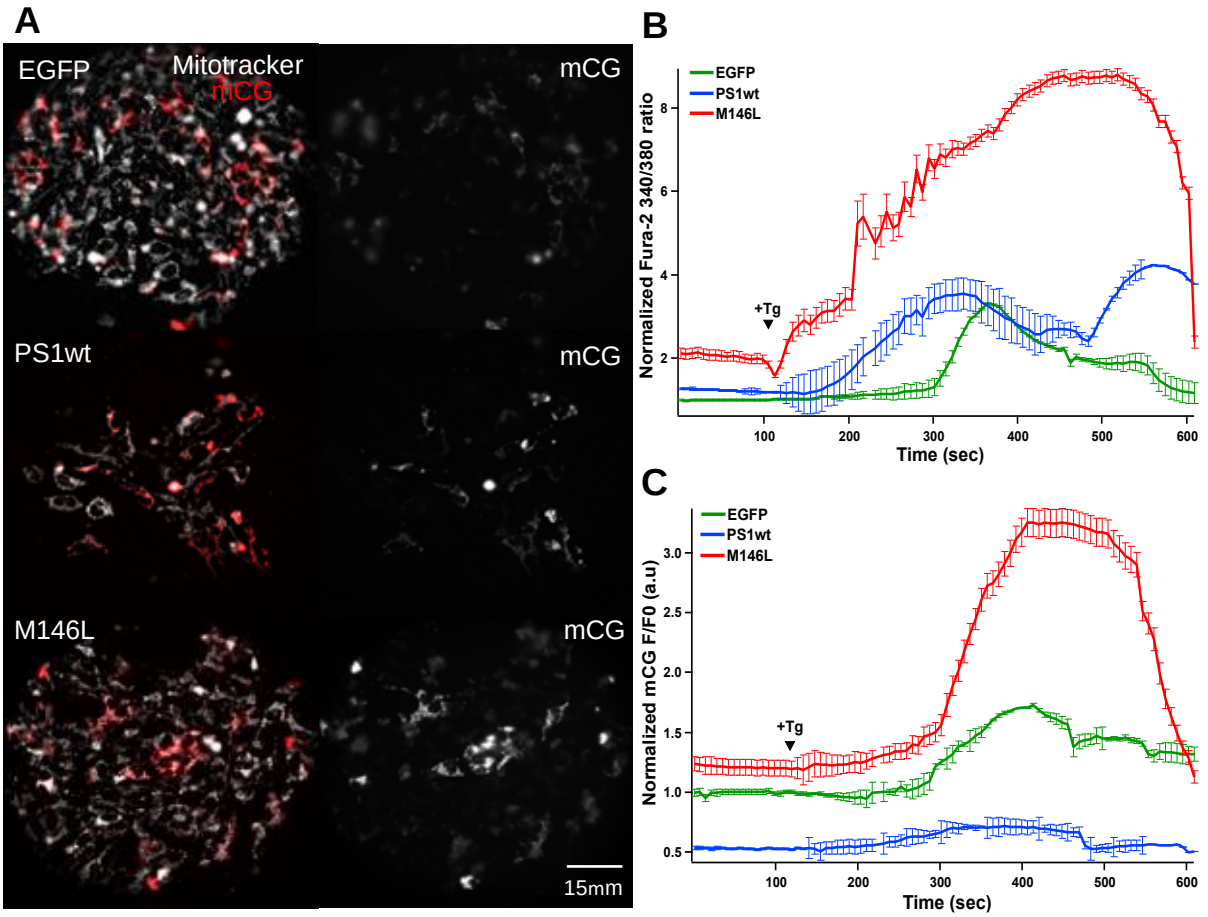

Figure 9: Increased [Ca^{2+}] in PS1-M146L expressing cells in response to ER Ca^{2+} release. **A)** Representative micrographs of the expression of mito-CAR-GECO1 (mCG), loaded with Fura-2. At 100 seconds, Tg (3 μM) was added to each cell line stably expressing either the empty pIRES vector EGFP, PS1wt or PS1-M146L. Cells were imaged using an epifluorescence microscope with a 20x objective at RT (560-nm excitation/600-750-nm emission) and deep red mitotracker (644/665 nm excitation/emission) to verify mitochondrial localization. **B)** Average traces of normalized Fura-2 340/380 ratios in each cell line. **C)** Average traces of relative level change of mCG fluorescence F/F0. The data represent the means of three experiments from different cell preparations. Bars represent the average +/- SEM of 3 independent experiments.

Using another experimental paradigm, we confirmed that upon BK stimulation the mean value of the $[Ca^{2+}]_c$ peak obtained was higher in cells expressing the mutant PS1-M146L (Figure 10). Figure 10B shows representative traces for each cell type analyzed demonstrating that the mean value of the peak obtained after BK stimulation was higher in cells expressing the mutant PS1-M146L.

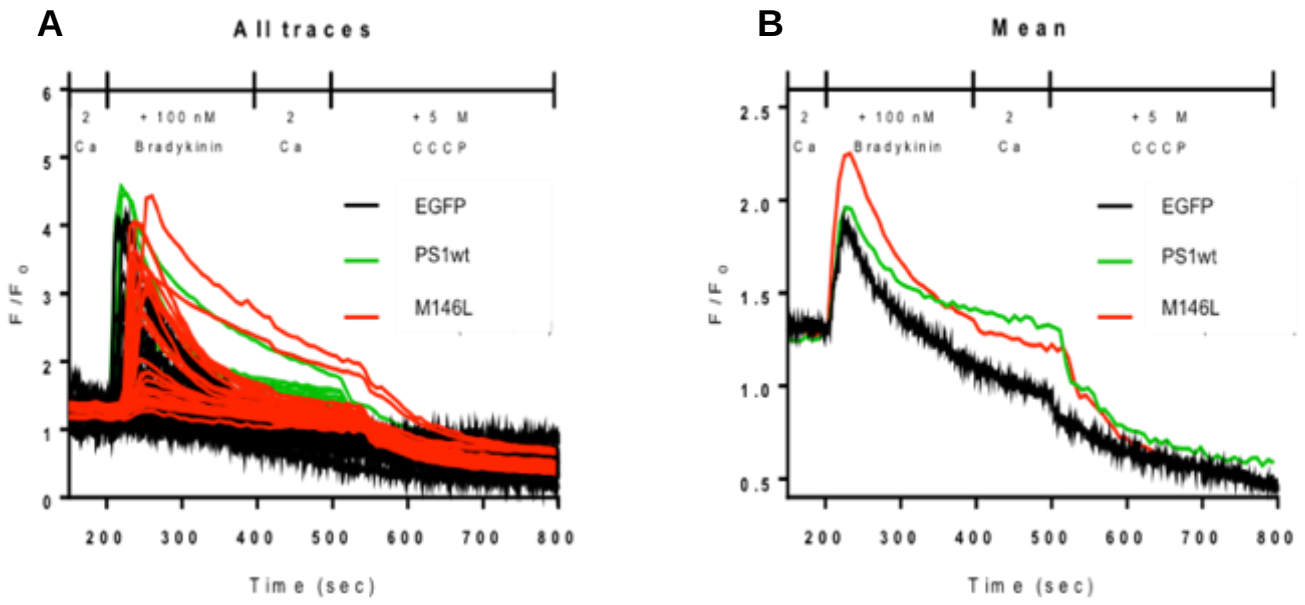

Figure 10: Increased mitochondrial $[Ca^{2+}]$ in mutant PS1-M146L expressing cells transfected with mCG in response to BK. Each cell type was transiently transfected with mCG1 and imaged 48-hr post-transfection using an epifluorescence microscope with a 20x objective at RT. The data represent 30 individual cells from one coverslip for each cell type and three coverslips for each and they show similar results. **A)** Show all traces analyzed in one coverslip of each cell line and **B)** The mean obtained of the previous graph (n=3).

As previously described in Figure 4, BK stimulation assays in SH-SY5Y cells were significantly improved when experiments were done in DMEM/FBS instead of Tyrode's solution. In a new set of experiments, cells were imaged using an epifluorescence microscope with a 20x objective at RT (560-nm excitation/600-750-nm emission) for

GFP (488-nm excitation/530-25-nm emission) and deep red MitoTracker (644/665 nm excitation/emission) to verify mitochondrial localization. We visually confirmed that cells expressing mutant PS1-M146L (GFP positive) had higher mCG fluorescence intensity in basal conditions compared with control cells (Figure 11).

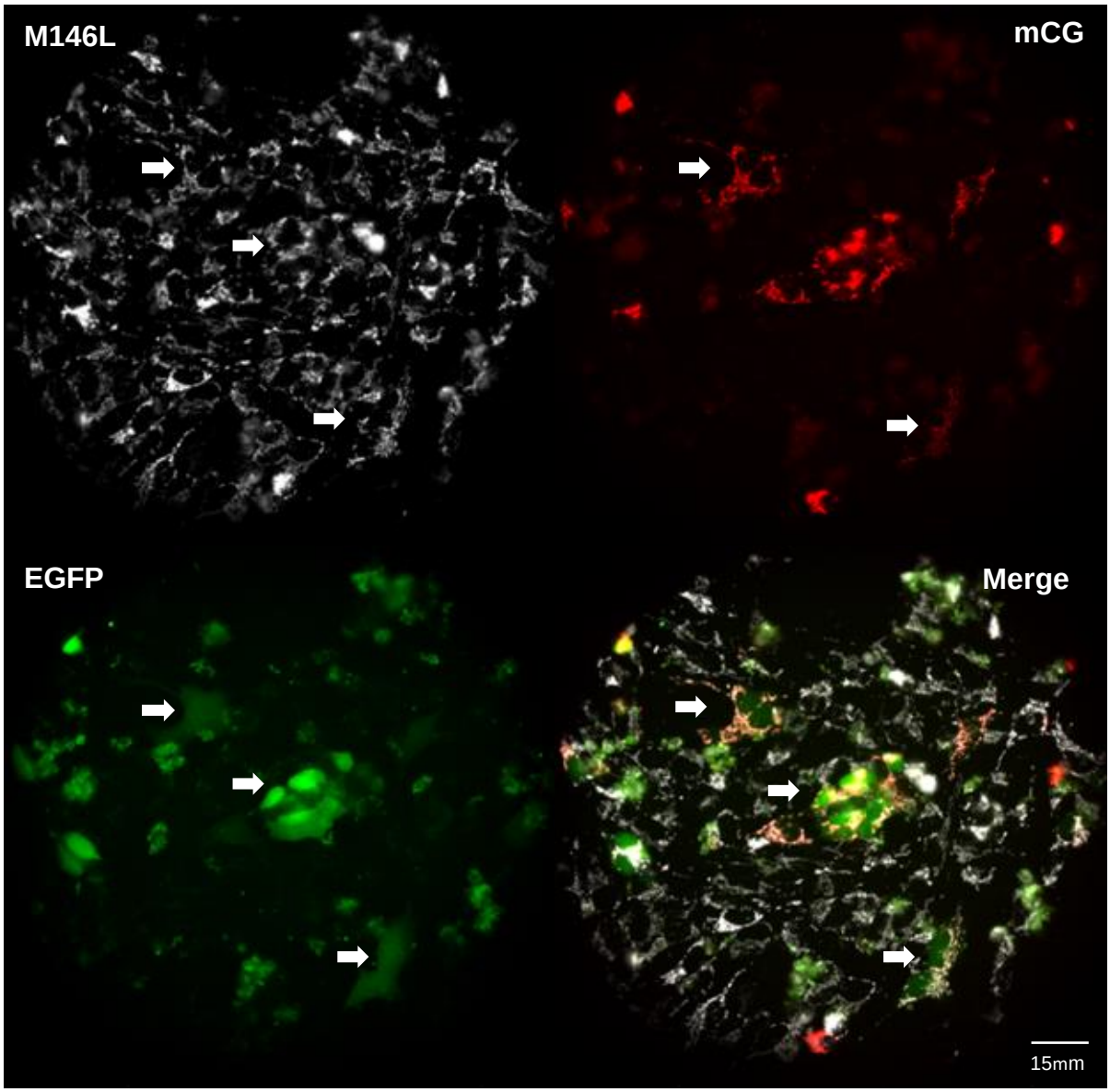

Figure 11: Representative imaging analysis of SH-SY5Y cells expressing mutant PS1-M146L. A) Cells loaded with deep red mitotracker (644/665 nm excitation/emission). **B)** positive PS1-M146L cells. **C)** EGFP expression from pIRES vector. **D)** Merge of three channels showing in yellow the co-localization of cells expressing mCG and EGFP and loaded with mitotracker (white arrows).

10.4.1 Measurement of $[Ca^{2+}]_m$ by imaging a FRET sensor.

To discard the possibility that mutant PS1-M146L expressing cells have brighter mCG signal due to higher transfection efficiency than control cells, we also tested a different mitochondrial Ca^{2+} sensor, the 4mtD3cpv second-generation chameleon. This sensor displays Ca^{2+} sensitivities tuned over a 100-fold range (0.6-160 μM), in which a Ca^{2+}-responsive element alters the efficiency of fluorescence resonance energy transfer (FRET) between the two fluorescent proteins, CFP and YFP and with a much larger dynamic range than the GECOs previously used and more sensitivity to small changes in mitochondrial Ca^{2+}. The absorption or emission spectrum is ratiometric, which changes with fluctuations in $[Ca^{2+}]$. This sensor was monitored by calculating the ratio of two different fluorescence emission intensities, termed the FRET ratio, which is the ratio of the acceptor (YFP) emission intensity to the donor (CFP) emission intensity (Park JG., Palmer AE, 2015).

Previously, we observed a consistent constitutive increase in $[Ca^{2+}]_c$ and $[Ca^{2+}]_m$ under stimulation with different agonists of ER Ca^{2+} release to levels that may be toxic in cells that expressed mutant PS1-M146L. The results with this FRET sensor recapitulated previous results, strongly confirming a significant higher $[Ca^{2+}]$ in the mitochondria, which was exacerbated under ER Ca^{2+} release in cells expressing the mutant PS1-M146L (Figure 12).

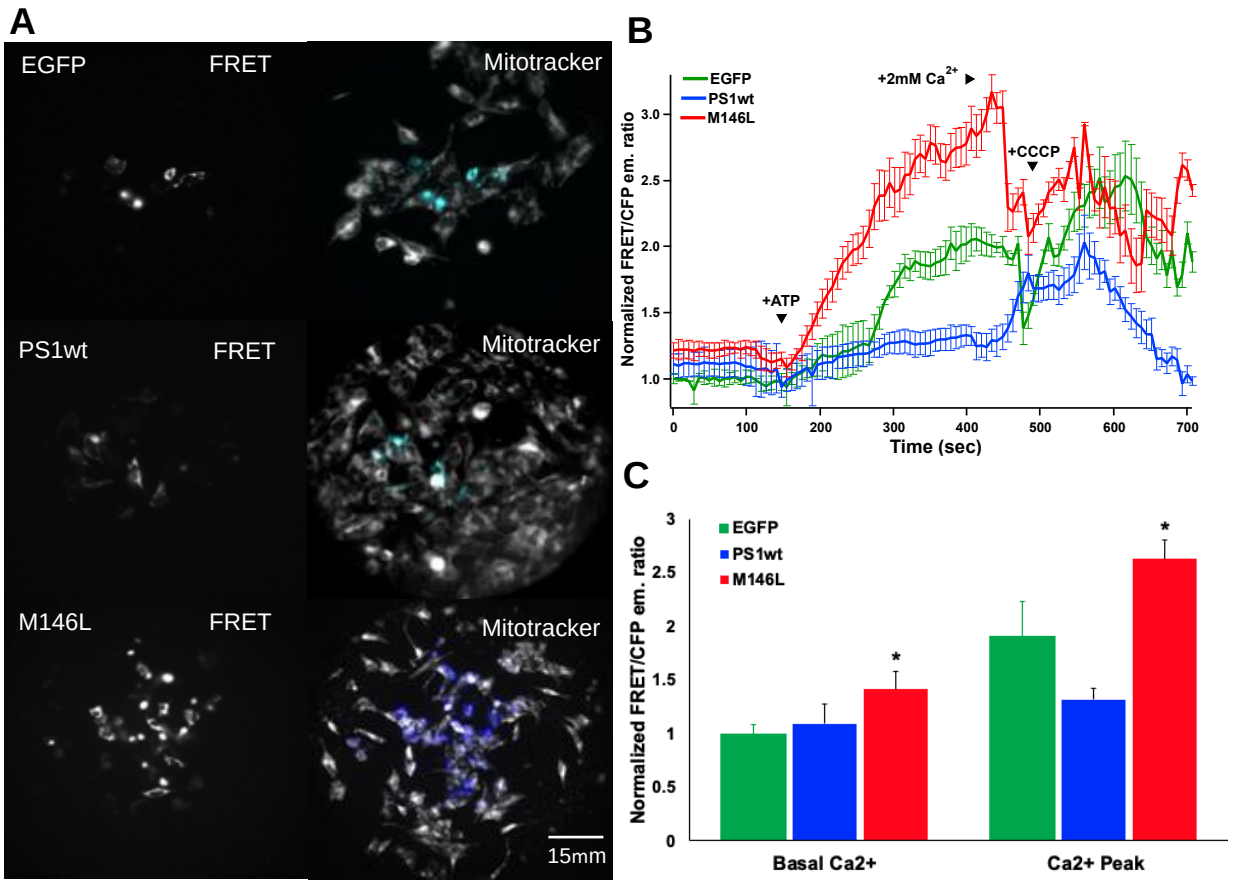

Figure 12: Comparison of basal $[Ca^{2+}]_m$ in SH-SY5Y cells transiently transfected with 4mtD3cpv (FRET sensor) and loaded with deep red mitotracker. **A)** Representative images of basal expressions in cells transiently transfected with 4mtD3cpv. Excitation of 4mtD3cpv was applied at 440 ± 10 nm, and emission was recorded at 480 and 535 nm. **B)** Average traces of normalized FRET emission ratio over time in each cell line perfused with 2 mM Tyrode´s solution and stimulated with ATP (10 µM), followed by CCCP addition (5 M). **C)** FRET emission ratio in basal conditions and after Tg stimulation. The data represent the means of 4 experiments from different cell preparations. Bars represent the average +/- SEM total mitochondrial Ca^{2+} relative content of 4 independent experiments. Significance was determined by one-way ANOVA with Dunnett's post-test using EGFP cells as control: *, $p < 0.05$.

10.5 Mitochondrial hypersensitivity to Ca^{2+} challenges in PS1-M146L cells is due to enhanced ER Ca^{2+} release.

Mitochondrial matrix Ca^{2+} content has a central role in metabolic regulation and cell death signaling. Ca^{2+} transfer to mitochondria must be finely regulated because excess Ca^{2+} will disturb OXPHOS, also increasing the generation of ROS that leads to cellular damage, a common feature in several neurodegenerative diseases, such as AD. In physiological conditions, transient opening of the mitochondrial transition pore (mPTP) can regulate Ca^{2+} levels in the mitochondrial matrix (Ichas, Jouaville et al. 1997). However, excess of Ca^{2+} levels and ROS generation in the mitochondria trigger a dysregulated opening of mPTP, causing the release of metabolites leading to loss of $\Delta\Psi_m$ and inhibition of OXPHOS among other effects (Rottenberg and Hoek 2017). To examine the effects of elevated matrix Ca^{2+} content on mPTP opening, we challenged permeabilized SH-SY5Y cells of each cell line with boluses of 2-3 µM Ca^{2+} (Figure 13). Cells were permeabilized in an intracellular-like medium lacking Ca^{2+} buffers (free $[Ca^{2+}]$ ~ 20 nM) and $[Ca^{2+}]_c$ and $\Delta\Psi_m$ were simultaneously measured using Fura-2 and TMRE, respectively. Tg was used to inhibit Ca^{2+} uptake into the ER, leading to a small increase in $[Ca^{2+}]_c$ that reached a steady state after ~300 sec. Later, CGP was added to inhibit NCLX-mediated mitochondrial Ca^{2+} extrusion. Under these conditions, MCU-mediated mitochondrial Ca^{2+} uptake plays the dominant role in determining $[Ca^{2+}]_c$. We applied several pulses of 2-3 µM $CaCl_2$ at ~500 sec causing a rapid rise in $[Ca^{2+}]_c$ followed by clearance of Ca^{2+} over 100-200 sec in all the cells analyzed. However, mutant PS1-M146L expressing cells exhibited greater sensitivity to successive Ca^{2+} challenges, causing a

dramatic loss of $\Delta\Psi_m$ after the third or fourth bolus of Ca^{2+} compared with control cells (Figure 13). Therefore, mPTP opening observed in cells expressing the mutant PS1-M146L emerges as a potential cause of mitochondrial dysfunction due to Ca^{2+} overload as a response of exaggerated Ca^{2+} release from the ER through the $InsP_3R$.

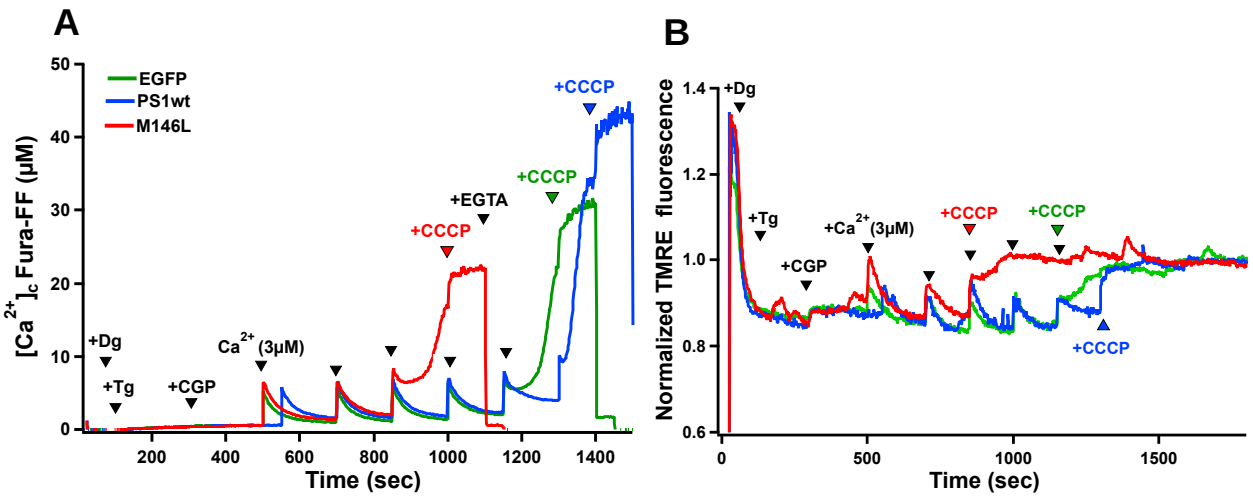

Figure 13: **Ca^{2+} uptake and efflux and $\Delta\Psi_m$ monitored in permeabilized SH-SY5Y cells monitored with Fura2-FF and TMRE, respectively and challenged with 3 μM Ca^{2+} boluses**. **A)** Representative traces of $[Ca^{2+}]_c$ and **B)** representative traces of normalized TMRE fluorescence intensity of the corresponding experiments. Cells were treated with 0.004% digitonin (Dg) to permeabilize plasma membrane, 2 μM thapsigargin (Tg) to block ER Ca^{2+} uptake, and 20 μM CGP37157 (CGP) to inhibit mitochondrial Ca^{2+} efflux, added at t=50, 100 and 300s, respectively as indicated. **B)** normalized for each trace.

Next, we measured differences in Tg-induced ER Ca^{2+} leak to compare and evaluate if the higher content of Ca^{2+} found in the mitochondria in mutant PS1-M146L cells could be a consequence of enhanced leak from the ER. As shown in Figure 14A, Tg addition revealed a more active ER Ca^{2+} leak in cells expressing mutant PS1-M146L compared with control PS1wt and EGFP cells. These results complement previous

observations that PS1-M146L causes an exaggerated Ca^{2+} release from the ER under basal conditions due to an increase in $InsP_3R$ activity (Cheung KH 2008) (Cheung, Mei et al. 2010). An increase of Ca^{2+} leak from the ER through sensitization of the $InsP_3R$ Ca^{2+} channel by direct interaction with FAD-linked PS mutants could be responsible for the sustained and progressive high levels of intracellular Ca^{2+} in cells expressing the mutant PS1-M146L. In the absence of Tg stimulation, as expected, no enhanced ER Ca^{2+} leak was observed in PS1-M146L cells (Figure 14C), having a Ca^{2+} signal dynamic similar to control cells in the absence of Tg (Figure 14E). In addition, the absence or presence of Tg did not affect the $\Delta\Psi_m$ in either of the cell lines studied (Figure 14 B&D&F).

Then we tested whether the absence of ER Ca^{2+} leak reduced the hypersensitivity of PS1-M146L cells to mPTP opening when challenged with successive boluses of Ca^{2+} (Figure 15). We repeated the experiment in the presence or absence of Tg. We found a slight improvement to Ca^{2+} challenge in the absence of Tg in PS1-M146L cells, indirectly suggesting a contribution of the ER Ca^{2+} leak to the mPTP opening stimulation and in consequence increased vulnerability of these cells. No significant differences were observed in control cells in the presence or absence or Tg, indicating that Ca^{2+} leak from the ER is not related to sensitivity to Ca^{2+} challenges.

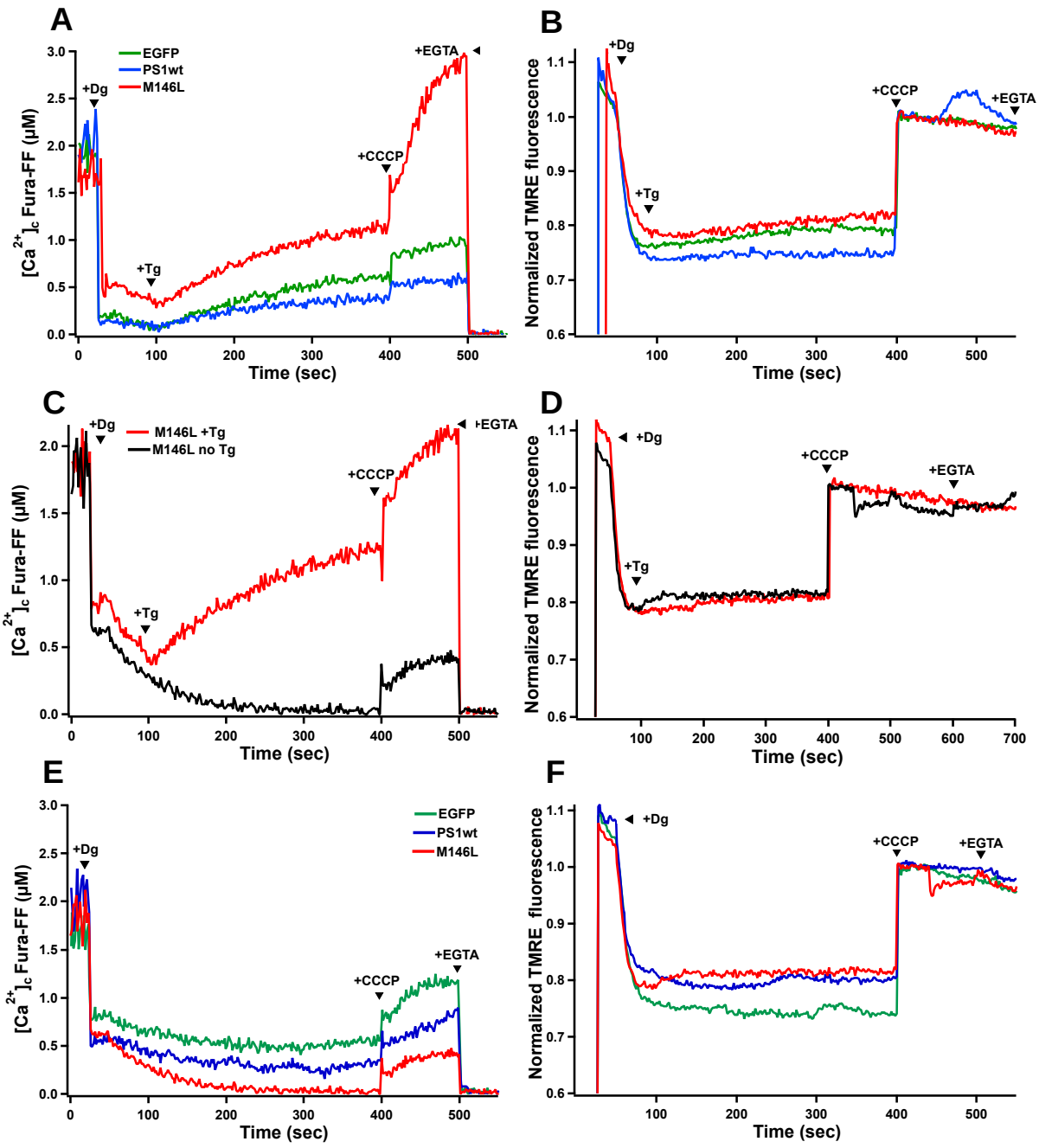

Figure 14: Elevated Ca^{2+} leak from the ER in PS1-M146L cells. **A)** Representative traces from 3 independent experiments of elevated Ca^{2+} leak from the ER after Tg addition in permeabilized cells expressing PS1-M146L and **B)** simultaneous $\Delta\Psi_m$ detection with TMRE. **C)** Representative traces of bath $[Ca^{2+}]$ in mutant PS1-M146L cells in the presence or absence of Tg and **D)** the TMRE analysis. **E)** Comparative graph of representative traces of each cell type in absence of Tg and **F)** normalized TMRE fluorescence intensity.

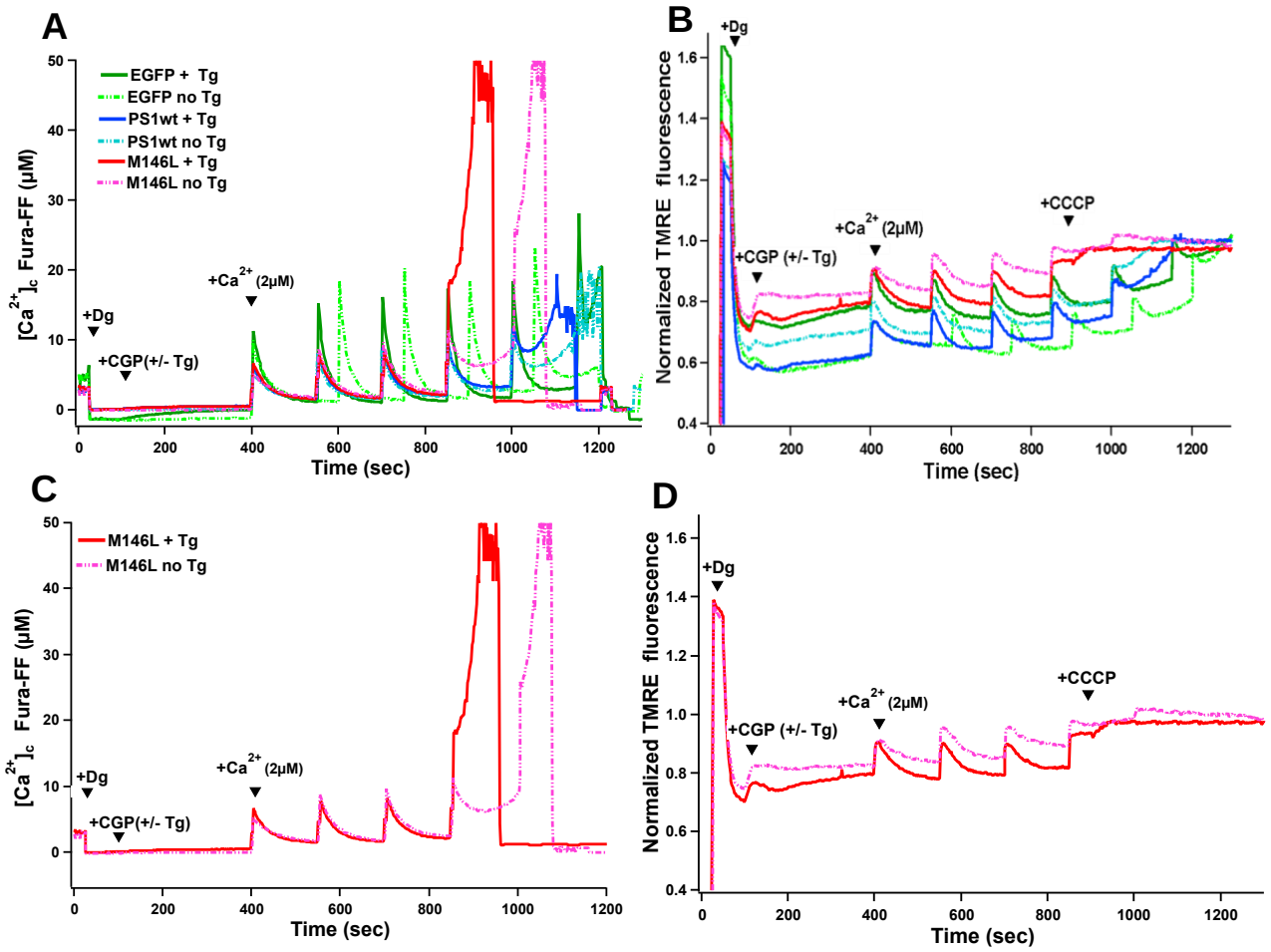

Figure 15: Ca^{2+} uptake and efflux and $\Delta\Psi_m$ monitored in permeabilized SH-SY5Y cells in the presence or absence of Tg. A) Representative traces of Ca^{2+} uptake and efflux and $\Delta\Psi_m$ monitored in permeabilized SH-SY5Y cells with FuraFF and TMRE, respectively, and challenged with 2 μM Ca^{2+} boluses in the presence or absence of Tg in each cell line. **B)** Representative traces of normalized TMRE fluorescence of each cell line analyzed in **A)** at different experimental conditions. **C)** and **D)** are traces just from the PS1-M146L cells to better visualize the differences in the presence or absence of Tg.

To confirm these results and explore more deeply the contribution of the ER Ca^{2+} leak on mitochondrial Ca^{2+} dynamics, we treated intact cells with BK to induce physiological $InsP_3R$-mediated Ca^{2+} release from the ER, and with Tg to trigger ER

Ca^{2+} leak (Figure 16). Briefly, the cells were loaded with the ratiometric cytoplasmic Ca^{2+} indicator Fura-2 and with Rhod-2 as a fluorescent mitochondrial Ca^{2+} indicator. As seen previously, PS1-M146L expressing cells showed a significantly higher level of basal $[Ca^{2+}]_c$ compared with control cells, and also higher leak from the ER after Tg stimulation (Figure 16A). However, the size of the $[Ca^{2+}]_m$ response to BK stimulation in the mutant PS1-M146L cells was lower than control cells (Figure 16B). These results consistently show that PS1-M146L cells present an increase in both cytoplasmic and mitochondrial Ca^{2+} levels, due to enhanced ER Ca^{2+} leak and Ca^{2+} release through the $InsP_3R$ resulting in exposure of mitochondria to elevated $[Ca^{2+}]_c$. On the other hand, it is possible that dysfunction in Ca^{2+} extrusion from mitochondria contributes to the elevated $[Ca^{2+}]_m$.

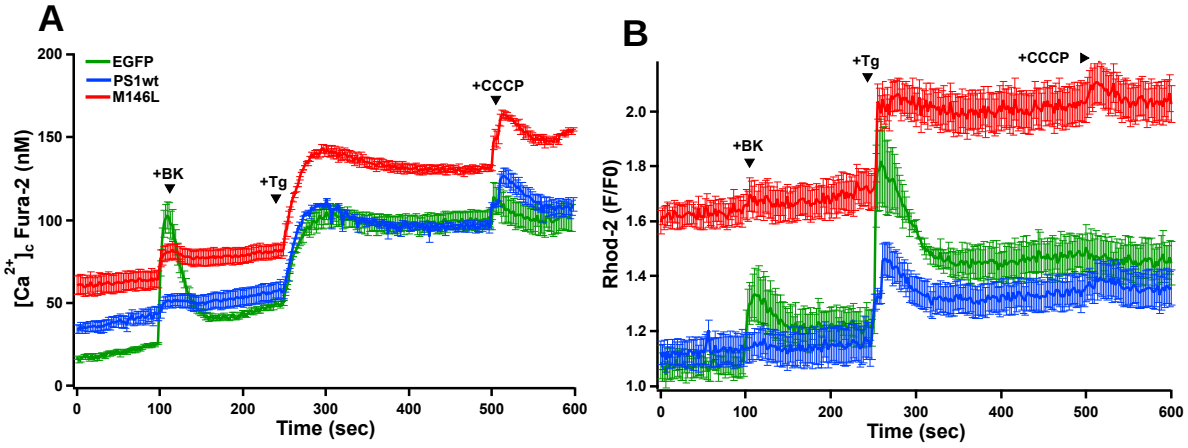

Figure 16: Increased mitochondrial $[Ca^{2+}]$ in mutant PS1-M146L expressing cells. A) Average traces of normalized Ca^{2+} influx and efflux on intact SH-SY5Y cells loaded with Fura-2 (**A**) and Rhod-2 (**B**). Cells were incubated in 2mM Ca^{2+} Tyrode's solution and then stimulated with BK. After Ca^{2+} transient cause by BK, cells were challenged with 2 μM Tg followed by CCCP. Data represent the means of three experiments from different cell preparations. Bars represent the average +/- SEM of 3 independent experiments.

10.6 Impaired mitochondrial Ca^{2+} efflux in PS1-M146L mutant cells.

Mitochondria extrude Ca^{2+} primarily through the Na^{+}/Ca^{2+} exchanger (NCLX). The ability of mitochondria to release Ca^{2+} is an important function and since the balance of Ca^{2+} entry and release is responsible for maintenance of mitochondrial Ca^{2+} homeostasis under normal and pathological conditions. In addition, the rate of Ca^{2+} transport through NCLX is significantly slower than the rate of Ca^{2+} uptake through MCU (Belosludtsev, Dubinin et al. 2019). The Na^{+}/Ca^{2+} exchanger is believed to be electrogenic with the stoichiometry of $3Na^{+}:1Ca^{2+}$. In many neurodegenerative disorders, mitochondrial Ca^{2+} is impaired, often leading to the toxic accumulation of mitochondrial free Ca^{2+}, previously called, mitochondrial Ca^{2+} overload. This mitochondrial Ca^{2+} overload is induced by imbalance between mitochondrial Ca^{2+} uptake and removal and often leads to mitochondrial opening of the mPTP and initiation of apoptosis (Ian Sekler, 2019).

We examined the expression of NCLX in stable SH-SY5Y cells. NCLX expression was lower in the PS1-M146L expressing cells compared to the control or PS1wt -expressing cells (Figure 17). To determine the contribution of NCLX to the mitochondrial Ca^{2+} overload and increased vulnerability to mPTP opening observed in mutant PS1-M146L expressing cells, we performed the mitochondrial Ca^{2+} uptake assay on permeabilized SH-SY5Y cells as above. As seen in Figure 18A-B, addition of CGP reduces the steady-state $[Ca^{2+}]_c$ ~300 sec after bolus Ca^{2+} addition in control cells while cells expressing the mutant PS1-M146L showed no differences in the presence or absence of CGP (Figure 18C). We observed these differences with more detail calculating the final change in $[Ca^{2+}]_c$ after the addition of Ca^{2+} in the presence or

absence of CGP. This final change was significantly different just in control cells, suggesting an effective inhibition of NCLX and the consequent decrease in $[Ca^{2+}]_c$ (Figure 18F). The transient matrix Ca^{2+} elevations have several effects on mitochondrial function and their final effects are dependent on a wide range of factors, one of them the mitochondrial Ca^{2+} efflux. The findings observed in PS1-M146L expressing cells showing no differences in $[Ca^{2+}]_c$ in the presence or absence of NCLX inhibitors revealed the importance of the significant decrease in NCLX expression and activity found.

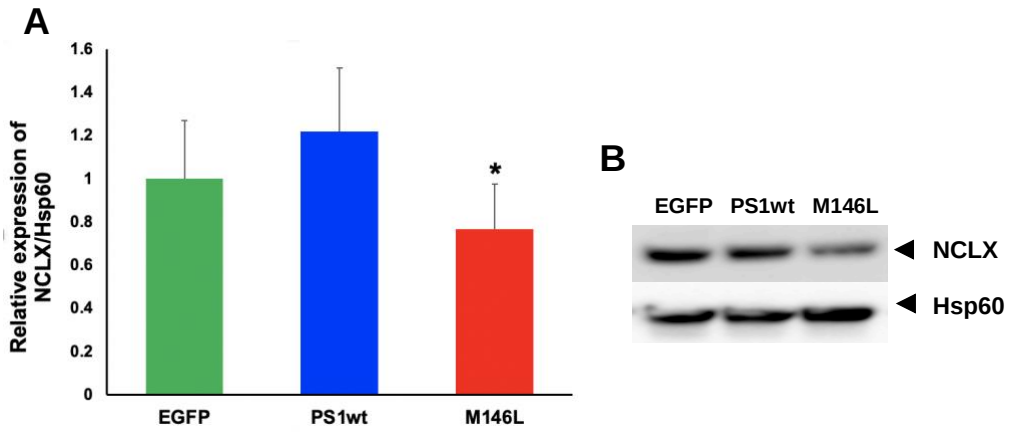

Figure 17: Decreased expression of NCLX in mutant PS1-M146L cells. Densitometric analysis (**A)** and **(B)** representative immuno-blot of NCLX expression normalized with the loading mitochondrial control Hsp60 protein, in SH-SY5Y cells stably transfected with EGFP only, PS1wt or mutant PS1-M146L. The data represent the means of 4 experiments from different cell preparations. Bars represent the average +/- SEM relative expression of NCLX from 4 independent experiments. Significance was determined by one-way ANOVA with Dunnett's post-test using EGFP cells as control: *, $p < 0.05$.

To examine more directly the role of NCLX on the Ca^{2+}-extrusion capacity of mitochondria in cells expressing mutant PS1-M146L, we measured mitochondrial Ca^{2+}

uptake in permeabilized SH-SY5Y cells in the presence or absence of CGP. CGP addition revealed constitutive MCU-mediated Ca^{2+} uptake in mutant PS1-M146L cells but no uptake in control cells (Figure 19A, red trace), which could possibly be attributed to the elevated $[Ca^{2+}]_c$ (~1 µM) in PS1-M146L cells relative to control cells (0.6-0.8 µM) at the time CGP was added. Nevertheless, the total amount of Ca^{2+} released from the mitochondria after CCCP addition was similar across all cell lines (Figure 19). The most significant difference was observed in $[Ca^{2+}]_m$ in mutant cells in the presence of CGP, which was higher relative to control cells, and even higher after CCCP addition. We also performed experiments in the presence of either low (1 mM) or high (10 mM) bath $[Na^+]$. Under low-$[Na^+]$ conditions, all cells show an increase in the steady-state $[Ca^{2+}]_c$ after uptake, although this may be due to a reduction in $\Delta\Psi_m$. However, the Ca^{2+} release from the mitochondria in the mutant PS1-M146L cells after CCCP addition was still higher in both conditions compared with control cells (Figure 20).

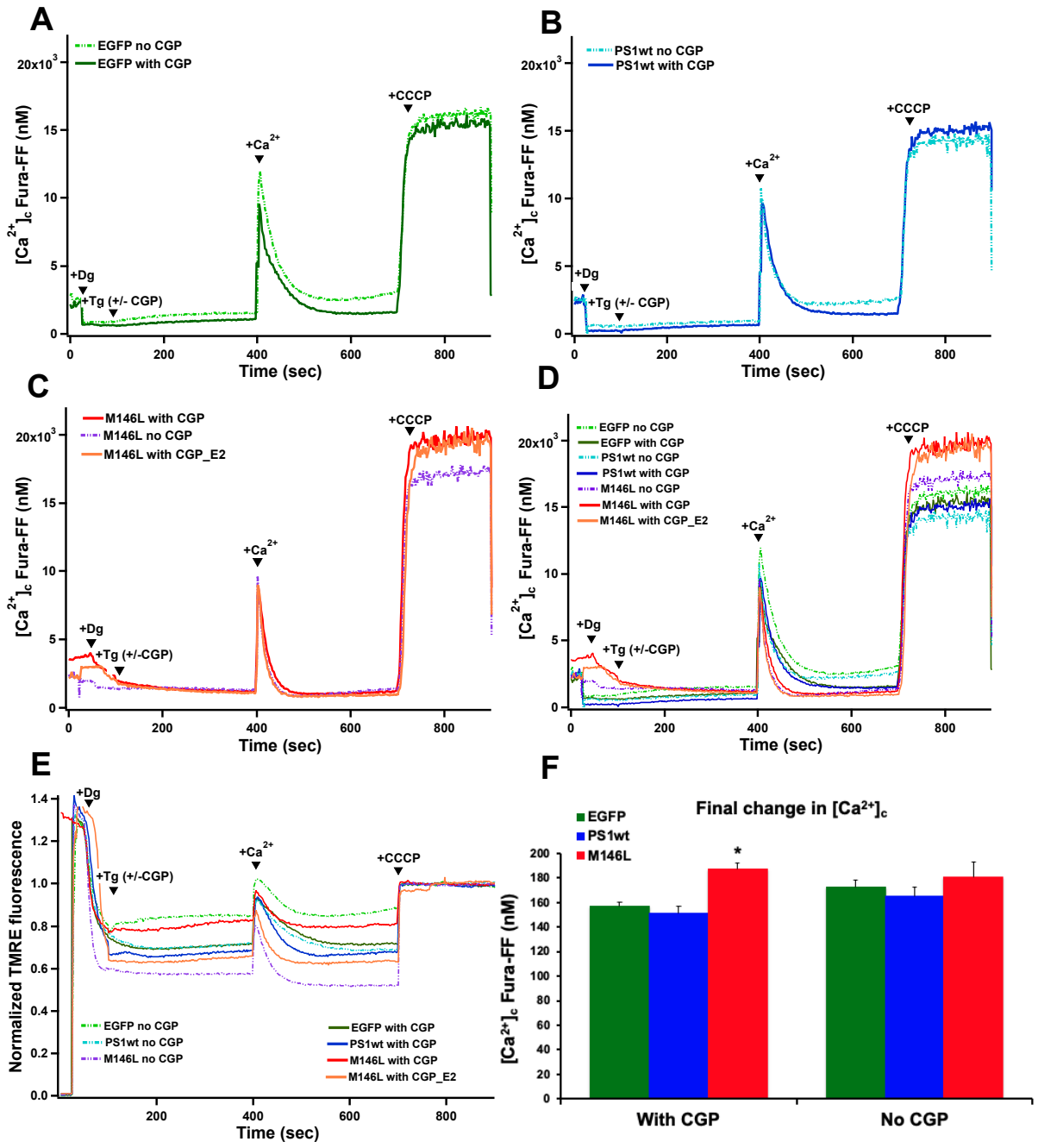

Figure 18: Ca^{2+} uptake and $\Delta\Psi_m$ monitored in permeabilized SH-SY5Y cells with Fura2-FF and TMRE, respectively, and challenged with 2 µM Tg in the presence or absence of CGP. **A)** and **B)** are representative traces of $[Ca^{2+}]_c$ in control cells expressing EGFP or PS1wt respectively. **C)** Representative traces in mutant PS1-M146L cells. **D)** Graph with all cell lines analyzed to compare among the different conditions evaluated. **E)** Representative traces of TMRE fluorescence of the corresponding experiments (n=3). **F)** Summary of the final change in $[Ca^{2+}]_c$, after CCCP addition. The data represent the means of 4 experiments from different cell preparations. Bars represent the average +/- SEM of final change in $[Ca^{2+}]_c$ of 4 independent experiments. Significance was determined by one-way ANOVA with Dunnett's post-test using EGFP cells as control: *, $p < 0.05$.

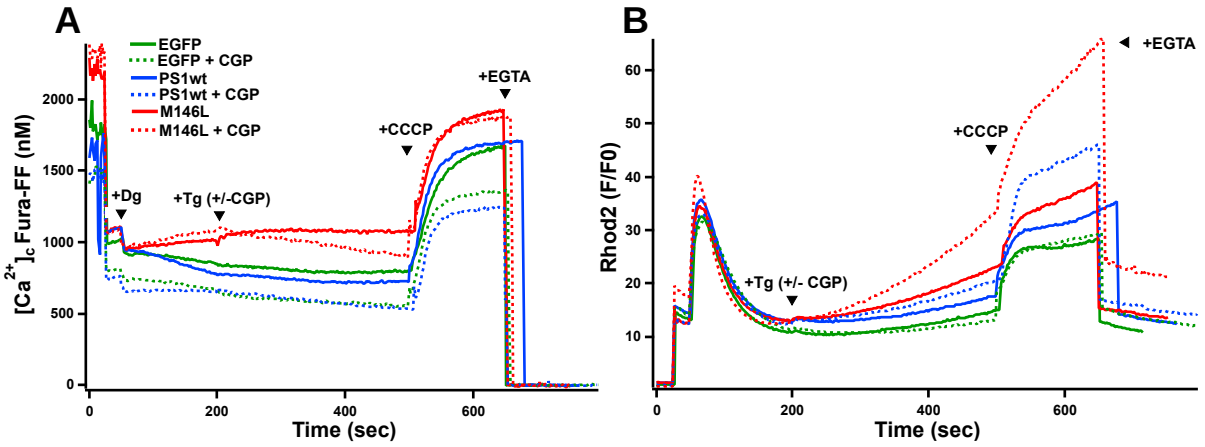

Figure 19: Cytoplasmic and mitochondrial Ca^{2+} uptake and efflux in permeabilized SH-SY5Y cells with Tg in the presence or absence of CGP. A) Representative traces of cytoplasmic and mitochondrial Ca^{2+} in permeabilized SH-SY5Y cells stably expressing EGFP only, PS1wt or PS1-M146L with Fura-2-FF and Rhod-2. Cells were challenged at 200 sec with Tg to induce ER Ca^{2+} leak in the presence or absence of NCLX inhibitor CGP. At 500 sec CCCP was added to cause a dissipation of $\Delta\Psi_m$ and release a^{2+} accumulated in the mitochondria. $[Ca^{2+}]_c$ was calibrated upon addition of ionomycin and EGTA to obtain the F_{max} and F_{min} respectively. **B)** Rhod-2 corresponding traces of mitochondrial Ca^{2+} (n=3).

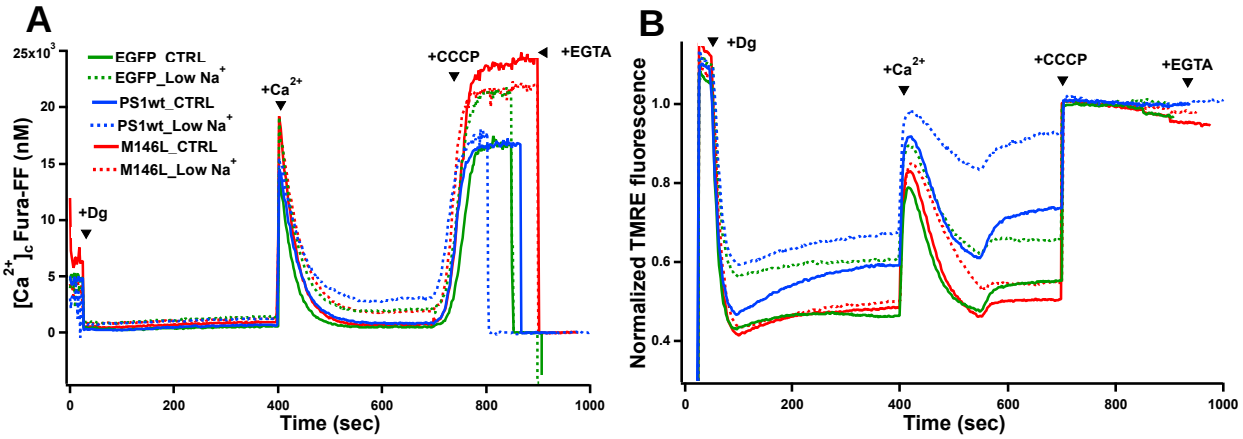

Figure 20: Effect of low $[Na^+]$ on mitochondrial Ca^{2+} uptake in permeabilized SH-SY5Y cells stably overexpressing either EGFP, PS1wt or mutant PS1-M146L. A) Mitochondrial Ca^{2+} uptake in permeabilized SH-SY5Y cells stably overexpressing either only EGFP, PS1wt or mutant PS1-M146L. Cells were treated with 0.004% digitonin (Dg) to permeabilize plasma membrane, 2 µM thapsigargin (Tg) to block ER Ca^{2+} uptake, and with normal or low Na^+ levels (10 mM or 1 mM) to explore NCLX activity. **B)** Representative traces of normalized TMRE fluorescence of each cell line analyzed in A) n=2 independent experiments.

10.7 Inhibition of ER Ca^{2+} leak protects mutant PS1-M146L cells from mitochondrial Ca^{2+} overload.

Next, we tested if preventing Tg-induced net ER Ca^{2+} leak in the presence or absence of NCLX activity would protect the mutant PS1-M146L-expressing cells from mPTP opening in response to successive Ca^{2+} boluses. Using the same experimental settings described previously for permeabilized-cell assays, addition of 3 μM free Ca^{2+} again led to a transient uptake of Ca^{2+} by mitochondria, followed by complete loss of $\Delta\Psi_m$ in mutant PS1-M146L expressing cells. Addition of Tg alone or Tg and CGP (Figure 21) increased the sensitivity to Ca^{2+}-induced depolarization. Remarkably, in the absence of both Tg and CGP, mutant cells were able to resist more than three boluses of 3 μM free Ca^{2+}, improving considerably the Ca^{2+} uptake capacity.

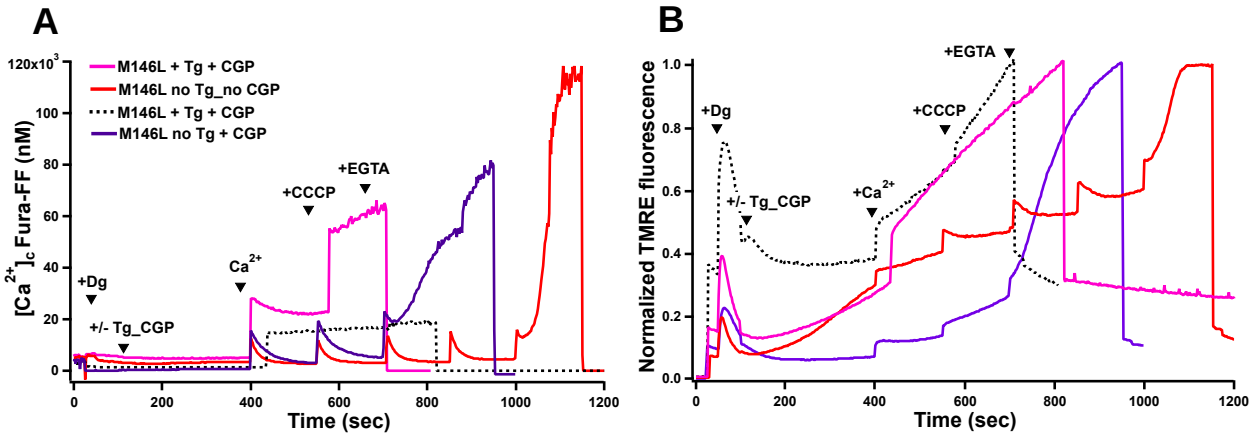

Figure 21: Effects of Tg and CGP on Ca^{2+} uptake/buffering capacity and $\Delta\Psi_m$ in permeabilized mutant PS1-M146L cells. Ca^{2+} uptake and efflux and $\Delta\Psi_m$ monitored in permeabilized SH-SY5Y cells challenged with 3 μM Ca^{2+} boluses in the presence or absence of Tg and CGP. **A** and **B** are representative traces of $[Ca^{2+}]_c$ signals and TMRE fluorescence respectively (n=3).

Mitochondrial sense and shape Ca^{2+} signals during cell stimulation via their ability to take up and subsequently release Ca^{2+} ions. This Ca^{2+} sequestration in the mitochondrial matrix contributes to the buffering of cytosolic Ca^{2+} elevations and serves as a signal that activates mitochondrial Ca^{2+} dependent processes (Glancy and Balaban 2012). Our results indicate that a prolonged accumulation of Ca^{2+} that can potentially trigger mPTP activation. Partial mPTP opening is often insufficient to trigger cell death and requires an additional "death" signal, constituting so-called two-hit mechanism of mPTP opening (Reynolds 1999). One other possible important "hit" is the levels of reactive oxygen species (ROS) in the mutant PS1-M146L expressing cells. Previously, we showed an enhanced generation of ROS as a result of an exaggerated Ca^{2+} signaling caused by PS1-M146L in DT40 and PC12 cells (Muller, Cheung et al. 2011).

However, whether expression of the PS1-M146L mutant enhances ROS production in SH-SY5Y cells has not been explored. To test this, cells were simultaneously loaded with MitoSOX, a red mitochondrial superoxide indicator, and Fura-2, in order to monitor cytoplasmic Ca^{2+} dynamics and ROS production in a high-speed spectrofluorometer. Briefly, cells were permeabilized in an intracellular-like medium lacking Ca^{2+} buffers (free $[Ca^{2+}] \sim 20$ nM using the low affinity ratiometric indicator Fura-2 to measure $[Ca^{2+}]_c$ (Figure 22B) and MitoSOX to simultaneously monitor ROS production (Figure 22A). Under these conditions, cells expressing mutant PS1-M146L showed a slight increase in basal ROS production, which was enhanced significantly after BK addition and later CCCP addition, compared to control cells.

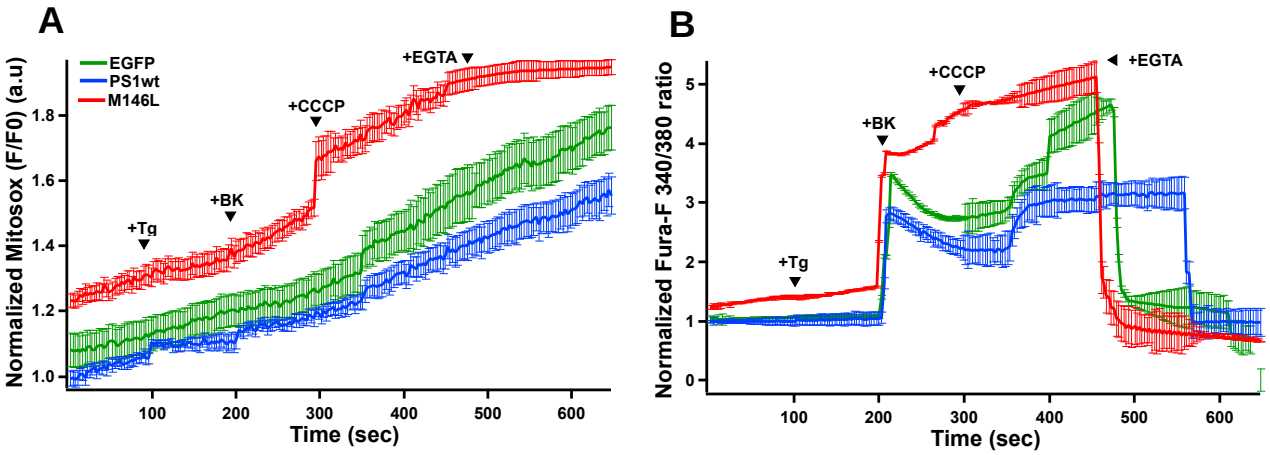

Figure 22: ROS and [Ca^{2+}] determinations in permeabilized SH-SY5Y cells. **A)** Average traces of normalized MitoSOX fluorescence. Cells were loaded with 5 μM MitoSOX red mitochondrial superoxide indicator and Fura-2-FF was used to measure bath [Ca^{2+}]. At 100 sec Tg was added and at 200 sec cells were stimulated with BK and ~100 sec later with CCCP. **B)** Average traces of normalized Fura-FF 340/380 ratio. The data represent the means of three experiments from different cell preparations. Bars represent the average +/- SEM of 3 independent experiments.

In addition, we similarly determined ROS levels in intact SH-SY5Y cells. Under these experimental settings, the fluorescence signal obtained was very low and noisy. We were unable to detect any changes in the presence of Tg, BK or CCCP and the results only suggest a slightly higher fluorescence signal in cells expressing PS1-M146L compared with control cells (Figure 23A). On the other hand, the data obtained to determine the relative intracellular Ca^{2+} levels with Fura-2, showed an increased basal signal in PS1-M146L expressing cells and a response to Tg, BK and CCCP (Figure 23 B). Nevertheless, we were unable to have conclusions for the lack of more experiments in this experimental setting.

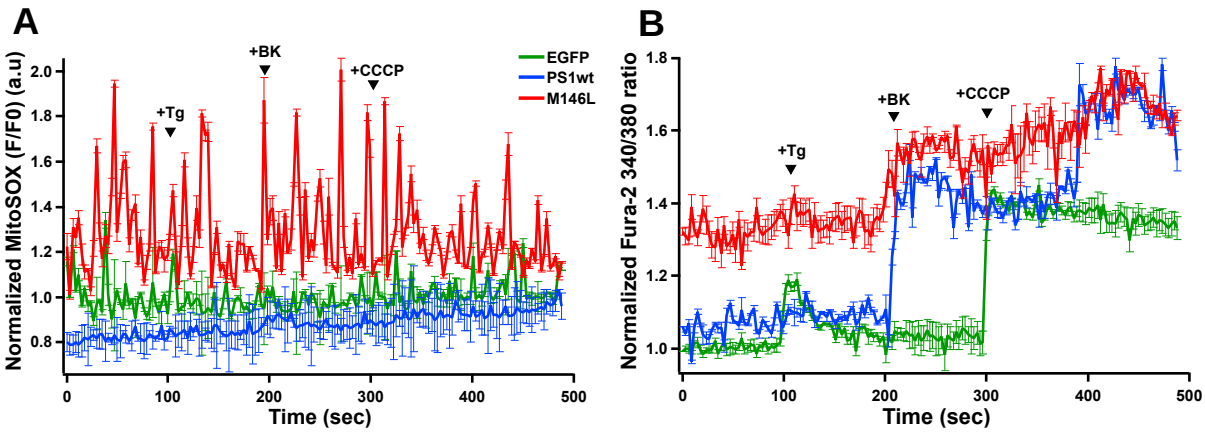

Figure 23: ROS and Ca^{2+} in intact SH-SY5Y cells. **A)** Average traces of normalized MitoSox fluorescence. Cells were loaded with 5 µM MitoSOX red mitochondrial superoxide indicator and Fura-2. At 100 sec Tg was added and at 200 sec the cells were stimulated with BK and ~100 sec later with CCCP. **B)** Average traces of normalized Fura-2 340/380 ratio determination. The data represent the means of three experiments from different cell preparations. Bars represent the average +/- SEM of 2 independent experiments.

10.8 Mitochondrial Ca^{2+} uptake in FAD patient's fibroblasts

Mitochondrial Ca^{2+} extrusion is equally critical as the Ca^{2+} uptake in order to achieve mitochondrial Ca^{2+} dependent signaling functions without triggering cell death. The above experiments demonstrate that mutations in PS1 cause no differences in MCU-mediated Ca^{2+} uptake between the cell lines analyzed, indicating that MCU activity is unaffected. However, we found that mutations in PS1 cause mitochondrial Ca^{2+} overload associated with reduced NCLX expression, which was correlated with increased the susceptibility to mPTP opening. The results also recapitulated previous observations that the expression of mutant PS1-M146L led to increased Ca^{2+} release from the ER through $InsP_3R$ under resting conditions or upon BK stimulation.

To complement our study of the role of mutant PS1-M146L in the neuronal cell line SH-SY5Y, we explored the role of mutant PS1 expression in human patient

fibroblasts. These cells present technical advantages for the study of mitochondrial-induced toxicity, because they were isolated from patients by minimally-invasive methods and present specific cumulative cellular damage due to mutations in PS1 or PS2. Human skin fibroblasts were purchased from Coriell Institute (Table 1, Materials and Methods) and cultured with EMEM with Earle's salts and 15% FBS, following provider instructions. We first investigated the impact of the mutant PS1 on mitochondrial Ca^{2+} uptake in fibroblast lines derived from human FAD patients (A246E PS1 mutation) and normal individuals. Mitochondrial Ca^{2+} uptake determinations were performed using $4x10^6$ fibroblasts suspended in ICM and permeabilized with Dg, and $[Ca^{2+}]_c$ and $\Delta\Psi_m$ were monitored simultaneously. The PSI-A246E fibroblasts showed a higher initial $[Ca^{2+}]_c$ compared with control fibroblasts, recapitulating the same phenotype observed in SH-SY5Y cells expressing the PS1 mutant (Figure 24A). The addition of Tg induced a Ca^{2+} leak from the ER in both cell lines, which was greater in A246E cells.

Next, CGP was added to inhibit NCLX, which caused a small depolarization but no significant mitochondrial Ca^{2+} uptake in control cells. On the other hand, the addition of CGP in PS1-A246E fibroblasts caused a complete loss of $\Delta\Psi_m$ (Figure 24B). In control cells, Ca^{2+} uptake was observed after addition of 1 μM free Ca^{2+}, further depolarizing the mitochondria. Subsequent addition of 3 μM free Ca^{2+} led to a transient uptake of Ca^{2+} by mitochondria, followed by complete loss of $\Delta\Psi_m$. In A246E cells, no uptake was observed after addition of 1 μM or 3 μM free Ca^{2+} due to the loss of $\Delta\Psi_m$, but 4 μM additional Ca^{2+} was released from mitochondria after addition of CCCP relative to control cells (Figure 24).

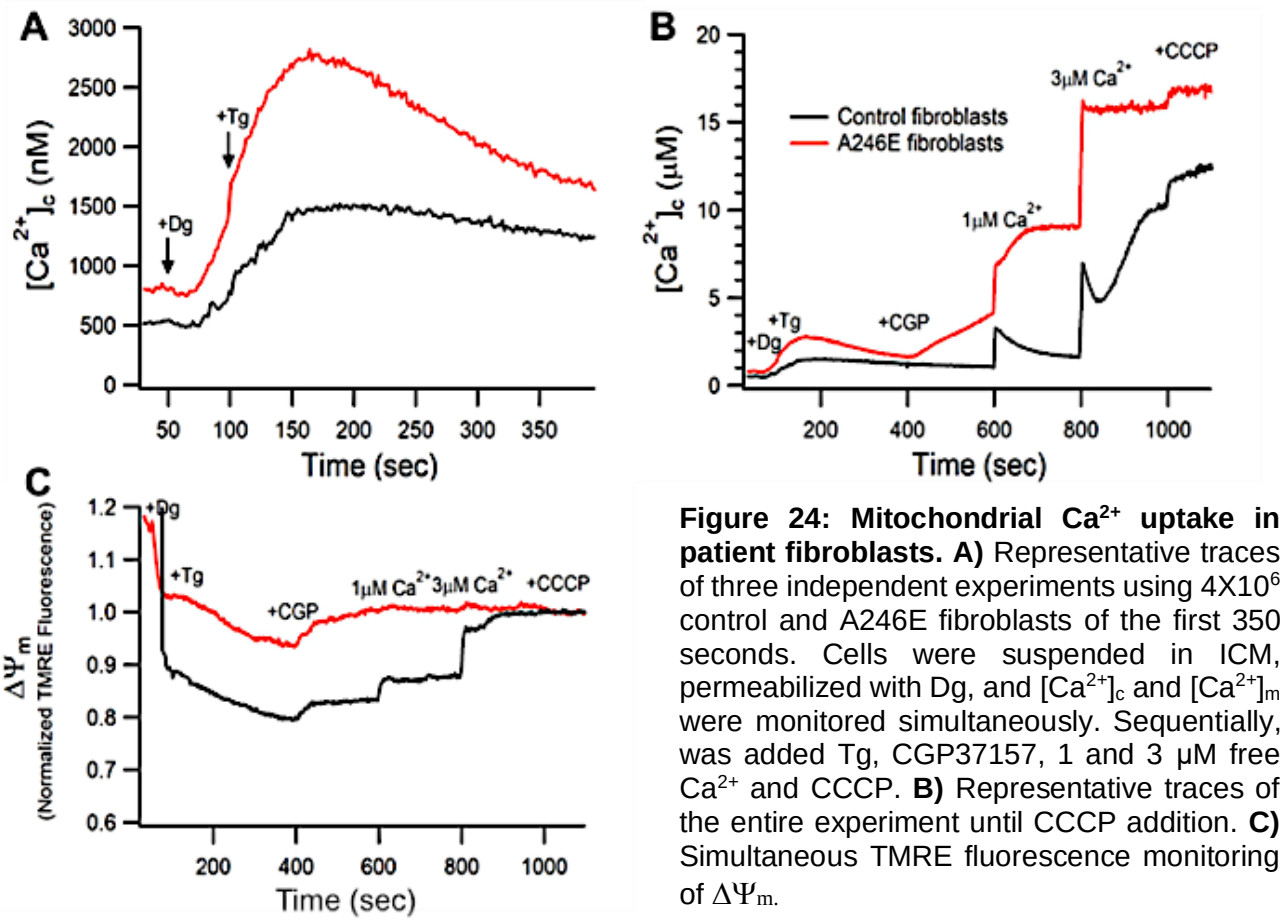

Figure 24: Mitochondrial Ca^{2+} uptake in patient fibroblasts. A) Representative traces of three independent experiments using $4X10^6$ control and A246E fibroblasts of the first 350 seconds. Cells were suspended in ICM, permeabilized with Dg, and $[Ca^{2+}]_c$ and $[Ca^{2+}]_m$ were monitored simultaneously. Sequentially, was added Tg, CGP37157, 1 and 3 μM free Ca^{2+} and CCCP. **B)** Representative traces of the entire experiment until CCCP addition. **C)** Simultaneous TMRE fluorescence monitoring of $\Delta\Psi_m$.

Control and PS1-A246E fibroblasts were incubated in ECM (Extracellular-like medium) with 0.1 mM EGTA for 30-40 minutes prior to being suspended in ICM to deplete intracellular Ca^{2+}stores. This pre-incubation in 0-Ca^{2+} reduced the initial $[Ca^{2+}]_c$ in both cell lines and greatly improved $\Delta\Psi_m$ in A246E cells (Figure 25A and B). Under these conditions, 3 μM free Ca^{2+} again led to a transient uptake of Ca^{2+} by mitochondria in control cells, followed by complete loss of $\Delta\Psi_m$ (Figure 25C). On the other hand, PS1-A246E cells showed enhanced Ca^{2+} uptake/buffering and $\Delta\Psi_m$ relative to control

cells, suggesting that A246E cells have developed mechanisms to protect mitochondria from constitutively elevated $[Ca^{2+}]_c$.

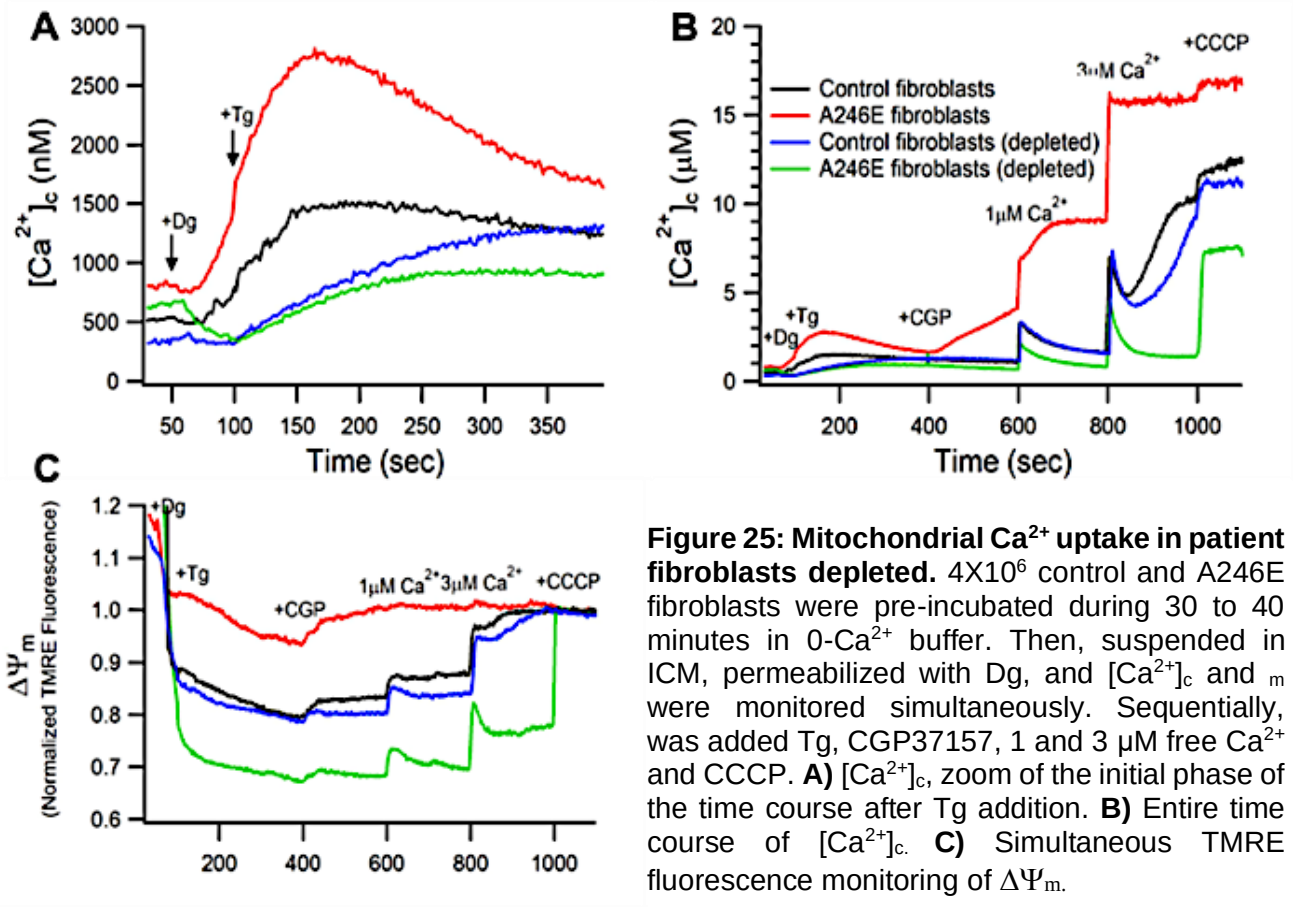

Figure 25: Mitochondrial Ca^{2+} uptake in patient fibroblasts depleted. $4X10^6$ control and A246E fibroblasts were pre-incubated during 30 to 40 minutes in 0-Ca^{2+} buffer. Then, suspended in ICM, permeabilized with Dg, and $[Ca^{2+}]_c$ and $_m$ were monitored simultaneously. Sequentially, was added Tg, CGP37157, 1 and 3 µM free Ca^{2+} and CCCP. **A)** $[Ca^{2+}]_c$, zoom of the initial phase of the time course after Tg addition. **B)** Entire time course of $[Ca^{2+}]_c$. **C)** Simultaneous TMRE fluorescence monitoring of $\Delta\Psi_m$.

10.9 Cytoplasmic and mitochondrial Ca^{2+} in human skin fibroblasts.

We assessed mitochondrial Ca^{2+} uptake in these cells by imaging a genetically-encoded mitochondrial Ca^{2+} sensors while simultaneously measuring [Ca^{2+}] with Fura-2. A disadvantage of working with human fibroblasts was the very slow proliferation rate in culture. Thus, our first approach was to transiently transfect mCG1 using Effectene transfection reagent (Qiagen), special for primary cells due to its low cytotoxicity. Cells were grown in 10-cm tissue-culture dishes and were imaged using an epifluorescence microscope with a 20x objective at RT. Fluorescence images of mCG1 (560-nm excitation/600-750-nm emission) were collected.

The first set of patient fibroblasts analyzed included AG06840 (FAD), AG07559 (control) and AG08243 (SAD). The fibroblasts from the both the SAD patient and FAD patients showed higher basal mCG1 fluorescence compared to control fibroblasts (Figure 26). However, in another set of patient's fibroblasts, control cells (AG07621) showed similar fluorescence intensity compared with FAD patients (AG08711 and A246E) (Figure 27). Finally, in the third set of patient's fibroblasts analyzed, FAD patient AG06848 showed a significant increase in mCG1 fluorescence intensity compared with control cells (AG08179) and with SAD patient (AG07374) (Figure 28). Although we observed a very high variability among the different patients studied, there was a tendency found in high basal mitochondrial Ca^{2+} in fibroblasts from FAD patients.

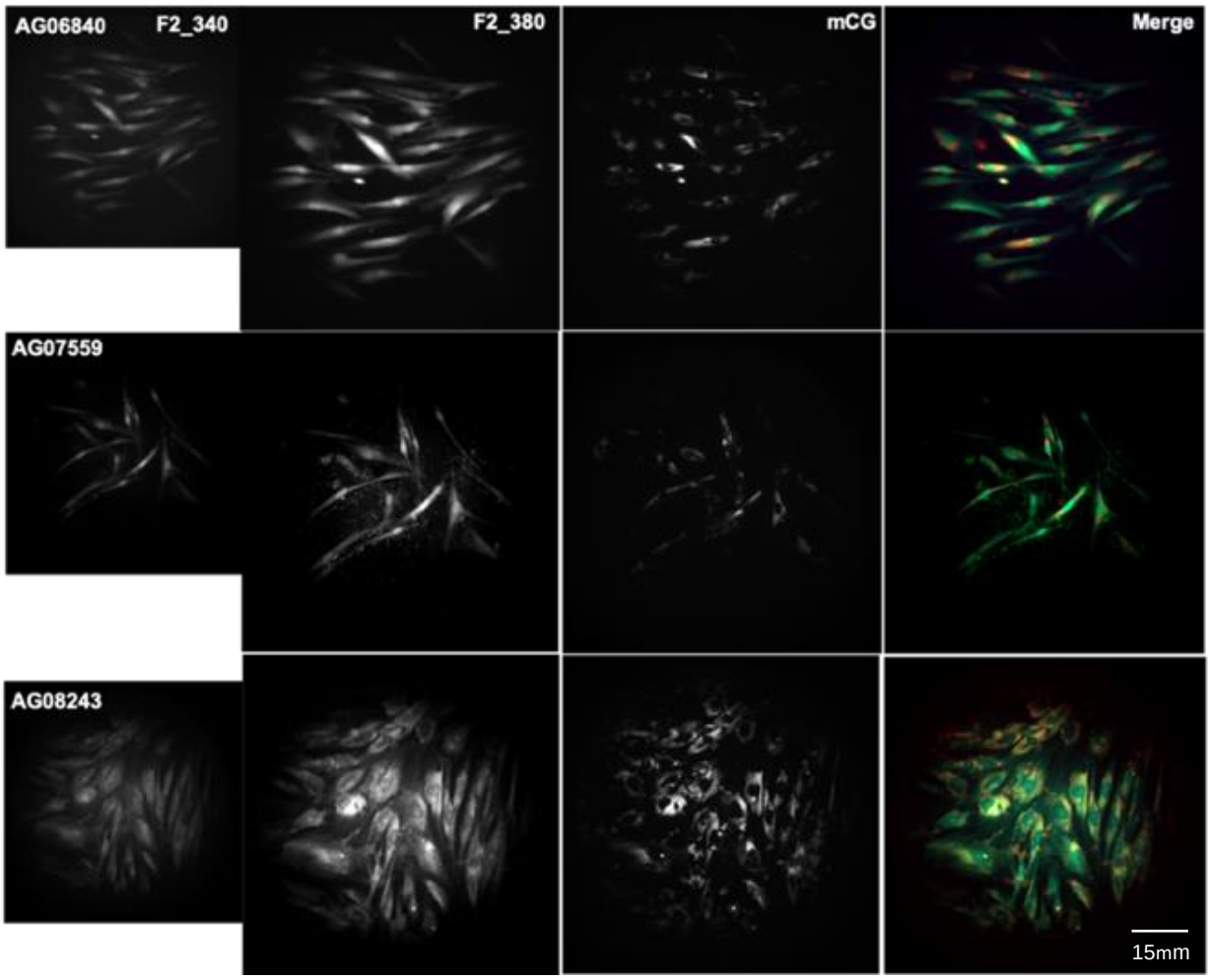

Figure 26: Cytoplasmic and mitochondrial [Ca^{2+}] in patient fibroblasts (Set 1). Representative micrographs of basal Fura-2 and mCG fluorescence from three different patients, AG06840 (FAD), AG07559 (control) and AG08243 (SAD). Fibroblast transiently transfected with mCG (48 hrs) were loaded with Fura-2 in 2mM Ca^{2+} Tyrode's solution.

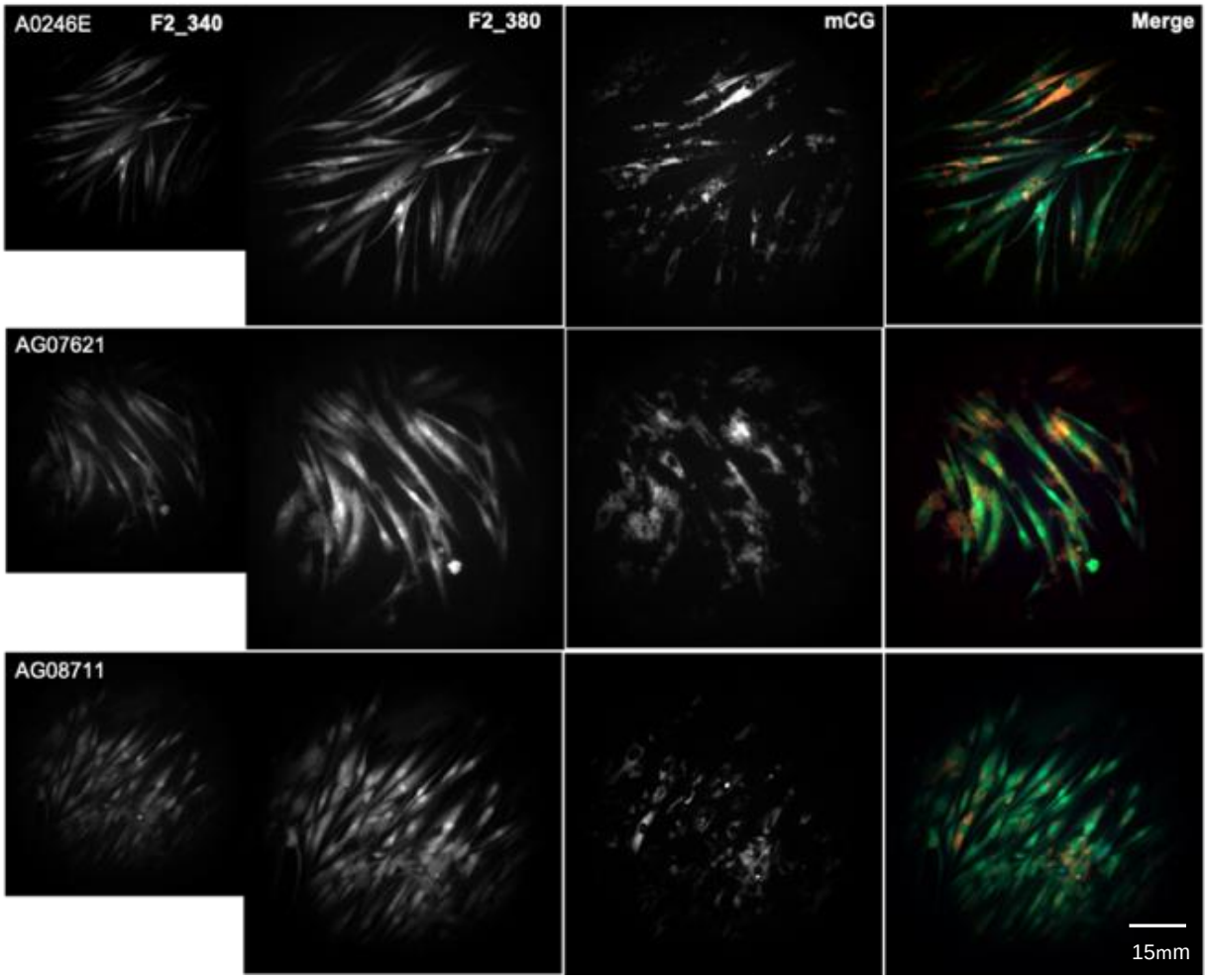

Figure 27: Cytoplasmic and mitochondrial [Ca^{2+}] in patient fibroblasts (Set 2). Representative micrographs of basal Fura-2 and mCG fluorescence from three different patients, A246E (FAD), AG07621 (control) and AG08711 (FAD). Fibroblast transiently transfected with mCG (48 hrs) were loaded with Fura2-am in 2 mM Ca^{2+} Tyrode's solution.

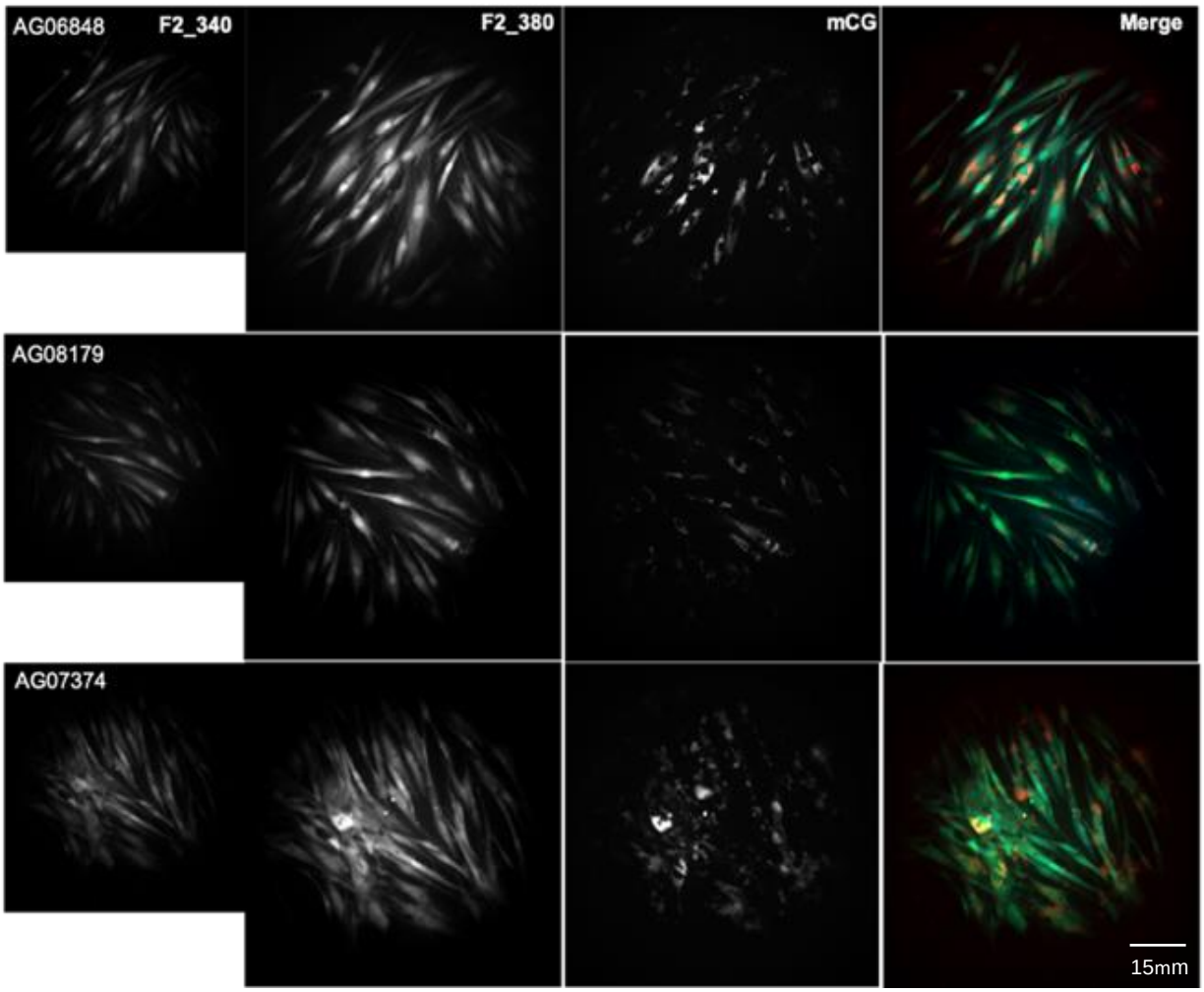

Figure 28: Cytoplasmic and Mitochondrial [Ca^{2+}] imaging in patient fibroblasts (Set 3). Representative micrographs of basal Fura-2 and mCG fluorescence in patient fibroblasts from three different patients, AG06848 (FAD), AG08179 (control) and AG087374 (SAD). Fibroblast transiently transfected with mCG (48 hrs) were loaded with Fura-2 in 2mM Ca^{2+} Tyrode's solution.

We performed these Ca^{2+} imaging experiments in at least three different cell preparations from each patient on different days. To trigger ER Ca^{2+} release through $InsP_3R$, we stimulated patient fibroblasts with 100 nM BK. The BK response within each

cell line and between experiments was highly variable. Some cells responded to BK stimulation very quickly with a strong Ca^{2+} transient while other cells responded with a significant delay after stimulation and a number of cells did not respond (Figure 29). A summary of the relative cytoplasmic and mitochondrial basal Ca^{2+} was determined for each experiment from time 0 to before BK stimulation (Figure 29A and B respectively).

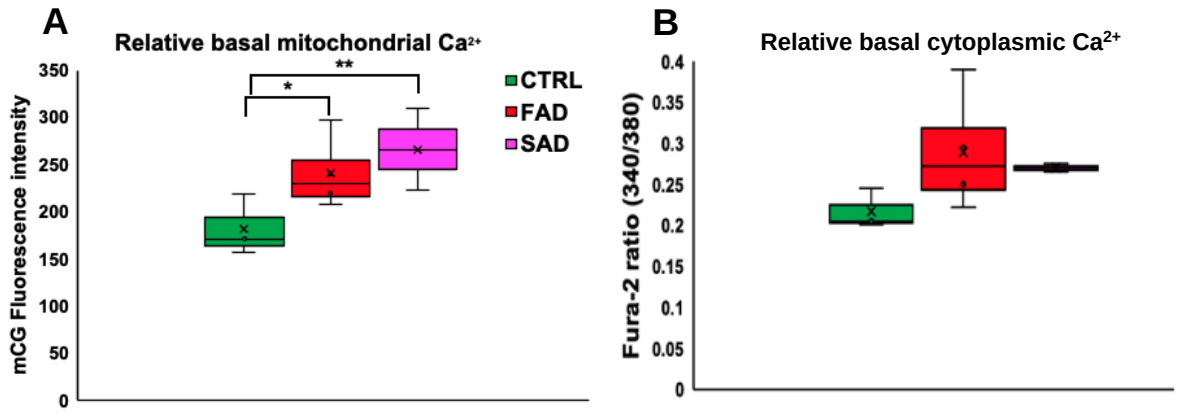

Figure 29: Relative basal mitochondrial [Ca^{2+}] in patient fibroblasts. Summary of basal Ca^{2+} levels from all patient fibroblasts studied and described in Table 1: CTRL subjects (green box), FAD patients (red box) and SAD patients (pink box). **A)** Mitochondrial Ca^{2+} of fibroblasts transiently transfected with mCG (48 hrs). **B)** Cytoplasmic Ca^{2+} in human fibroblasts loaded with ratiometric Fura-2. Control patients: AG07621, AG08179. FAD patients: AG068840, AG06848, AG08711, AG09908 and A246E. SAD patients: AG08243 and AG07374. Significance was determined by one-way ANOVA with Bonferroni (paired comparison) post-test using subject control cells as control: *, $p < 0.05$.

Although we could visually confirm a good transfection efficiency of mCG1 in patient's fibroblasts and identified important differences between patients, this mCG1 sensor did not show significant changes under experimental challenges such as CCCP stimulation. Some cells responded as expected to CCCP with an increase in mCG1 fluorescence, while others did not. Due to this lack of sensitivity of mCG1 sensor, we decided to transiently transfect patients' fibroblasts with the FRET sensor 4mtD3cpv

previously described and used on SH-SY5Y cells (Figure 30, 31, 32). FAD patients showed a significantly higher FRET fluorescence intensity compared with control cells (Figure 30, 31, 32) and with fibroblasts from SAD patients, specifically AG07374 (Figure 31).

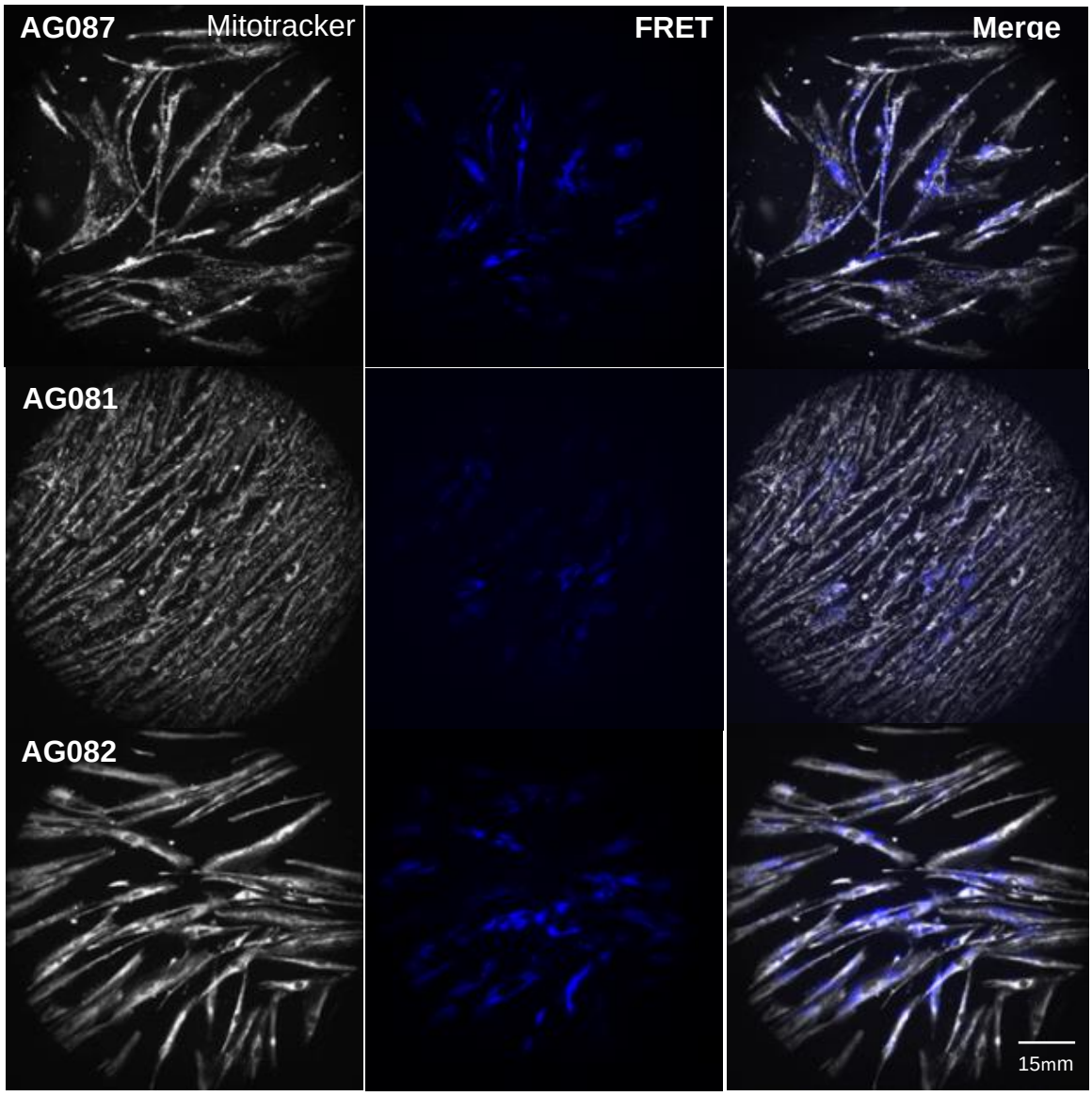

Figure 30: Mitochondrial [Ca^{2+}] imaging in patient fibroblasts (Set 1). Representative micrographs of first set of patient fibroblasts loaded with deep red mitotracker and transiently transfected with 4mtD3cpv (FRET sensor). AG08711 (FAD), AG08179 (control) and AG08243 (SAD). FRET signal corresponds to emission ratio of CFP/YFP.

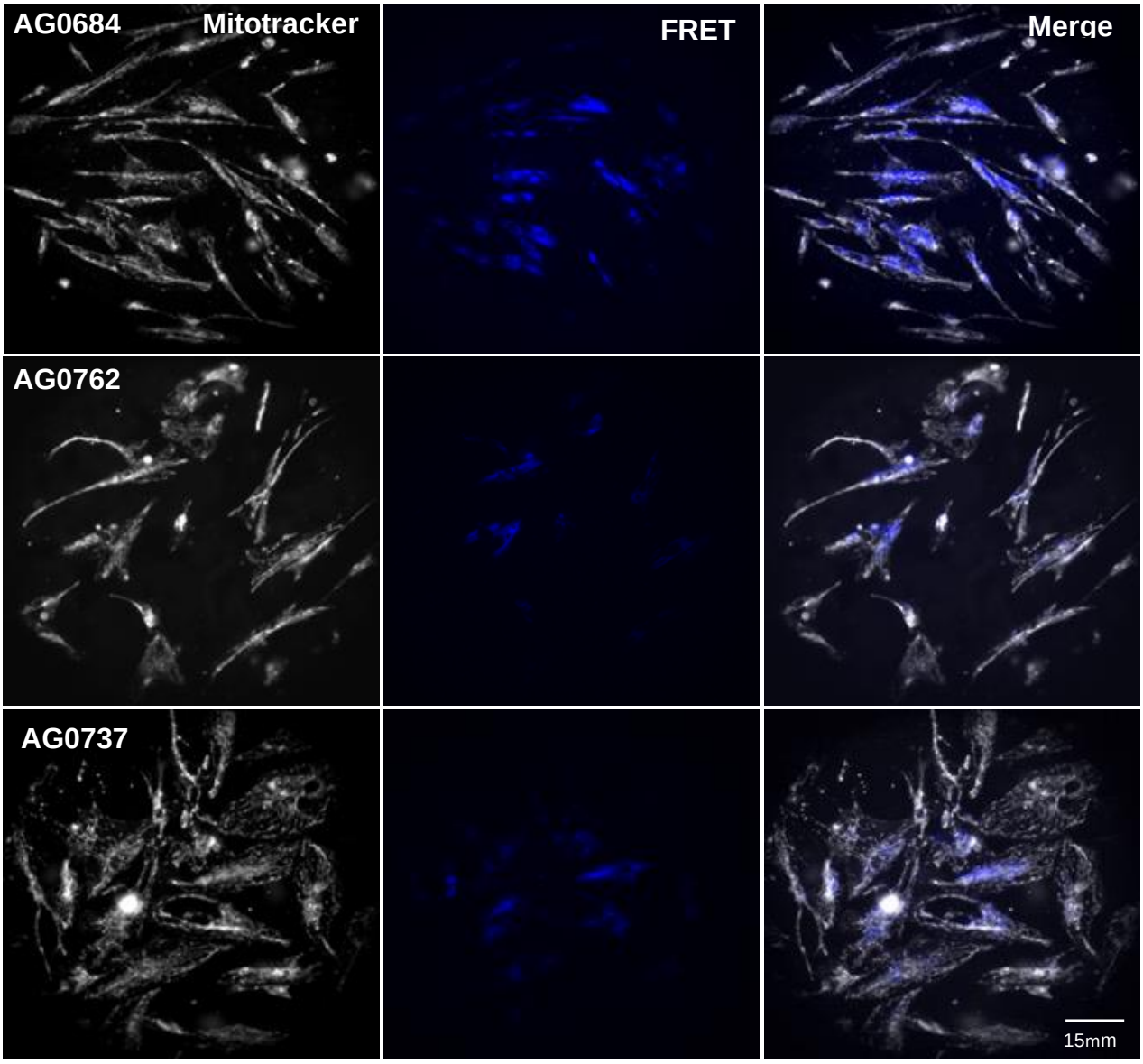

Figure 31: Mitochondrial [Ca^{2+}] imaging in patient fibroblasts (Set 2). Representative micrographs of second set of patient fibroblasts loaded with deep red mitotracker and transiently transfected with 4mtD3cpv (FRET sensor). AG06848 (FAD), AG07621 (control) and AG07374 (SAD). FRET signal corresponds to emission ratio of CFP/YFP.

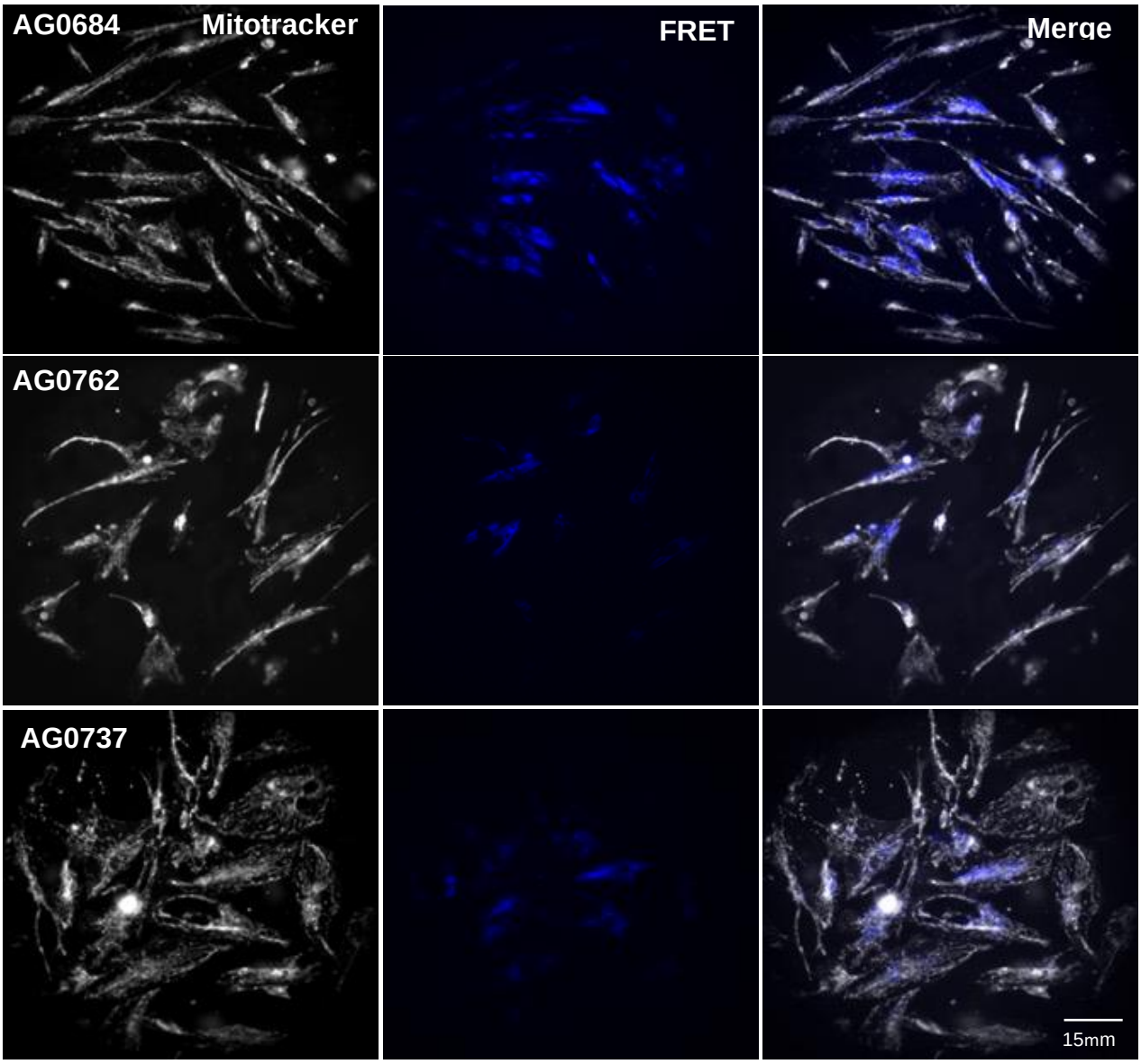

Figure 31: Mitochondrial [Ca^{2+}] imaging in patient fibroblasts (Set 3). Representative micrographs of second set of patient fibroblasts loaded with deep red mitotracker and transiently transfected with 4mtD3cpv (FRET sensor). AG06848 (FAD), AG07621 (control) and AG07374 (SAD). FRET signal corresponds to emission ratio of CFP/YFP.

As with the previous set of experiments, we performed these Ca^{2+} imaging experiments in at least three different cell preparations of each patient in different days. To trigger ER Ca^{2+} release through $InsP_3R$, we stimulated patient fibroblasts with 100 µM ATP. However, the ATP response was also very variable as previously observed in mCG1 experiments (Figure 33). Relative mitochondrial basal Ca^{2+} was determined for each experiment from time 0 to before ATP stimulation (Figure 33A).

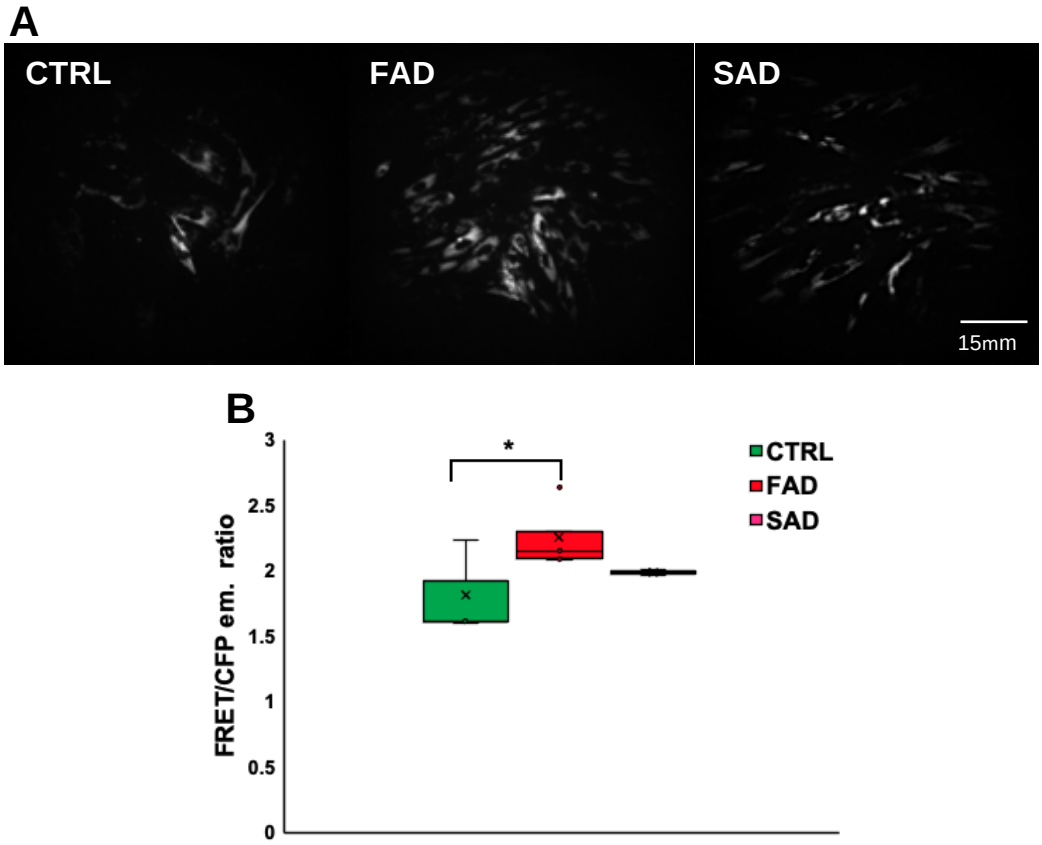

Figure 33: Summary of relative basal mitochondrial [Ca^{2+}] in patient fibroblasts with FRET sensor. A) Representative micrograph of FRET signal intensity to compare FAD, SAD and control patients. **B)** Basal FRET signal ratio over CFP fluorescence intensity in all group of fibroblasts studied. Summary of relative mitochondrial Ca^{2+}. (n=3 for each patient). The significance of basal Ca^{2+} relative values were determined by Student's t test, *, $p<0.05$.

We also determined the relative change of FRET signal after ATP and CCCP stimulation. As we can see in Figure 34A, a change in FRET signal was observed after ATP stimulation in cells from FAD patients. We also observed, after CCCP addition, that FAD fibroblasts had an increase in FRET signal compared with control cells. This increase was also higher but not significant in fibroblast obtained from SAD patients.

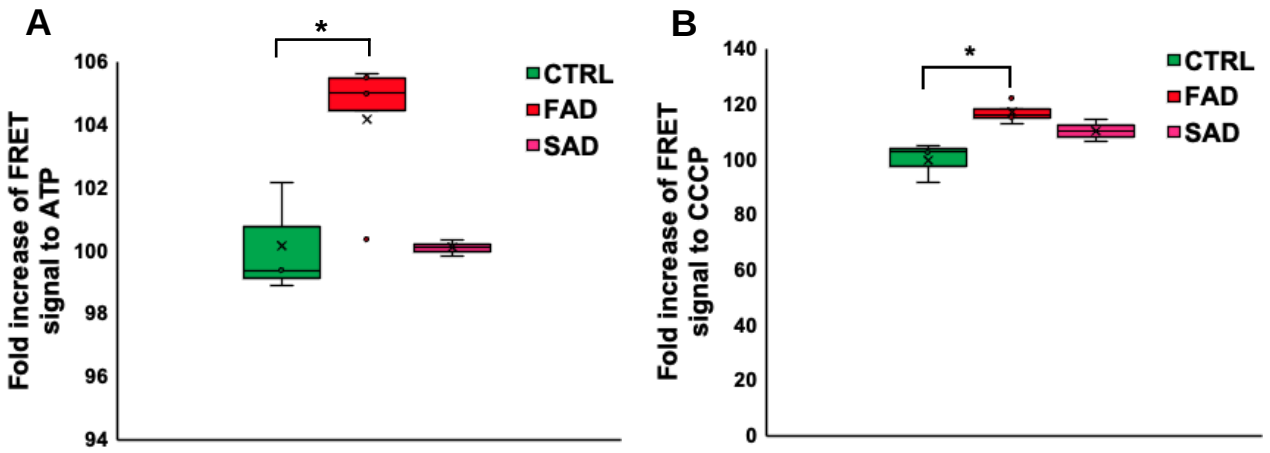

Figure 34: Summary of mitochondrial [Ca^{2+}] response to ATP and CCCP in patient fibroblasts. A) Fold increase of FRET signal after ATP stimulation**. B)** Fold increase of FRET signal after CCCP stimulation**.** Cells were perfused in 2 mM Ca^{2+} Tyrode´s solution and at 100 sec stimulated with 100 μM ATP and at 400 sec CCCP was added. (n=3 for each patient) The significance of ATP Ca^{2+} relative values were determined by Student's t test, *, $p<0.05$.

Although the results with the FRET sensor showed significant differences after ATP stimulation on human skin fibroblasts from FAD patients, the results had high variability and fibroblasts from SAD patients did not show significant differences after ATP stimulation.

Ca^{2+} indicators for use in mitochondria where concentrations of Ca^{2+} can change over three orders of magnitude (~ 0.1 μM to ~100 μM) are not optimized for

several reasons. To explore and determine the best tool for mitochondrial Ca^{2+} imaging, we also tested a low affinity R-GECO1 called LAR-GECO1 (K_D ~20 µM) with ~10-fold increase in fluorescence intensity upon binding of Ca^{2+}. Following the same experimental conditions used for the previous sensors, in another set of experiments we determined the basal mitochondrial Ca^{2+} levels in human fibroblasts. As is shown in Figure 35, a set of patient fibroblasts transiently transfected with LAR-GECO1 and see that FAD fibroblast had basal fluorescence intensity higher than control and SAD cells. In the second set of experiments, FAD fibroblasts presented an increase in basal fluorescence compared with control patients, but similar to FAD cells from PSEN2 patients (AG09908) (Figure 36). Finally, in the third set of experiments, the fluorescence intensity of LAR-GECO1 was just slightly higher in FAD and SAD cells compared with control fibroblast AG08179 (Figure 37).

In this set of experiments, we observed significant variability in the responses to ATP among the different patients studied and between experiments from the same patient. However, the average of basal mitochondrial and cytoplasmic relative Ca^{2+} levels were significantly higher in fibroblasts obtained from FAD patients (Figure 38 A and B). The cytoplasmic and mitochondrial [Ca^{2+}] peak in response to ATP was also higher in FAD and SAD patients but not statistically significant compared to control patients (Figure 38 C and D).

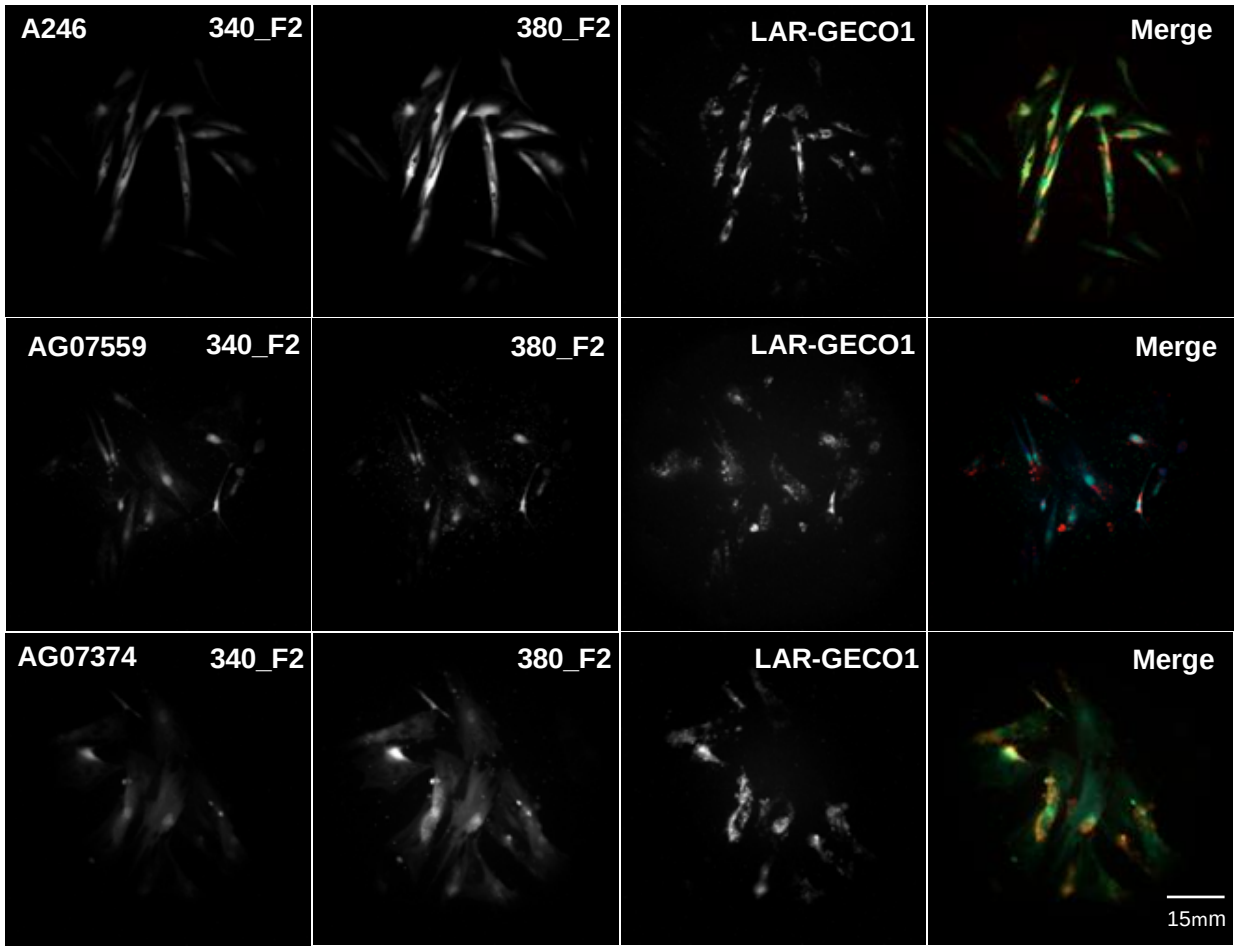

Figure 35: Mitochondrial [Ca^{2+}] imaging in patient fibroblasts with LAR-GECO1 (Set 1). Representative micrographs of first set of patient fibroblasts loaded with Fura-2 and transiently transfected with low affinity Ca^{2+} sensor, LAR-GECO1. Cells used in this set were A246E (FAD), AG07559 (control) and AG07374 (SAD).

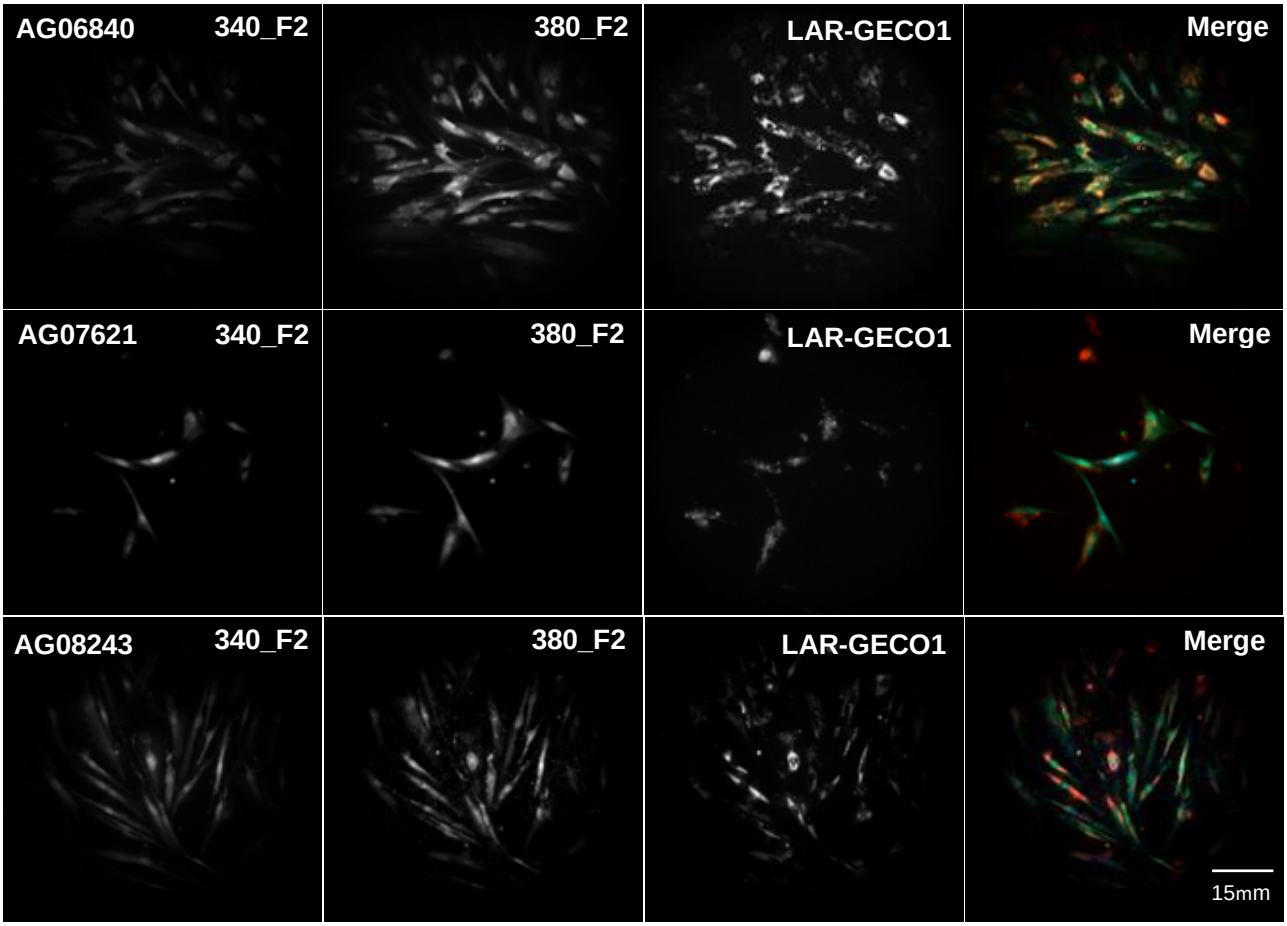

Figure 36: Mitochondrial [Ca^{2+}] imaging in patient fibroblasts with LAR-GECO1 (Set 2). Representative micrographs of first set of patient fibroblasts loaded with Fura-2 and transiently transfected with low affinity Ca^{2+} sensor, LAR-GECO1. Cells used in this set were AG06840 (FAD), AG07621 (control) and AG08243 (SAD).

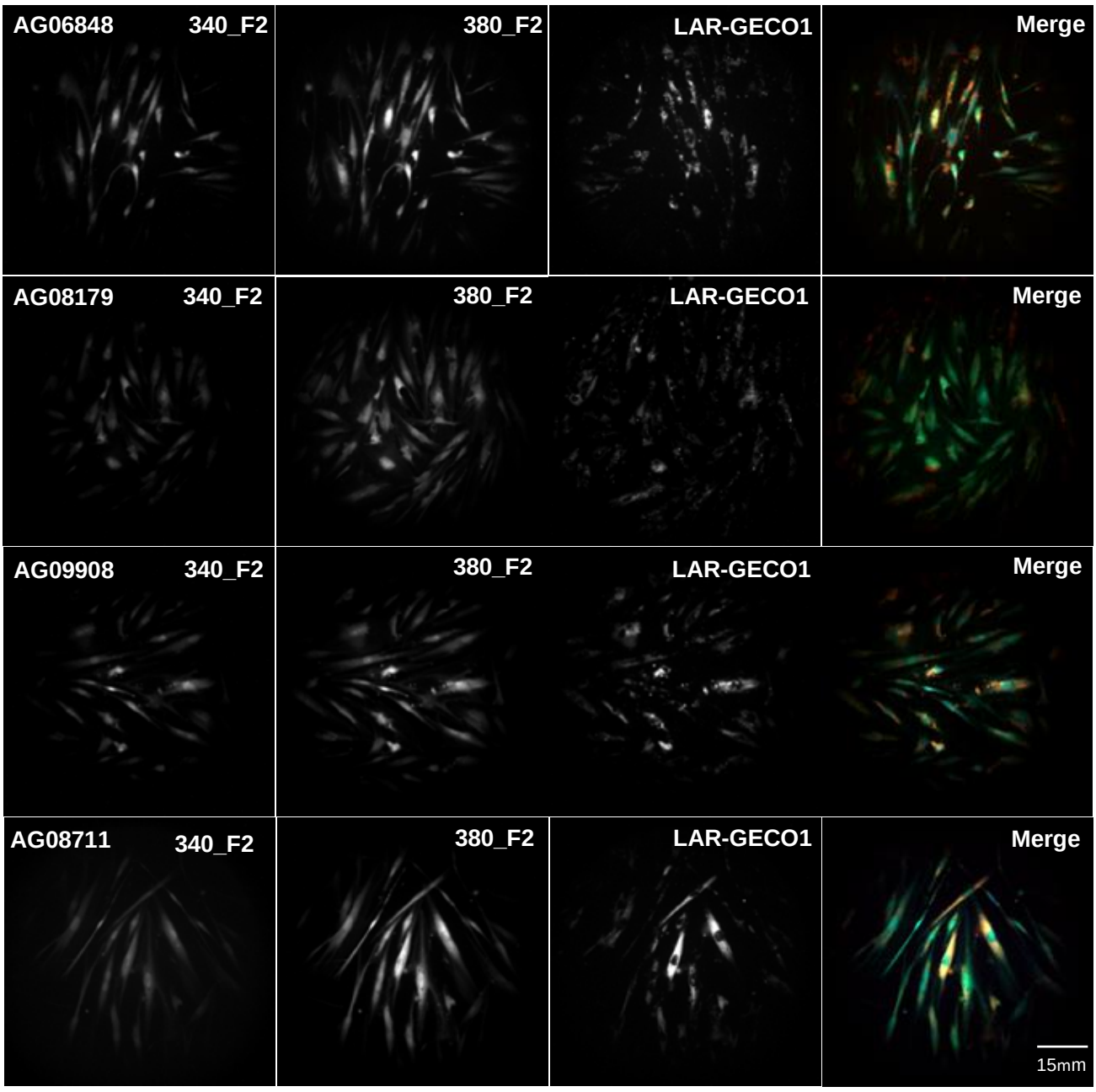

Figure 37: Mitochondrial [Ca^{2+}] imaging on patient fibroblasts (Set 3). Representative micrographs of patient fibroblasts loaded with Fura-2 (340/380 nm) and transiently transfected with low affinity Ca^{2+} sensor, LAR-GECO1. Cells used in this set were AG06848 (FAD), AG08179 (control) and AG09908 (FAD_PSEN2) and AG08711 (FAD).

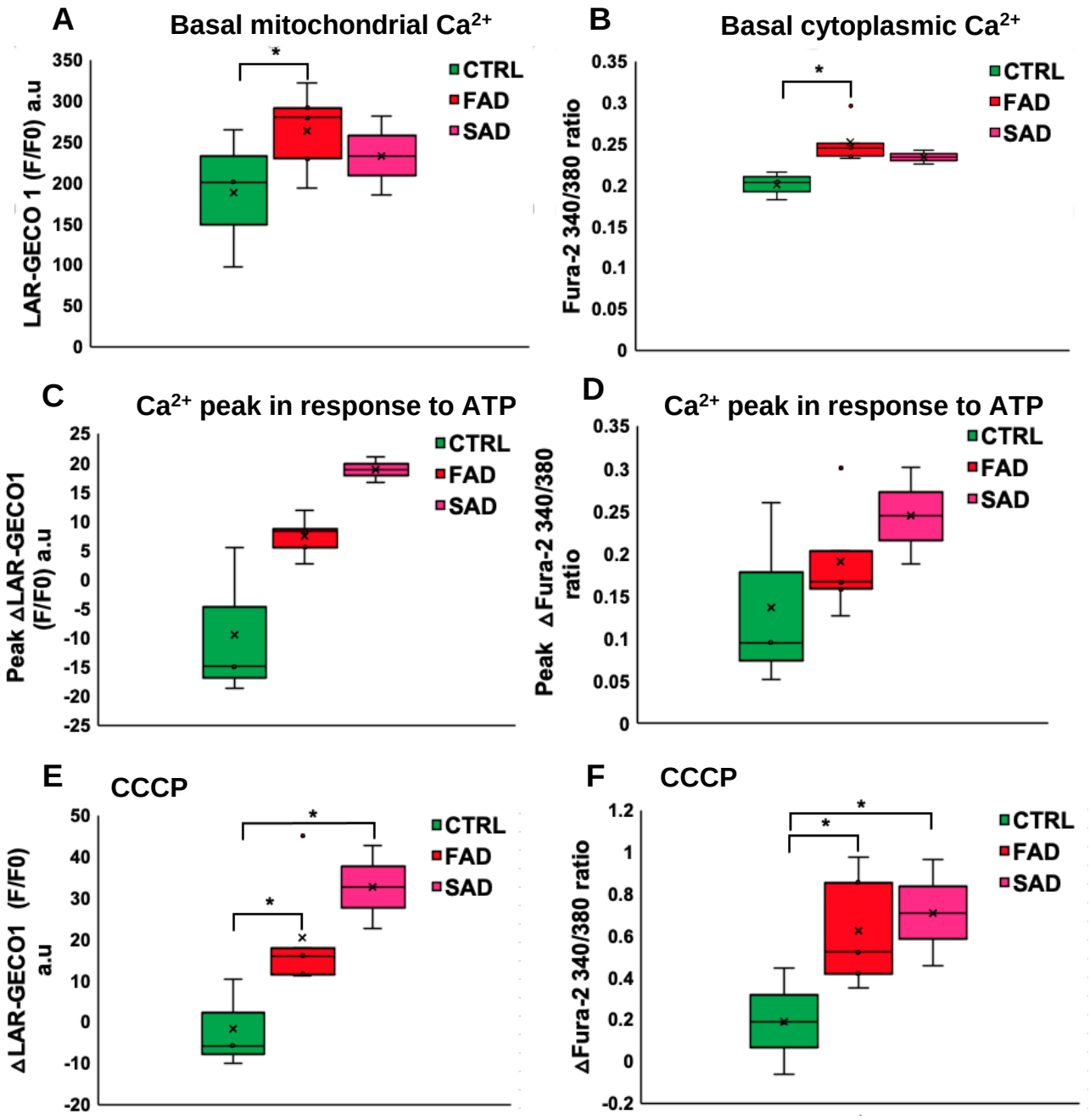

Figure 38: Summary of mitochondrial and cytoplasmic [Ca^{2+}] imaging in patient fibroblasts. A) Summary of basal mitochondrial Ca^{2+} on control, FAD and SAD fibroblasts loaded with Fura-2 and transiently transfected with low affinity Ca^{2+} sensor, LAR-GECO1. **B)** Summary of basal cytoplasmic Ca^{2+}**. C)** Peak mitochondrial Ca^{2+} levels in each experimental group after ATP stimulation (100 µM) and **D)** cytoplasmic [Ca^{2+}] peak in three different set of cells from FAD, control or SAD patients. **E)** Summary of total relative mitochondrial Ca^{2+} levels after CCCP stimulation on each group of patients and **F)** total relative cytoplasmic Ca^{2+} levels. N=3 independent experiments/patient. The significance of basal, peak and total Ca^{2+} relative values were determined by Student's t test, *, $p<0.05$.

10.10 Aim 1d. Determining the expression levels of the proteins responsible for mitochondrial Ca^{2+} homeostasis in mutant PS1-M146L SH-SY5Y cells and FAD human skin fibroblast from FAD patients.

We determined the expression levels of MCU and associated proteins, specifically MICU2 and MCUR1 by Western blot in the SH-SY5Y cell lines described previously. Unexpectedly, we found a significant increase in the expression of MCU in cells expressing PS1wt but not in cells expressing either EGFP only or mutant PS1-M146L (Figure 39). However, MICU2 and MCUR1 had no significant differences among different cell lines tested (Figure 39). We used the Hsp60 protein in order to identify possible differences in mitochondrial mass among the cell lines, however no significant differences were observed on the relative expression of hsp60 in the mutant PS1-M146L compared with control cells PS1wt or EGFP (empty vector) cells (Figure 39).
We also examined the relative expression of levels of these proteins in human skin fibroblasts from FAD, control and SAD patients. However, there was significant variability in the expression levels of Hsp60, MCU and MCUR1 proteins (Figure 40), suggesting different roles and contributions of each one of these proteins on the Ca^{2+} levels observed in previous experiments.

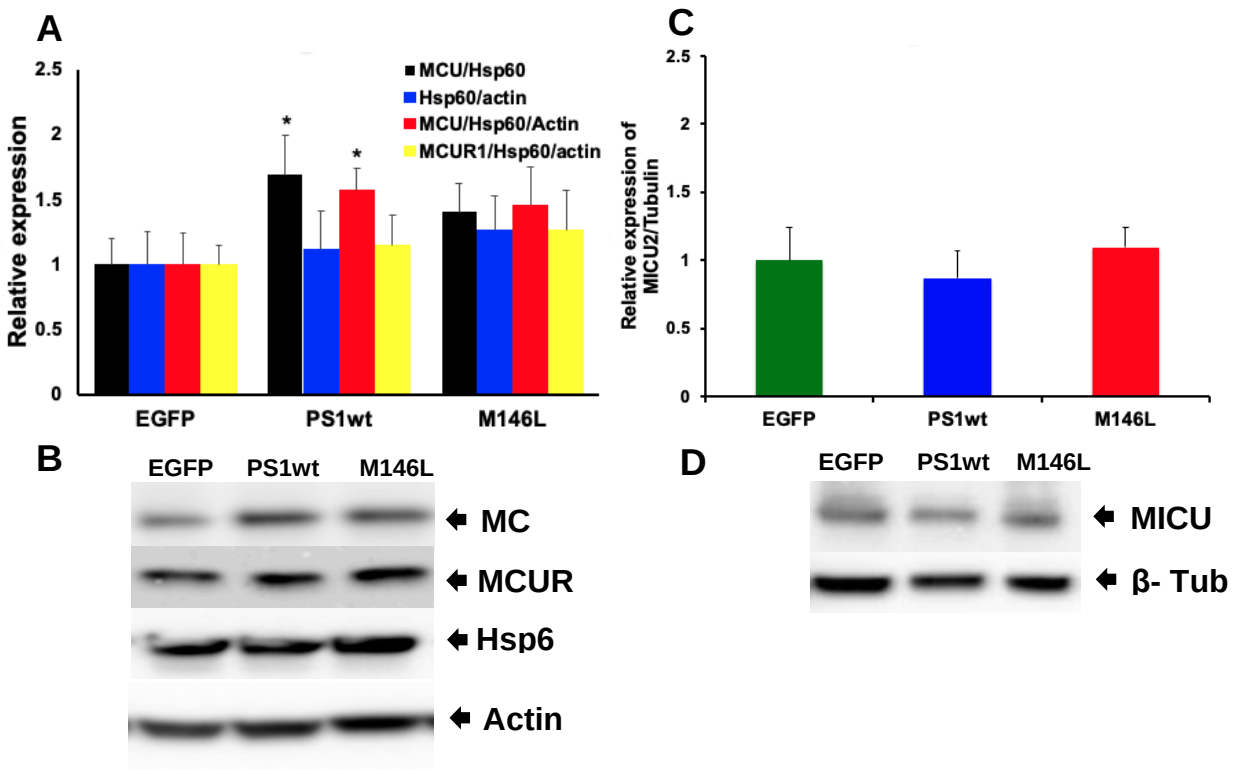

Figure 39: Relative expression levels of the main proteins responsible for mitochondrial Ca^{2+} uptake in SH-SY5Y cells. A) Relative expression levels of MCU in SH-SY5Y cells stably transfected either with EGFP (empty vector), PS1wt or PS1-M146L. **B)** Representative immuno-blots of MCU and MCUR1 normalized with mass of mitochondrial proteins (Hsp60) and with the loading control actin. **C)** Relative expression of MICU2 normalized to β-tubulin as a loading control. **D)** Representative immuno-blots of MICU2. The data represent the means of three experiments from different cell preparations. Bars represent the average +/- SEM of 3 independent experiments.

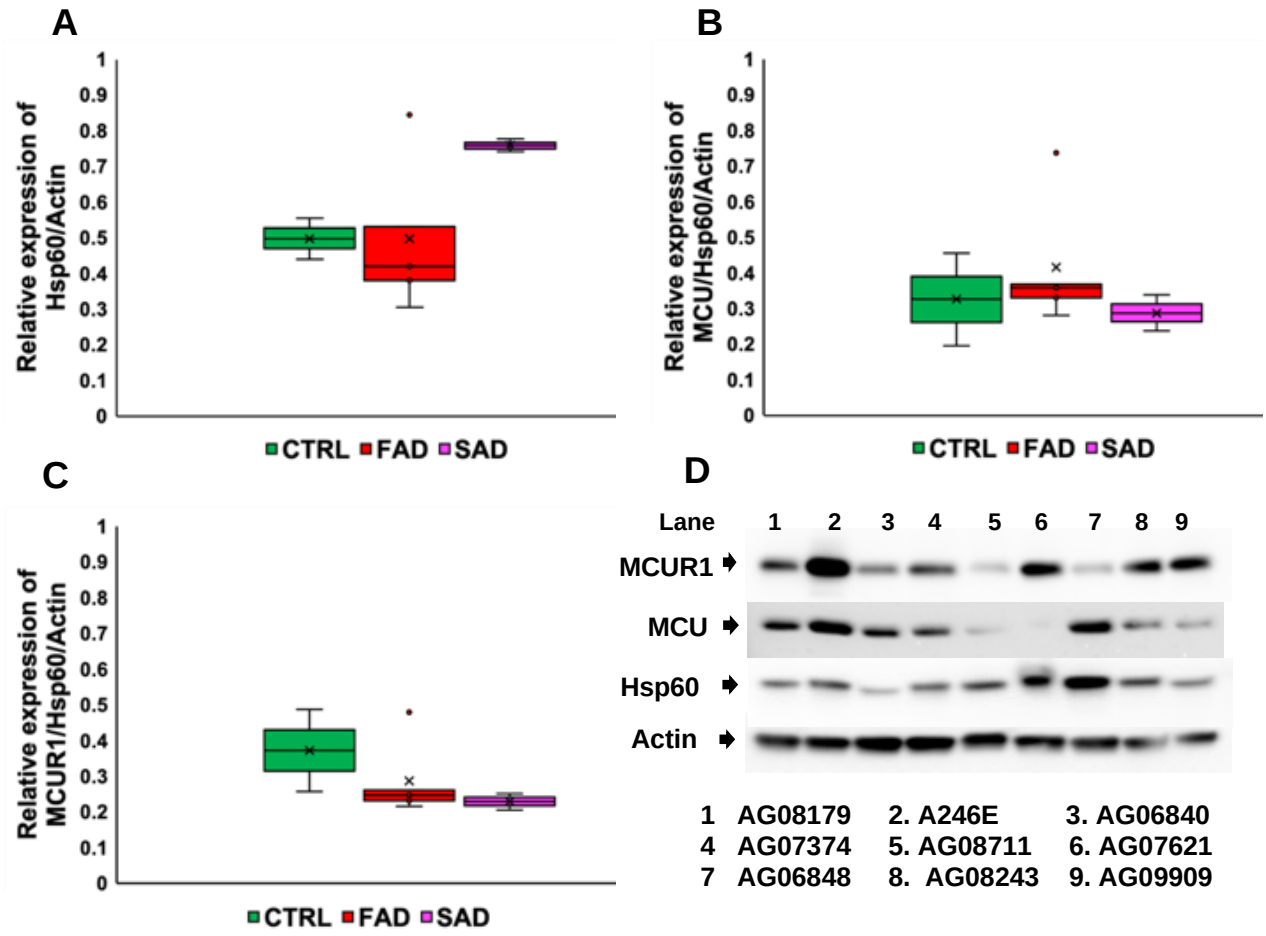

Figure 40: Relative expression levels of the main proteins responsible of mitochondrial Ca^{2+} uptake in human fibroblasts. A) Relative expression levels of Hsp60 as a ubiquitous mitochondrial marker on fibroblasts isolated from FAD, control and SAD patients **B)** Relative expression levels of MCUR1 normalized by mitochondrial marker and actin as a loading control. **C)** Relative expression of MCU normalized by Hsp60 and with actin as a loading control. **D)** Representative immuno blots of MCUR1, MCU, Hsp60 and actin from each patient. Control patients: AG07621, AG08179. FAD patients: AG068840, AG06848, AG08711, AG09908 and A246E. SAD patients: AG08243 and AG07374. N=3 independent experiments/patient.

As an important player of the phenotype found on SH-SY5Y cells related with Ca^{2+} extrusion from the mitochondria, we also determined the levels of NCLX in fibroblasts from patients. The results suggest a common possible cause of mitochondrial Ca^{2+} overload between SH-SY5Y cells and fibroblast isolated form FAD

patients, in which nearly all of them show a decrease in the relative expression of NCLX. However, one FAD patient had a significant increase in NCLX levels (Figure 41). For this reason, it would be important to expand our study to more patients to have a considerable number of patients to compare, and to determine if enhanced NCLX expression is correlated with slower disease progression in FAD. Our results show an important dysregulation in Ca^{2+} handling mechanism where NCLX has a relevant role. The lower expression levels observed on mutant PS1-M146L expressing cells could explain the increased mitochondrial Ca^{2+} levels that together with the higher Ca^{2+} release from the ER has severe consequences on the mitochondrial function.

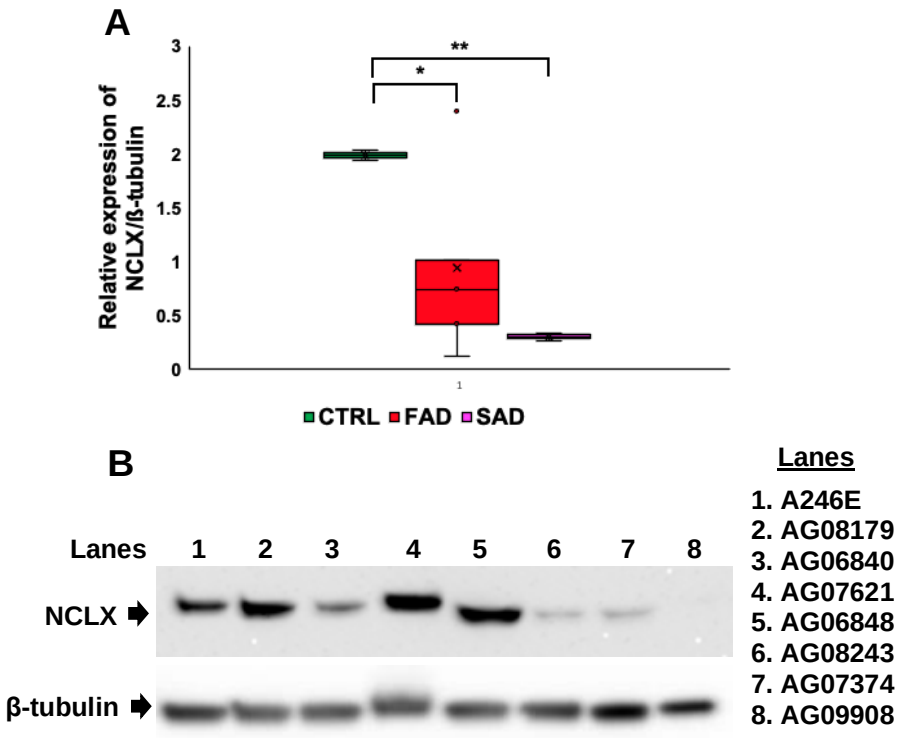

Figure 41: Expression levels of NCLX in skin fibroblasts. **A)** Summary of relative expression levels of NCLX in skin fibroblasts isolated from FAD, control and SAD patients **B)** Representative immuno-blots of NCLX and tubulin as loading control from each patient. Control patients: AG07621, AG08179. FAD patients: AG06840, AG06848, AG09908 and A246E. SAD patients: AG08243 and AG07374. N=3 independent experiments/patient. The significance of basal relative expression values was determined by Student's t test, *, $p<0.05$.

10.11 Mitochondrial function and the role of the IP_3R-MCU axis in mutant PS1-M146L SH-SY5Y cells and human skin fibroblast isolated from FAD patients.

To determine the role of Ca^{2+} release through $InsP_3R$ and mitochondrial Ca^{2+} uptake in regulating oxygen consumption rate (OCR), we performed OCR assays as a measure of mitochondrial activity in SH-SY5Y cell lines using a Seahorse XF-96 metabolic flux analyzer. We performed mitochondria stress-test assays as described by Nicholls (Nicholls, Darley-Usmar et al. 2010), in which the OCR was measured under basal conditions followed by sequential additions of the ATP synthase inhibitor oligomycin (1 μM), the uncoupling agent that collapses the proton gradient and disrupts the mitochondrial membrane potential, FCCP (1 μM), and complex I and a complex III inhibitor rotenone and antimycin A (1 μM) respectively to shut down mitochondrial respiration. This protocol allowed us an estimation of basal respiration, proton leak, maximal respiration, spare capacity, non-mitochondrial respiration and ATP production. First, we found a significant decrease in the global OCR in cells expressing the mutant PS1-M146L (Figure 42 & 43). When we analyze the different parameters individually, we find that the basal respiration was significantly diminished in PS1-M146L cells compared with control cells (Figure 44 A). Differences in basal OCR suggest an altered ATP consumption or altered ATP synthesis in these mutant cells. Indirectly, measurement of the additional parameters allowed us to elucidate the possible contributing factors. The ATP production and the maximal respiration were also statistically lower in these cells (Figure 44 B and C). To test the effect of Ca^{2+} release through the $InsP_3R$ in OCR, we pre-incubated the cells in the presence of 5 μM of XeB,

a specific $InsP_3R$ inhibitor. We found just a slight increase in basal OCR in the presence of XeB, but no significant differences were observed in maximal respiration in mutant PS1-M146L expressing cells (Figure 42 B & 44). However as expected, control cells, PS1wt and EGFP in the presence of XeB had an important decrease on OCR.

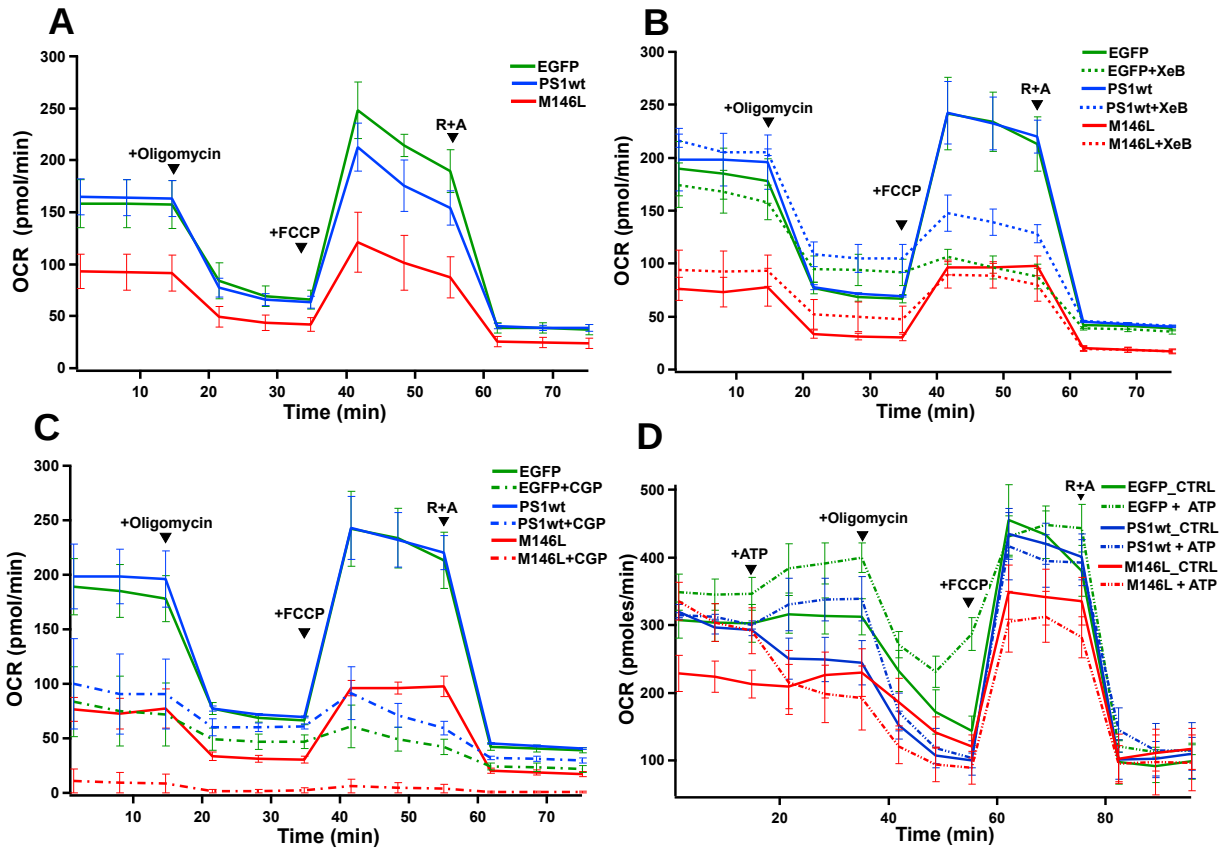

Figure 42: OCR responses to XeB, CGP and ATP in SH-SY5Y cells. A) Averaged traces of OCR in SH-SY5Y cells stably transfected with EGFP, PS1wt or mutant PS1-M146L. Injection of 1 µM oligomycin, 1 µM FCCP and 1 µM of Rotenone plus antimicin A was added sequentially to assess mitochondrial function. **B)** Averaged traces of OCR in SH-SY5Y cells in the presence or absence of 2 µM XeB. **C)** Averaged traces of OCR in SH-SY5Y cells in the presence or absence of NCLX inhibitor, CGP. **D)** Averaged traces of OCR in SH-SY5Y cells upon 10 µM ATP stimulation (n=3 in each condition).

To evaluate the role of NCLX on OCR, we pre-incubated the SH-SY5Y cells for 30 min at RT with the NCLX inhibitor CGP. The results presented in Figures 42 C & 44, showed a decrease in all the possible parameters evaluated in this assay in all the cell lines studied, however CGP-mediated NCLX inhibition in mutant PS1-M146L cells had an even more toxic effect due to their intrinsic vulnerability observed in different tests.

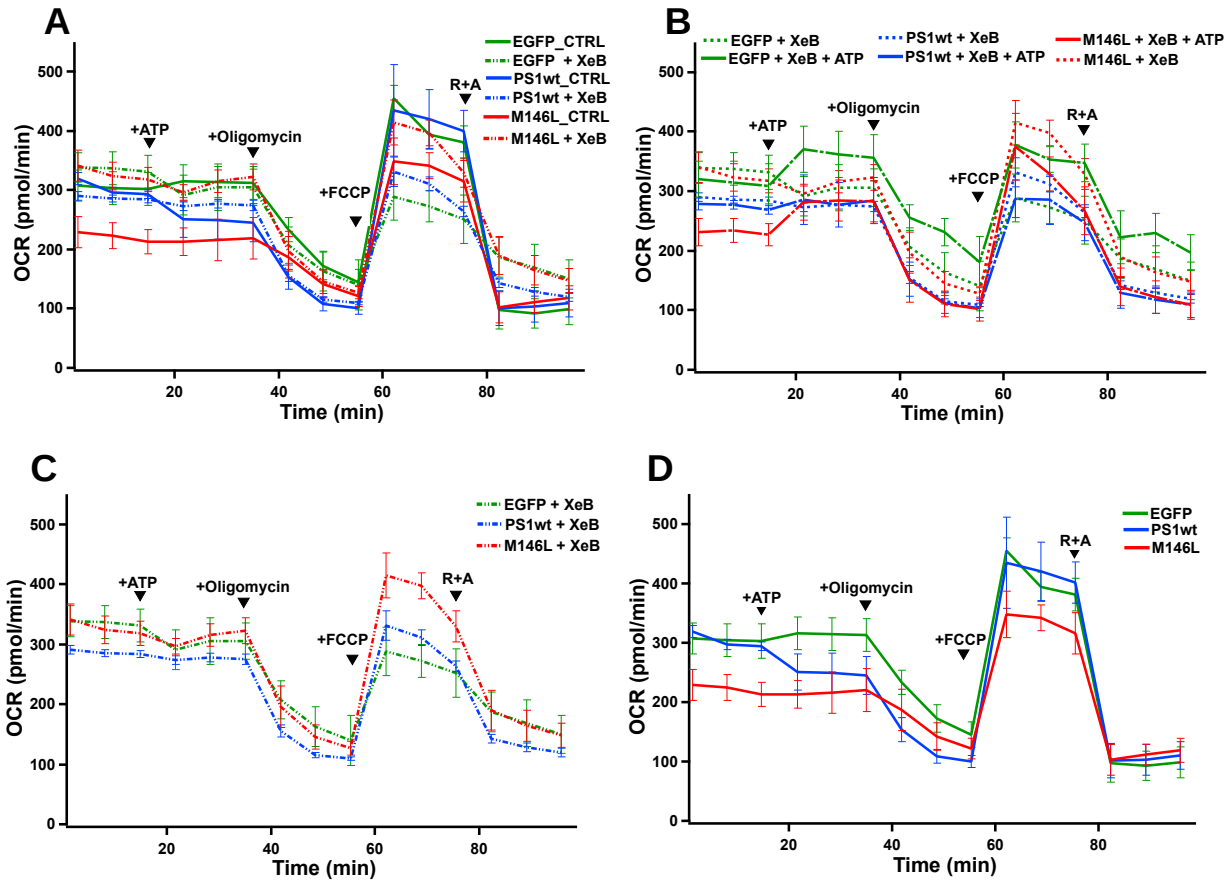

Figure 43: Inhibition of InsP$_3$R improved OCR in PS1 mutant M146L cells. Averaged traces of OCR in SH-SY5Y cells stably transfected with EGFP, PS1wt or mutant PS1-M146L. Injection of 1 µM oligomycin, 1 µM FCCP and 1 µM of Rotenone plus antymicin was added sequentially to assess mitochondrial function. Averaged traces of OCR in SH-SY5Y cells **A)** in the presence or absence of 5 µM XeB; **B)** in the presence or absence of 5 µM XeB with or without ATP stimulation. **C)** Same traces showed in panel A but just under XeB incubation. **D)** Control traces A without XeB (n=3).

Finally, we evaluated the effect of a more physiological Ca^{2+} release through the $InsP_3R$ upon ATP stimulation on OCR in the SH-SY5Y cells. This stimulation caused a significant increase in basal OCR in all the cells evaluated, however, no significant changes were observed in the rest of the parameters examined with the mito-stress assay (Figure 42 D & 44).

In another set of experiments, we increased the XeB concentration from 2 µM to 5 µM in order to see a bigger effect on the OCR. At this XeB concentration, we could see a more important increase in basal OCR in cells expressing the mutant PS1-M146L, although no significant differences were observed in the rest of control cells (Figure 43 A & 44). Under the effect of 5 µM XeB, mutant PS1-M146L expressing cells had a recovery in mitochondrial function, increasing not just basal levels of OCR as well as maximal respiration under ATP stimulation (Figures 43 B & 44). Thus, we found a decrease in OCR in cells expressing the mutant PS1-M146L despite having increased mitochondrial Ca^{2+} levels. This dysfunction might explain the lower ATP production observed in several models of FAD. Remarkably, the mitochondrial dysfunction found in FAD cells, can be reverted upon inhibition of ER Ca^{2+} release through the $InsP_3R$ with XeB.

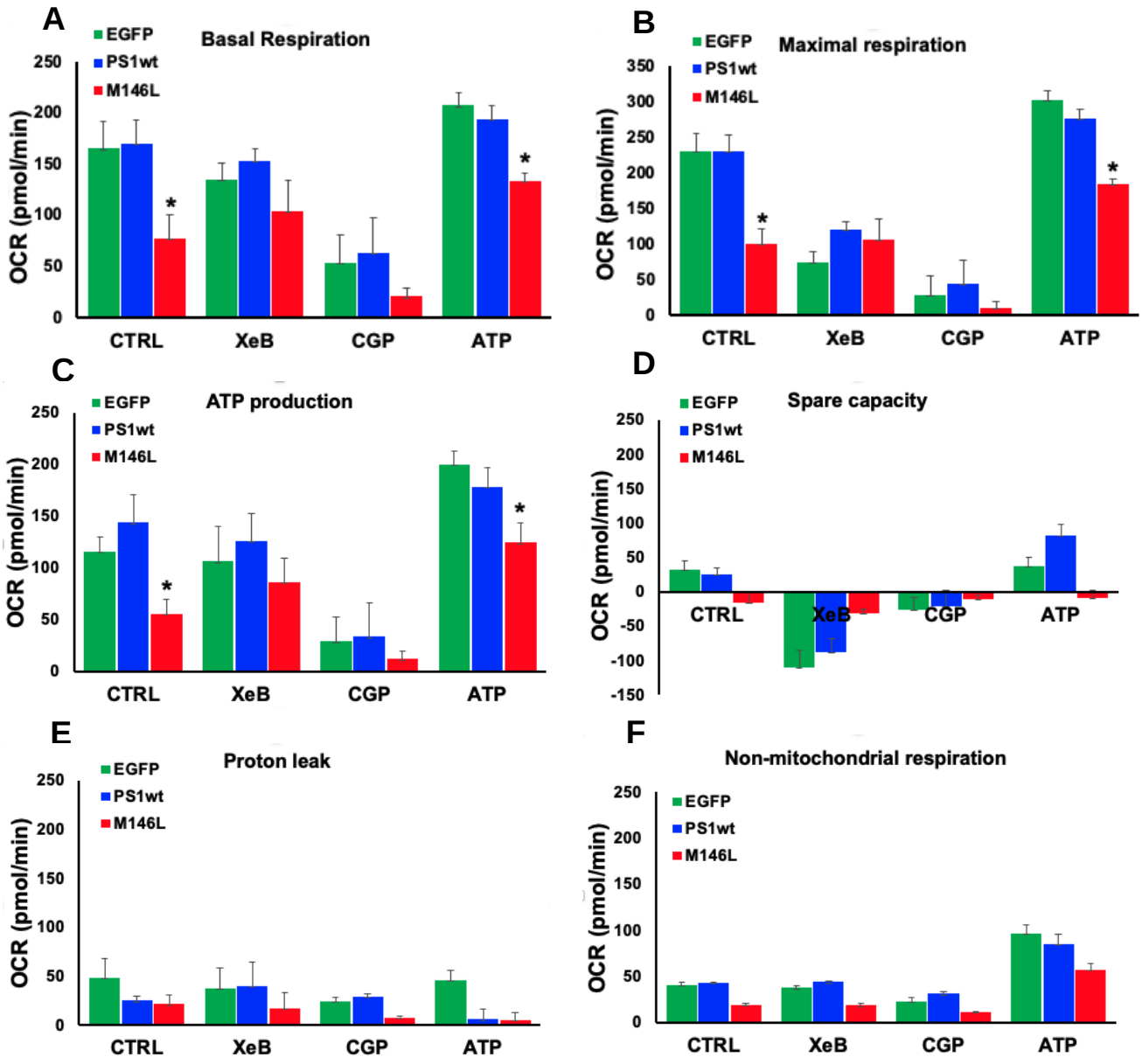

Figure 44: Summary of different parameters evaluated from mito stress assays in SH-SY5Y cells stably expressing EGFP only, PS1wt or PS1-M146L. The data represent the means of three experiments from different cell preparations. Bars represent the average +/- SEM of 3 independent experiments. Significance was determined by one-way ANOVA with Bonferroni (paired comparison) post-test using control subjects as control: *, $p < 0.05$.

10.12. Determining the role of Ca^{2+} release through IP_3R-MCU axis in regulating OCR in skin fibroblasts from FAD patients

We also determined mitochondrial function parameters using the mito-stress assay on human skin fibroblasts isolated from FAD, control and SAD patients. As previously observed in this FAD model, we found high variability among the 10 patients evaluated (Figure 45).

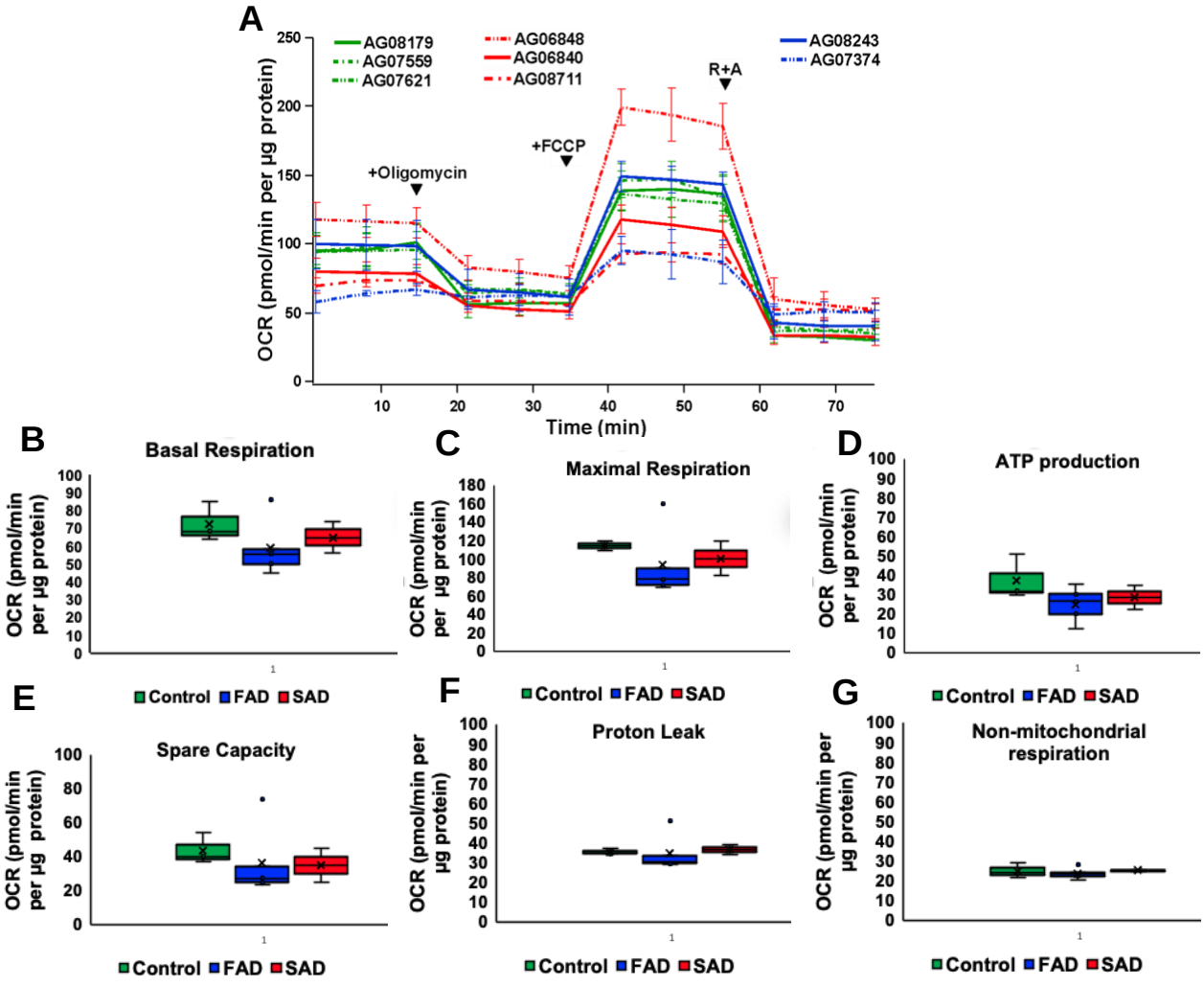

Figure 45: Mitochondrial function parameters on human skin fibroblasts. A) Averaged traces of OCR in human skin fibroblast isolated from FAD, control and SAD patients. Injection of 1 µM oligomycin, 1 µM FCCP and 1 µM of Rotenone plus antymicin was added sequentially to assess mitochondrial function. **B-G)** Summary of different mitochondrial function parameters evaluated from mito-stress assays. (n=3). Control patients: AG07621, AG08179 and AG07559. FAD patients: AG068840, AG06848, AG08711, AG09908 and A246E. SAD patients: AG08243 and AG07374.

Figure 45 shows a marked tendency of a decrease in basal and maximal OCR in FAD patients (red bars in Figure 45 B). However, the patient AG06848 (FAD) had a normal basal OCR compared to control cells and also the highest maximal respiration of the group. We also evaluated the effects of inhibition of ER Ca^{2+} release through the $InsP_3R$ using XeB. This $InsP_3R$ specific inhibitor reduced in all the patients evaluated, the levels of OCR, either basal and maximal, with no significant differences among FAD, SAD and control group of patients (Figure 46 and 47 for summary).

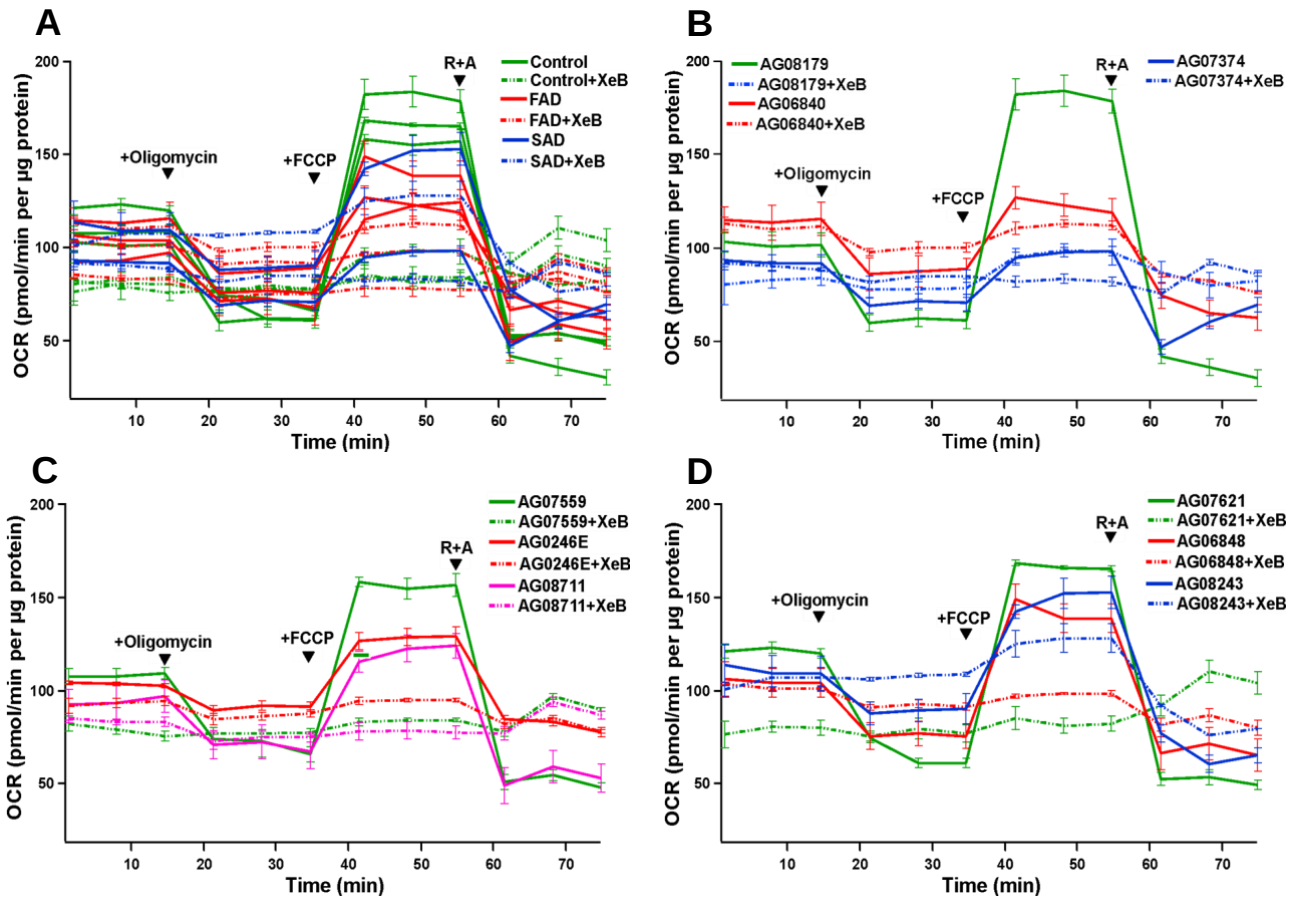

Figure 46: OCR responses to XeB in human skin fibroblasts. A) Averaged traces of OCR in human skin fibroblasts cells from control (green traces), FAD (red traces) and SAD (blue) patients. Injection of 1 µM oligomycin, 1 µM FCCP and 1 µM of Rotenone plus antymicin was added sequentially to assess mitochondrial function in the presence (continued line traces) or absence of 5 µM XeB (discontinued line). **B)** First set of cells from Control (AG08179), FAD (AG06840) and SAD (AG07374) patients. **C)** Second set of cells from Control (AG07559), FAD (AG0246E) and FAD (AG08711) patients. **D)** Third set of cells from Control (AG07621), FAD (AG06848) and SAD (AG08243) patients. (n=3).

Figure 47 presents a summary of mitochondrial functional parameters in human skin fibroblasts in the presence or absence of XeB. A significant reduction in basal OCR was observed in FAD and SAD patients compared with control individuals (Figure 47 A). In the presence of XeB we observed a significant increase in OCR in SAD patients compared with control fibroblasts, however the OCR levels in SAD and FAD patients were not improved in the presence of XeB compared with the basal levels in the absence of this $InsP_3R$ inhibitor. Similar results were obtained regards the maximal respiration parameter (Figure 47 B), observing an important decrease in the maximal respiration of FAD patients compared with control cells. No significant differences were observed among the different patient fibroblasts in ATP production in the presence or absence of XeB (Figure 47 C). An interesting result obtained in these set of experiments was the significant decrease in the spare capacity response in FAD and SAD cells, suggesting an alteration in the amount of extra ATP that can be produced by OXPHOS in case of a sudden increase in energy demand in these cells (Figure 47 D). In the presence of XeB the spare capacity of all the cells were dramatically reduced.

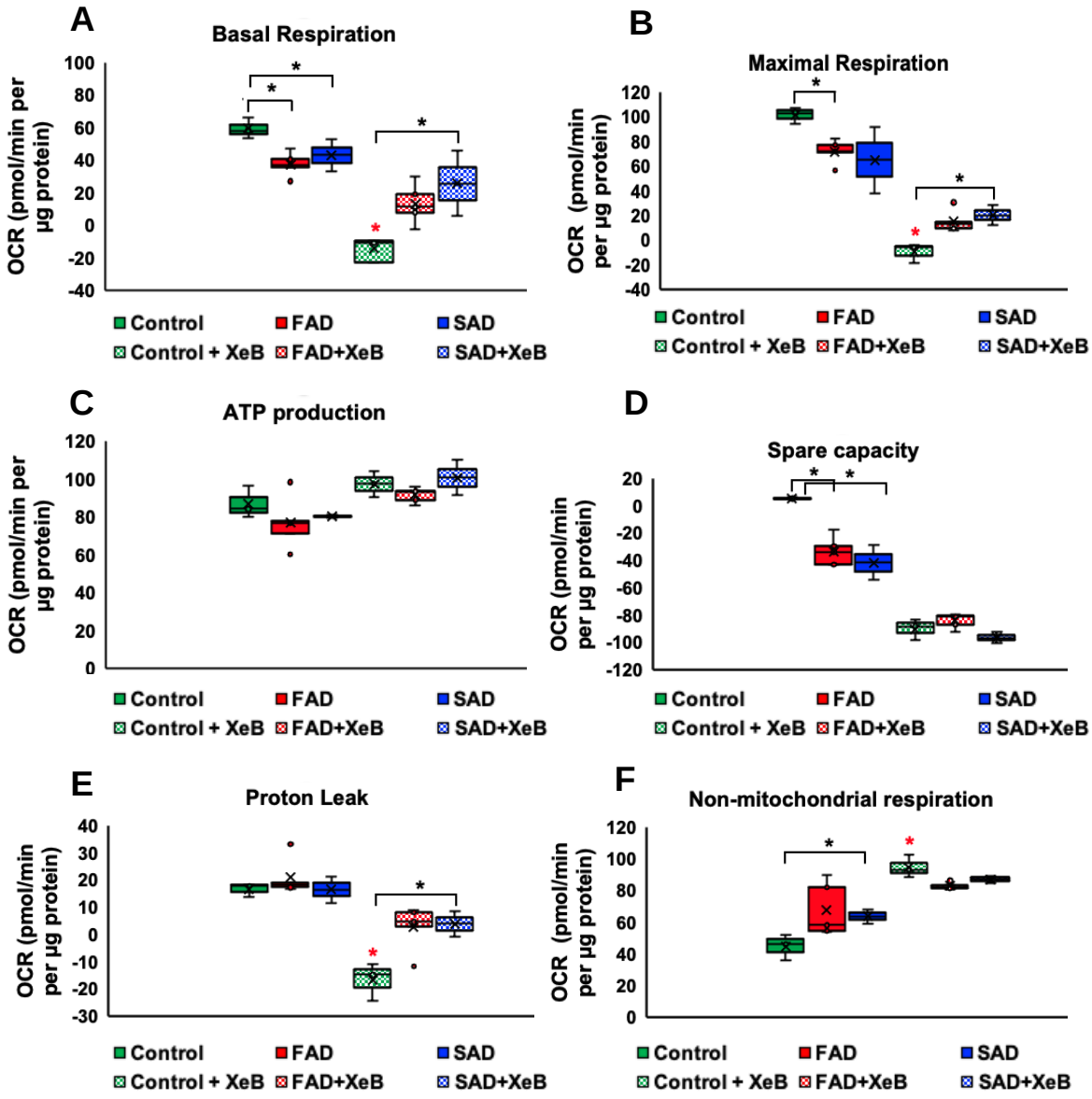

Figure 47: Summary of mitochondrial functional parameters in human skin fibroblasts in the presence or absence of XeB. A) Comparison of basal respiration in all human skin fibroblast isolated from FAD, control and SAD patients. **B)** Comparisons of maximal respiration between fibroblasts isolated from FAD, control and SAD patients. **C)** Comparisons of ATP production between fibroblast isolated from FAD, control and SAD patients. **D)** Comparison of the spare capacity, **E)** proton leak and **F)** non-mitochondrial respiration. Data summarized as the mean ± SEM, and statistical significance of differences between means was assessed using unpaired t tests or analysis of variance (ANOVA) for repeated measures at the 95% level (* $p < 0.05$).

10.13 Role of $InsP_3R$–MCU Ca^{2+} transfer in the expression levels and activity of PDH and α-KGDH in PS1-M146L SH-SY5Y cells, and in human skin fibroblasts isolated from FAD patients.

As an important parameter of mitochondrial function, we evaluated the relative expression of phospho-PDH (p-PDH), IDH and α-KGDH in different experimental models described previously. Ca^{2+} that enters the mitochondrial matrix stimulates the TCA cycle by activating these enzymes that are extremely sensitive to Ca^{2+}, where PDH is activated by Ca^{2+}-sensitive phosphatase activity. The TCA cycle produces the reducing equivalents (NADH and $FADH_2$) that power the ETC, which produces a proton gradient across the mitochondrial inner membrane. H^+ flows down its electrochemical gradient through the ATP synthase leading to biogenesis of ATP. Almost all of the processes involved in the regulation of neuronal membrane potential, excitability and propagation of action potentials exhibit a dependence on [ATP]. Thus, we explored the effect of $InsP_3R$–MCU Ca^{2+} transfer on the expression of p-PDH, IDH and α-KGDH in two different sets of experiments.

We found a significant decrease of p-PDH in PS1-M146L SH-SY5Y-expressing cells that correlated with the higher mitochondrial [Ca^{2+}] levels found with different approaches in these cells throughout this study (Figure 48 A-D). As we expected, the addition of XeB in these cells significantly reverted the levels of p-PDH as a consequence of ER Ca^{2+} release inhibition through the $InsP_3R$ (Figure 48 C). No significant effects of XeB were observed in control cells. We also evaluated the

expression of α-KGDH and IDH, finding an increase in the relative expression of these metabolic enzymes compared with control cells (Figure 49).

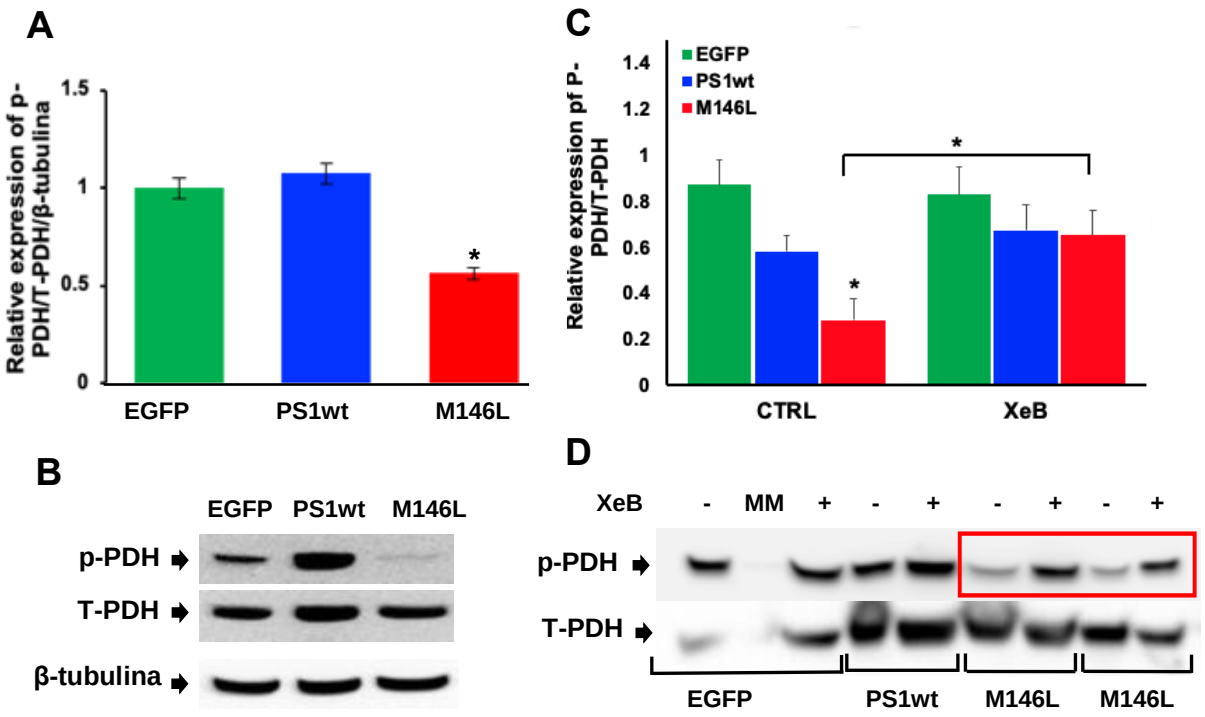

Figure 48: Inhibition of $Insp_3R$ rescues expression of p-PDH in PS1 mutant M146L expressing cells. A) Relative expression levels of p-PHD on SH-SY5Y cells stably transfected with either EGFP only, PS1wt or M146L **B)** Representative immuno blots of p-PHD normalized for total-PHD levels and tubulin as loading control. **C)** Relative expression of p-PHD in the presence or absence of 5 µM XeB. **D)** Representative immuno blots of p-PHD normalized for total-PHD levels in the presence or absence of 5 µM XeB. Results are summarized from 3 experiments under basal conditions. Asterisks indicate $p<0.05$.

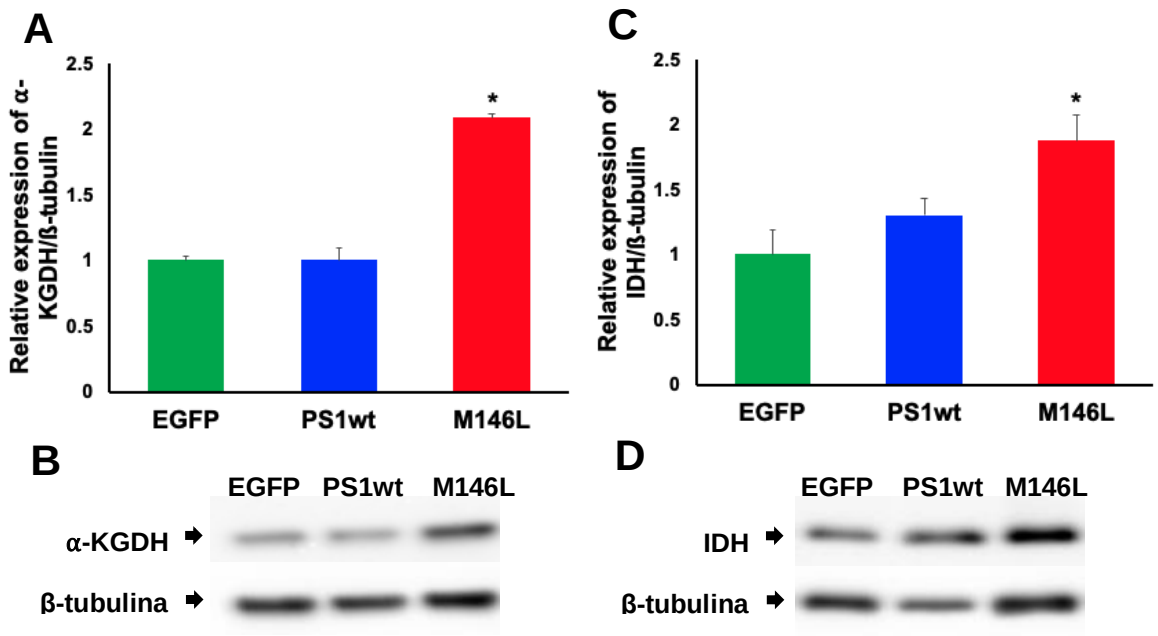

Figure 49: Increased expression levels of α-KGDH and IDH in PS1-M146L expressing cells. A) Summary of relative expression levels of **α-**KGDH and **C)** IDH in SH-SY5Y cells stably transfected with either EGFP only, PS1wt or PS1-M146L **B)** Representative immune-blots of **α-**KGDH normalized by tubulin as loading control. **C)** Relative expression of IDH normalized by tubulin as loading control. **D)** Representative immuno blots of IDH. Results are summarized from 3 experiments under basal conditions. Asterisks indicate $p<0.05$.

To confirm the results regarding p-PDH and α-KGDH expression, we measured their expression in human skin fibroblasts isolated from FAD, control and SAD patients. As in previous assays, we found a great variability in the relative expression of p-PHD and α-KGDH among the different patients. Nevertheless, we found a significant decrease in the FAD patient samples compared with the control group studied. Recapitulating the results observed in SH-SY5Y cells, we also found an increase in the expression of α-KGDH in the FAD patient group compared with controls (Figure 50).

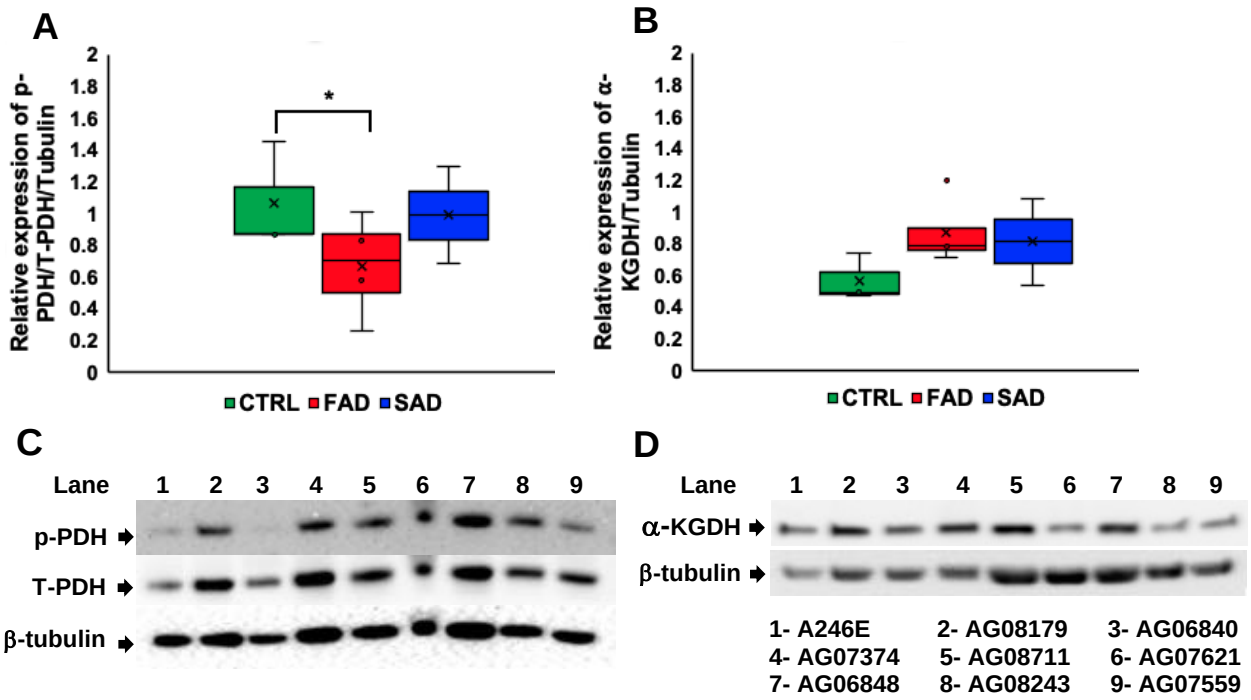

Figure 50: A) Summary of expression levels of p-PHD and α-KGDH in human skin fibroblast from FAD, control and SAD patients. **B)** Representative immuno blots of p-PDH normalized for total-PDH levels and tubulin as loading control. **C)** Relative expression levels of α-KGDH and corresponding representative immunoblot (**D).** Differences between groups were assessed using unpaired t tests or analysis of variance (ANOVA) for repeated-measures at the 95% level (* $p < 0.05$).

Although we identified a similar finding in the SAD group, our results weren't statistically significant, and these results may be due to the small number of subjects studied compared with the other two other groups.

11. DISCUSSION

Our laboratory has previously revealed the involvement of $InsP_3R$ in exaggerated $[Ca^{2+}]_i$ signaling observed in many FAD experimental models (Cheung, Shineman et al. 2008) (Muller, Cardenas et al. 2011) (Shilling, Muller et al. 2014). Although the mechanisms are still controversial, these observations indicate that increased Ca^{2+} release caused by FAD PSs is an early phenotype and could accordingly contribute to disease pathogenesis (Honarnejad and Herms 2012).

Although age is the single most accepted and powerful risk factor of AD, there are a number of hypotheses regarding the underlying mechanisms of AD pathogenesis. Here we described a possible underlying mechanism involving an increase of Ca^{2+} in AD that impinges on mitochondrial function in FAD models. Higher levels of mitochondrial $[Ca^{2+}]$ due to an exaggerated ER Ca^{2+} leak and release under basal and stimulation conditions with agonists of the $InsP_3R$, a decrease of mitochondrial Ca^{2+} extrusion capacity (decreased NCLX expression) and an increase in ROS production, may explain the increased vulnerability and eventual death of these cells due to progressive mitochondrial dysfunction.

Mitochondria are organelles that play multiple important functions in the cell. However, the main function is the production of energy in the form of ATP and almost all other processes inside mitochondria are related or dependent on bioenergetics. Thus, ATP synthesis by oxidative phosphorylation is coupled with mitochondrial respiration and regulated by Ca^{2+} in the matrix. Furthermore, there have been numerous reports indicating that mitochondrial function is disrupted in early-stage AD (Chen, Tang et al.

2006). These include diminished glucose metabolism, mitochondrial enzymatic failure, and increased ROS production (before Aβ and tau tangles have begun forming). Whether these mitochondrial-associated dysfunctions are sufficient to cause neurodegenerative pathogenesis such as in FAD remains uncertain, as they may also evolve secondarily to a different underlying pathology. A decline in mitochondrial function may be a natural process of aging but may normally be compensated by adaptive changes. A loss of these compensatory mechanisms, or a "second trigger" may convert a subclinical decline into a clinically relevant neurodegenerative phenotype such AD. PSs are the major AD genes whose mutation contributes to over 90% of FAD cases and affects cytoplasmic Ca^{2+} in AD neurons. Ca^{2+} signaling plays a central role in regulating many physiological processes and the progressive and excessive Ca^{2+} entry into mitochondria can lead to opening of a mPTP causing the collapse of membrane potential and loss of ATP production resulting in apoptosis (Kroemer, Galluzzi et al. 2007). Furthermore, it has been shown that the inhibition of mPTP opening pharmacologically using cyclosporine-A or genetically (CypD KO) reduces neuronal dysfunction and degeneration in AD models (Du, Guo et al. 2008) (Du, Guo et al. 2011). How these Ca^{2+} entry pathways affected lead to development of the AD remains unclear.

In several experimental AD models intracellular [Ca^{2+}] is elevated, and these elevated [Ca^{2+}] appear to be toxic to cells and trigger subsequent pathological processes, which drive AD pathogenesis. But what are the causes of these increased of [Ca^{2+}] in AD? We have focused on the role of PS1, where a significant body of research in our lab and others suggests that AD-bearing PS mutants cause Ca^{2+}

dysregulation independently of its gamma-secretase function and beta-amyloid accumulation and due to changes in activity of RyR and $InsP_3R$, showing an enhanced Ca^{2+} release via both ER-resident channels. Previously, we documented that a reduction in $[Ca^{2+}]_i$ ameliorates the pathology in animal models, specifically targeting the activity or expression of $InsP_3R$ (Shilling D, et al, 2014). However, it is still not well understood how altered levels of Ca^{2+} in cells expressing mutant PS1 affect mitochondrial function. It is also well known that under conditions of Ca^{2+} overload due to sustained release from the stores such as the ER appear to be toxic to cells and trigger subsequent pathological processes such as opening of the mPTP, which may drive AD pathogenesis. Our results were clear on the SH-SY5Y cells, however on the human skin fibroblasts the results were less evident maybe for their bioenergetics properties differ from a neuronal phenotype.

The results in this work recapitulated previous observations that the expression of mutant PS1-M146L or A246E in patient fibroblasts led to increased Ca^{2+} release from the ER through $InsP_3R$ under resting conditions or upon stimulation with BK or ATP. This can account for why we observed higher basal $[Ca^{2+}]$ in both models studied. This increase in $[Ca^{2+}]_c$ is theorized to cause mitochondrial Ca^{2+} overload, which is linked to excessive ROS generation and metabolic and mitochondrial dysfunction. However, direct evidence of mitochondrial Ca^{2+} overload is scarce. In our investigation we observed in both FAD models, using different tools and approaches, a significant increase in basal mitochondrial $[Ca^{2+}]$ in cells expressing mutant PS1 which increased further upon Tg inhibition of SERCA activity. However, our data revealed no differences

in MCU-mediated Ca^{2+} uptake between the cell lines analyzed, indicating that MCU activity is unaffected.

In addition, it is also widely recognized that mitochondrial Ca^{2+} can directly influence cell death signaling through the opening of the mPTP and indirectly through its effects on ROS production. Here, we demonstrated that mitochondrial Ca^{2+} overload causes the opening of the mPTP in cells expressing mutant PS1-M146L, making them more vulnerable to small perturbances in Ca^{2+} homeostasis. However, this vulnerability can be successfully reverted inhibiting the ER Ca^{2+} release with $Insp_3R$ specific inhibitor (XeB) or through the absence of ER Ca^{2+} leak with Tg.

Another source of mitochondrial Ca^{2+} overload found during this work was impaired mitochondrial Ca^{2+} efflux due to a significant decrease of NCLX expression in mutant PS1-M146L expressing cells. This unexpected finding could explain another possible trigger of Ca^{2+} homeostasis dysregulation, which can contribute to AD progression promoting in addition to the enhanced ER Ca^{2+} release to metabolic dysfunction and cell death. There are several mechanisms by which Ca^{2+} can cause the activation of apoptosis, such as the increase in OMM permeability and also mPTP opening causing the collapse of membrane potential and loss of ATP production. In this work we demonstrated the enhanced vulnerability of mutant PS1-M146L cells in response to Ca^{2+} overload challenged with 2-3 μM of Ca^{2+} boluses. This vulnerability was recovered by inhibiting the ER Ca^{2+} leak and was fully impair in the presence of CGP, a NCLX inhibitor, strongly suggesting more than one possible trigger for cell death.

Associated with the metabolic dysfunction and in agreement with the mitochondrial Ca^{2+} overload, we found a significant increase in p-PDH in mutant PS1-M146L expressing cells and also in FAD patients' fibroblasts, which was reverted upon XeB incubation, strongly suggesting Ca^{2+} overload through the involvement of $InsP_3R$. We also found a decrease in OCR, suggesting diminished ATP production in the mutant cells in both models used. Diminished mitochondrial respiration may indicate that overall metabolism is suppressed in these cells, maybe because of energy stress. On the other hand, we observed a mitochondrial matrix [Ca^{2+}] increase, which would be predicted to increase OXPHOS. In agreement with our previous results (Muller, Cheung et al. 2011), we also observed an increase in ROS production in cells expressing the mutant PS1-M146L, which correlates with AD progression and mitochondrial dysfunction. All these findings support our working hypothesis that mitochondrial Ca^{2+} overload through $InsP_3R$-MCU axis and lack of NCLX expression are disrupted in FAD leading to cellular dysfunction and promoting a pathological cycle essential to disease progression. Last year, impaired mitochondrial Ca^{2+} efflux was suggested to be a major contributor to the disease progression in a mouse model of AD associated with a loss in expression and functionality of NCLX (Jadiya, Kolmetzky et al. 2019). Genetic rescue of NCLX expression in 3xTg-AD mice completely ablated age-associated cognitive decline and reducing neuronal pathology. This is the first study that directly examined the role of mitochondrial Ca^{2+} signaling in AD with the disease progression, using similar experimental strategies that the one using in our investigation. Their results complement those from my study, however, the models used here have important differences and also important advantages and disadvantages. The cellular models

used in both studies, specifically brain-derived cell lines such as the human SH-SY5Y or the mouse N2a cell line, differ in their bioenergetics and neurotoxic properties from primary neurons (LePage, Dickey et al. 2005). On the other hand, the AD mouse model and the data obtained from them raises important questions to consider. A wide variety of human APP and PS constructs have been introduced into the mouse genome. Most of these lines of mice produce substantial deposits of amyloid but the most classic AD-associated pathologies never develop (Herrup 2015). Overexpression of human APP in mice does not produce tangles, neurodegeneration or AD-like dementia, but the advantages are that the mouse produces plaques, shows memory deficits and Aβ is toxic to neurons in culture. A crucial experiment lacking in this work is to determine if rescuing NCLX expression can correct in part the mitochondrial dysfunction due to alterations in Ca^{2+} efflux mechanism in cells expressing the mutant PS1-M146L.

A robust amount of evidence suggests other causes for mitochondrial Ca^{2+} overload, such as Aβ-induced increases in ER-mitochondrial contacts, which could result in elevated ER-to-mitochondria Ca^{2+} transfer and promote matrix overload (Area-Gomez, Del Carmen Lara Castillo et al. 2012) (Del Prete, Suski et al. 2017, Calvo-Rodriguez, Hou et al. 2020). In our work we demonstrated no significant differences in rates of MCU-mediated Ca^{2+} uptake between the cell lines analyzed (Figure 1), indicating that MCU activity is unaffected.

We have examined specifically the effects of mutant PS1-M146L, the main cause of FAD, proposing a mechanism of cellular toxicity that involve a Ca^{2+} dyshomeostasis triggering mitochondrial dysfunction which may contribute to synaptic and neuronal damage in FAD patients. Here we show new alternatives to develop therapies that

could treat AD without relying of the amyloid hypothesis, pointing to a critical role in ER Ca^{2+} leak and mitochondrial Ca^{2+} uptake through MCU or possible enhancing Ca^{2+} extrusion from the mitochondria through NCLX as possible candidates. We clearly demonstrated that preventing ER Ca^{2+} leak through the InsP3R with XeB could serve as a therapeutic approach to avoid mPTP activation.

12. CONCLUSION

In summary, our findings demonstrate that constitutively high basal Ca^{2+} levels provoke mitochondrial Ca^{2+} overload via ER Ca^{2+} leak and decreased Ca^{2+} efflux due to a decreased NCLX expression leading to cell death.

13. BIBLIOGRAPHY

Area-Gomez, E., A. de Groof, E. Bonilla, J. Montesinos, K. Tanji, I. Boldogh, L. Pon and E. A. Schon (2018). "A key role for MAM in mediating mitochondrial dysfunction in Alzheimer disease." Cell Death Dis **9**(3): 335.

Area-Gomez, E., M. Del Carmen Lara Castillo, M. D. Tambini, C. Guardia-Laguarta, A. J. de Groof, M. Madra, J. Ikenouchi, M. Umeda, T. D. Bird, S. L. Sturley and E. A. Schon (2012). "Upregulated function of mitochondria-associated ER membranes in Alzheimer disease." EMBO J **31**(21): 4106-4123.

Baughman, J. M., F. Perocchi, H. S. Girgis, M. Plovanich, C. A. Belcher-Timme, Y. Sancak, X. R. Bao, L. Strittmatter, O. Goldberger, R. L. Bogorad, V. Koteliansky and V. K. Mootha (2011). "Integrative genomics identifies MCU as an essential component of the mitochondrial calcium uniporter." Nature **476**(7360): 341-345.

Belosludtsev, K. N., M. V. Dubinin, N. V. Belosludtseva and G. D. Mironova (2019). "Mitochondrial Ca2+ Transport: Mechanisms, Molecular Structures, and Role in Cells." Biochemistry (Mosc) **84**(6): 593-607.

Berridge, M. J. (2013). "Dysregulation of neural calcium signaling in Alzheimer disease, bipolar disorder and schizophrenia." Prion **7**(1): 2-13.

Berridge, M. J. (2014). "Calcium signalling and psychiatric disease: bipolar disorder and schizophrenia." Cell Tissue Res **357**(2): 477-492.

Boyman, L., G. S. Williams, D. Khananshvili, I. Sekler and W. J. Lederer (2013). "NCLX: the mitochondrial sodium calcium exchanger." J Mol Cell Cardiol **59**: 205-213.

Brand, M. D. and D. G. Nicholls (2011). "Assessing mitochondrial dysfunction in cells." Biochem J **435**(2): 297-312.

Bubber, P., V. Haroutunian, G. Fisch, J. P. Blass and G. E. Gibson (2005). "Mitochondrial abnormalities in Alzheimer brain: mechanistic implications." Ann Neurol **57**(5): 695-703.

Cahalan, M. D. (2009). "STIMulating store-operated Ca(2+) entry." Nat Cell Biol **11**(6): 669-677.

Calvo-Rodriguez, M., S. S. Hou, A. C. Snyder, E. K. Kharitonova, A. N. Russ, S. Das, Z. Fan, A. Muzikansky, M. Garcia-Alloza, A. Serrano-Pozo, E. Hudry and B. J. Bacskai (2020). "Increased mitochondrial calcium levels associated with neuronal death in a mouse model of Alzheimer's disease." Nat Commun **11**(1): 2146.

Cardenas, C., R. A. Miller, I. Smith, T. Bui, J. Molgo, M. Muller, H. Vais, K. H. Cheung, J. Yang, I. Parker, C. B. Thompson, M. J. Birnbaum, K. R. Hallows and J. K. Foskett (2010). "Essential regulation of cell bioenergetics by constitutive InsP3 receptor Ca2+ transfer to mitochondria." Cell **142**(2): 270-283.

Chakroborty, S., J. Kim, C. Schneider, C. Jacobson, J. Molgo and G. E. Stutzmann (2012). "Early presynaptic and postsynaptic calcium signaling abnormalities mask underlying synaptic depression in presymptomatic Alzheimer's disease mice." J Neurosci **32**(24): 8341-8353.

Chaudhuri, D., Y. Sancak, V. K. Mootha and D. E. Clapham (2013). "MCU encodes the pore conducting mitochondrial calcium currents." Elife **2**: e00704.

Chen, J., X. Q. Tang, J. L. Zhi, Y. Cui, H. M. Yu, E. H. Tang, S. N. Sun, J. Q. Feng and P. X. Chen (2006). "Curcumin protects PC12 cells against 1-methyl-4-phenylpyridinium ion-induced apoptosis by bcl-2-mitochondria-ROS-iNOS pathway." Apoptosis **11**(6): 943-953.

Cheung, K., L. Mei, D. O. Mak, I. Hayashi, T. Iwatsubo, D. E. Kang and J. K. Foskett (2010). "Gain-of-function enhancement of IP3 receptor modal gating by familial Alzheimer's disease-linked presenilin mutants in human cells and mouse neurons." Sci Signal **3**(114): ra22.

Cheung, K., D. Shineman, M. Muller, C. Cardenas, M. Lijuan, J. Yang, T. Tomita, T. Iwatsubo, V. M.-Y. Lee and J. K. Foskett (2008). "Mechanism of Ca2+ disruption in Alzheimer's disease by presenilin regulation of InsP(3) receptor channel gating." Neuron **58**(6): 871-883.

Cheung KH, S. D., Müller M, Cárdenas C, Mei L, ,. Lee V and J. Foskett JK (2008). "Presenilin Regulation of InsP3 Receptor Channel Gating as a Mechanism of Ca2+ Disruption in Alzheimer's Disease." Neuron **58**: 871-883.

Cleary, J. P., D. M. Walsh, J. J. Hofmeister, G. M. Shankar, M. A. Kuskowski, D. J. Selkoe and K. H. Ashe (2005). "Natural oligomers of the amyloid-beta protein specifically disrupt cognitive function." Nat Neurosci **8**(1): 79-84.

Connolly, N. M. C., P. Theurey, V. Adam-Vizi, N. G. Bazan, P. Bernardi, J. P. Bolanos, C. Culmsee, V. L. Dawson, M. Deshmukh, M. R. Duchen, H. Dussmann, G. Fiskum, M. F. Galindo, G. E. Hardingham, J. M. Hardwick, M. B. Jekabsons, E. A. Jonas, J. Jordan, S. A. Lipton, G. Manfredi, M. P. Mattson, B. McLaughlin, A. Methner, A. N. Murphy, M. P. Murphy, D. G. Nicholls, B. M. Polster, T. Pozzan, R. Rizzuto, J. Satrustegui, R. S. Slack, R. A. Swanson, R. H. Swerdlow, Y. Will, Z. Ying, A. Joselin, A. Gioran, C. Moreira Pinho, O. Watters, M. Salvucci, I. Llorente-Folch, D. S. Park, D. Bano, M. Ankarcrona, P. Pizzo and J. H. M. Prehn (2018). "Guidelines on experimental methods to assess mitochondrial dysfunction in cellular models of neurodegenerative diseases." Cell Death Differ **25**(3): 542-572.

Cornejo, V. H. and C. Hetz (2013). "The unfolded protein response in Alzheimer's disease." Semin Immunopathol **35**(3): 277-292.

Cutler, R. G., J. Kelly, K. Storie, W. A. Pedersen, A. Tammara, K. Hatanpaa, J. C. Troncoso and M. P. Mattson (2004). "Involvement of oxidative stress-induced abnormalities in ceramide and cholesterol metabolism in brain aging and Alzheimer's disease." Proc Natl Acad Sci U S A **101**(7): 2070-2075.

De Stefani, D., A. Raffaello, E. Teardo, I. Szabo and R. Rizzuto (2011). "A forty-kilodalton protein of the inner membrane is the mitochondrial calcium uniporter." Nature **476**(7360): 336-340.

De Stefani, D., R. Rizzuto and T. Pozzan (2016). "Enjoy the Trip: Calcium in Mitochondria Back and Forth." Annu Rev Biochem **85**: 161-192.

Del Prete, D., J. M. Suski, B. Oulès, D. Debayle, A. S. Gay, S. Lacas-Gervais, R. Bussiere, C. Bauer, P. Pinton, P. Paterlini-Bréchot, M. R. Wieckowski, F. Checler and M. Chami (2017). "Localization and Processing of the Amyloid-β Protein Precursor in Mitochondria-Associated Membranes." J Alzheimers Dis **55**(4): 1549-1570.

Deluca, H. and G. Engstrom (1961). "Calcium uptake by rat kidney mitochondria." Proc Natl Acad Sci U S A **47**: 1744-1750.

Demuro, A. and I. Parker (2013). "Cytotoxicity of intracellular abeta42 amyloid oligomers involves Ca2+ release from the endoplasmic reticulum by stimulated production of inositol trisphosphate." J Neurosci **33**(9): 3824-3833.

Denton, R. M., P. J. Randle and B. R. Martin (1972). "Stimulation by calcium ions of pyruvate dehydrogenase phosphate phosphatase." Biochem J **128**(1): 161-163.

Du, H., L. Guo, F. Fang, D. Chen, A. A. Sosunov, G. M. McKhann, Y. Yan, C. Wang, H. Zhang, J. D. Molkentin, F. J. Gunn-Moore, J. P. Vonsattel, O. Arancio, J. X. Chen and S. D. Yan (2008). "Cyclophilin D deficiency attenuates mitochondrial and neuronal perturbation and ameliorates learning and memory in Alzheimer's disease." Nat Med **14**(10): 1097-1105.

Du, H., L. Guo, W. Zhang, M. Rydzewska and S. Yan (2011). "Cyclophilin D deficiency improves mitochondrial function and learning/memory in aging Alzheimer disease mouse model." Neurobiol Aging **32**(3): 398-406.

Fernandez-Morales, J. C., J. A. Arranz-Tagarro, E. Calvo-Gallardo, M. Maroto, J. F. Padin and A. G. Garcia (2012). "Stabilizers of neuronal and mitochondrial calcium cycling as a strategy for developing a medicine for Alzheimer's disease." ACS Chem Neurosci **3**(11): 873-883.

Francis, R., G. McGrath, J. Zhang, D. A. Ruddy, M. Sym, J. Apfeld, M. Nicoll, M. Maxwell, B. Hai, M. C. Ellis, A. L. Parks, W. Xu, J. Li, M. Gurney, R. L. Myers, C. S. Himes, R. Hiebsch, C. Ruble, J. S. Nye and D. Curtis (2002). "aph-1 and pen-2 are required for Notch pathway signaling, gamma-secretase cleavage of betaAPP, and presenilin protein accumulation." Dev Cell **3**(1): 85-97.

Gillardon, F., W. Rist, L. Kussmaul, J. Vogel, M. Berg, K. Danzer, N. Kraut and B. Hengerer (2007). "Proteomic and functional alterations in brain mitochondria from Tg2576 mice occur before amyloid plaque deposition." Proteomics **7**(4): 605-616.

Glancy, B. and R. S. Balaban (2012). "Role of mitochondrial Ca2+ in the regulation of cellular energetics." Biochemistry **51**(14): 2959-2973.

Green, K. N., A. Demuro, Y. Akbari, B. D. Hitt, I. F. Smith, I. Parker and F. M. LaFerla (2008). "SERCA pump activity is physiologically regulated by presenilin and regulates amyloid beta production." J Gen Physiol **132**(2): i1.

Greer, P. L. and M. E. Greenberg (2008). "From synapse to nucleus: calcium-dependent gene transcription in the control of synapse development and function." Neuron **59**(6): 846-860.

Hardy, J. and D. J. Selkoe (2002). "The amyloid hypothesis of Alzheimer's disease: progress and problems on the road to therapeutics." Science **297**(5580): 353-356.

Herrero-Mendez, A., A. Almeida, E. Fernández, C. Maestre, S. Moncada and J. P. Bolaños (2009). "The bioenergetic and antioxidant status of neurons is controlled by continuous degradation of a key glycolytic enzyme by APC/C-Cdh1." Nat Cell Biol **11**(6): 747-752.

Herrup, K. (2015). "The case for rejecting the amyloid cascade hypothesis." Nat Neurosci **18**(6): 794-799.

Honarnejad, K. and J. Herms (2012). "Presenilins: role in calcium homeostasis." Int J Biochem Cell Biol **44**(11): 1983-1986.

Iacono, D., S. M. Resnick, R. O'Brien, A. B. Zonderman, Y. An, O. Pletnikova, G. Rudow, B. Crain and J. C. Troncoso (2014). "Mild cognitive impairment and asymptomatic Alzheimer disease subjects: equivalent beta-amyloid and tau loads with divergent cognitive outcomes." J Neuropathol Exp Neurol **73**(4): 295-304.

Ichas, F., L. S. Jouaville and J. P. Mazat (1997). "Mitochondria are excitable organelles capable of generating and conveying electrical and calcium signals." Cell **89**(7): 1145-1153.

Itoh, K., K. Nakamura, M. Iijima and H. Sesaki (2013). "Mitochondrial dynamics in neurodegeneration." Trends Cell Biol **23**(2): 64-71.

Jadiya, P., D. W. Kolmetzky, D. Tomar, A. Di Meco, A. A. Lombardi, J. P. Lambert, T. S. Luongo, M. H. Ludtmann, D. Praticò and J. W. Elrod (2019). "Impaired mitochondrial calcium efflux contributes to disease progression in models of Alzheimer's disease." Nat Commun **10**(1): 3885.

Jaimovich, E., C. Mattei, J. L. Liberona, C. Cardenas, M. Estrada, J. Barbier, C. Debitus, D. Laurent and J. Molgo (2005). "Xestospongin B, a competitive inhibitor of IP3-mediated Ca2+ signalling in cultured rat myotubes, isolated myonuclei, and neuroblastoma (NG108-15) cells." FEBS Lett **579**(10): 2051-2057.

Khachaturian, Z. S. (1987). "Hypothesis on the regulation of cytosol calcium concentration and the aging brain." Neurobiol Aging **8**(4): 345-346.

Kroemer, G., L. Galluzzi and C. Brenner (2007). "Mitochondrial membrane permeabilization in cell death." Physiol Rev **87**(1): 99-163.

LaFerla (2002). "Calcium dyshomeostasis and intracellular signalling in Alzheimer's disease.". Nat Rev Neurosci **3**(11): 862-872.

LePage, K. T., R. W. Dickey, W. H. Gerwick, E. L. Jester and T. F. Murray (2005). "On the use of neuro-2a neuroblastoma cells versus intact neurons in primary culture for neurotoxicity studies." Crit Rev Neurobiol **17**(1): 27-50.

Lin, M. T. and M. F. Beal (2006). "Alzheimer's APP mangles mitochondria." Nat Med **12**(11): 1241-1243.

Liu, T., E. Takimoto, V. L. Dimaano, D. DeMazumder, S. Kettlewell, G. Smith, A. Sidor, T. P. Abraham and B. O'Rourke (2014). "Inhibiting mitochondrial Na+/Ca2+ exchange prevents sudden death in a Guinea pig model of heart failure." Circ Res **115**(1): 44-54.

Liu, Y. and X. Zhu (2017). "Endoplasmic reticulum-mitochondria tethering in neurodegenerative diseases." Transl Neurodegener **6**: 21.

Llorente-Folch, I., C. B. Rueda, B. Pardo, G. Szabadkai, M. R. Duchen and J. Satrustegui (2015). "The regulation of neuronal mitochondrial metabolism by calcium." J Physiol **593**(16): 3447-3462.

Luongo, T. S., J. P. Lambert, P. Gross, M. Nwokedi, A. A. Lombardi, S. Shanmughapriya, A. C. Carpenter, D. Kolmetzky, E. Gao, J. H. van Berlo, E. J. Tsai, J. D. Molkentin, X. Chen, M. Madesh, S. R. Houser and J. W. Elrod (2017). "The mitochondrial Na(+)/Ca(2+) exchanger is essential for Ca(2+) homeostasis and viability." Nature **545**(7652): 93-97.

Luongo, T. S., J. P. Lambert, A. Yuan, X. Zhang, P. Gross, J. Song, S. Shanmughapriya, E. Gao, M. Jain, S. R. Houser, W. J. Koch, J. Y. Cheung, M. Madesh and J. W. Elrod (2015). "The Mitochondrial Calcium Uniporter Matches Energetic Supply with Cardiac Workload during Stress and Modulates Permeability Transition." Cell Rep **12**(1): 23-34.

Mallilankaraman, K., C. Cardenas, P. J. Doonan, H. C. Chandramoorthy, K. M. Irrinki, T. Golenar, G. Csordas, P. Madireddi, J. Yang, M. Mueller, R. Miller, J. E. Kolesar, J. Molgo, B. Kaufman, G. Hajnoczky, J. K. Foskett and M. Madesh (2012). "MCUR1 is an essential component of mitochondrial Ca2+ uptake that regulates cellular metabolism." Nature Cell Biology **14**(12): 1336-+.

Mallilankaraman, K., P. Doonan, C. Cardenas, H. C. Chandramoorthy, M. Muller, R. Miller, N. E. Hoffman, R. K. Gandhirajan, J. Molgo, M. J. Birnbaum, B. S. Rothberg, D. O. Mak, J. K. Foskett and M. Madesh (2012). "MICU1 is an essential gatekeeper for MCU-mediated mitochondrial Ca(2+) uptake that regulates cell survival." Cell **151**(3): 630-644.

Mattson, M. P. (2004). "Pathways towards and away from Alzheimer's disease." Nature **430**(7000): 631-639.

Mullane, K. and M. Williams (2013). "Alzheimer's therapeutics: continued clinical failures question the validity of the amyloid hypothesis-but what lies beyond?" Biochem Pharmacol **85**(3): 289-305.

Muller, M., C. Cardenas, L. Mei, K. H. Cheung and J. K. Foskett (2011). "Constitutive cAMP response element binding protein (CREB) activation by Alzheimer's disease presenilin-driven inositol trisphosphate receptor (InsP3R) Ca2+ signaling." Proc Natl Acad Sci U S A **108**(32): 13293-13298.

Muller, M., K. H. Cheung and J. K. Foskett (2011). "Enhanced ROS generation mediated by Alzheimer's disease presenilin regulation of InsP3R Ca2+ signaling." Antioxid Redox Signal **14**(7): 1225-1235.

Nicholls, D. G., V. M. Darley-Usmar, M. Wu, P. B. Jensen, G. W. Rogers and D. A. Ferrick (2010). "Bioenergetic profile experiment using C2C12 myoblast cells." J Vis Exp(46).

Palty, R., W. F. Silverman, M. Hershfinkel, T. Caporale, S. L. Sensi, J. Parnis, C. Nolte, D. Fishman, V. Shoshan-Barmatz, S. Herrmann, D. Khananshvili and I. Sekler (2010). "NCLX is an essential component of mitochondrial Na+/Ca2+ exchange." Proc Natl Acad Sci U S A **107**(1): 436-441.

Payne, R., H. Hoff, A. Roskowski and J. K. Foskett (2017). "MICU2 Restricts Spatial Crosstalk between InsP." Cell Rep **21**(11): 3141-3154.

Peterson, C., G. E. Gibson and J. P. Blass (1985). "Altered calcium uptake in cultured skin fibroblasts from patients with Alzheimer's disease." N Engl J Med **312**(16): 1063-1065.

Plovanich, M., R. L. Bogorad, Y. Sancak, K. J. Kamer, L. Strittmatter, A. A. Li, H. S. Girgis, S. Kuchimanchi, J. De Groot, L. Speciner, N. Taneja, J. Oshea, V. Koteliansky and V. K. Mootha (2013). "MICU2, a paralog of MICU1, resides within the mitochondrial uniporter complex to regulate calcium handling." PLoS One **8**(2): e55785.

Popugaeva, E., E. Pchitskaya and I. Bezprozvanny (2018). "Dysregulation of Intracellular Calcium Signaling in Alzheimer's Disease." Antioxid Redox Signal **29**(12): 1176-1188.

Qiu, J., Y. W. Tan, A. M. Hagenston, M. A. Martel, N. Kneisel, P. A. Skehel, D. J. Wyllie, H. Bading and G. E. Hardingham (2013). "Mitochondrial calcium uniporter Mcu controls excitotoxicity and is transcriptionally repressed by neuroprotective nuclear calcium signals." Nat Commun **4**: 2034.

Raffaello, A., D. De Stefani, D. Sabbadin, E. Teardo, G. Merli, A. Picard, V. Checchetto, S. Moro, I. Szabo and R. Rizzuto (2013). "The mitochondrial calcium uniporter is a multimer that can include a dominant-negative pore-forming subunit." EMBO J **32**(17): 2362-2376.

Rasola, A. and P. Bernardi (2011). "Mitochondrial permeability transition in Ca(2+)-dependent apoptosis and necrosis." Cell Calcium **50**(3): 222-233.

Reynolds, I. J. (1999). "Mitochondrial membrane potential and the permeability transition in excitotoxicity." Ann N Y Acad Sci **893**: 33-41.

Rizzuto, R., P. Bernardi and T. Pozzan (2000). "Mitochondria as all-round players of the calcium game." J Physiol **529 Pt 1**: 37-47.

Rottenberg, H. and J. B. Hoek (2017). "The path from mitochondrial ROS to aging runs through the mitochondrial permeability transition pore." Aging Cell **16**(5): 943-955.

Rutter, G. A. and R. M. Denton (1988). "Regulation of NAD+-linked isocitrate dehydrogenase and 2-oxoglutarate dehydrogenase by Ca2+ ions within toluene-permeabilized rat heart mitochondria. Interactions with regulation by adenine nucleotides and NADH/NAD+ ratios." Biochem J **252**(1): 181-189.

Sekler, I. (2015). "Standing of giants shoulders the story of the mitochondrial Na(+)Ca(2+) exchanger." Biochem Biophys Res Commun **460**(1): 50-52.

Shilling, D., M. Muller, H. Takano, D.-O. D. Mak, T. Abel, D. A. Coulter and J. K. Foskett (2014). "Suppression of InsP(3) Receptor-Mediated Ca2+ Signaling Alleviates Mutant Presenilin-Linked Familial Alzheimer's Disease Pathogenesis." Journal of Neuroscience **34**(20): 6910-6923.

Slachevsky, A., M. Budinich, C. Miranda-Castillo, J. Núñez-Huasaf, J. R. Silva, C. Muñoz-Neira, S. Gloger, O. Jimenez, B. Martorell and C. Delgado (2013). "The CUIDEME Study: determinants of burden in chilean primary caregivers of patients with dementia." J Alzheimers Dis **35**(2): 297-306.

Stutzmann, G. E., I. Smith, A. Caccamo, S. Oddo, I. Parker and F. Laferla (2007). "Enhanced ryanodine-mediated calcium release in mutant PS1-expressing Alzheimer's mouse models." Ann N Y Acad Sci **1097**: 265-277.

Su, B., X. Wang, L. Zheng, G. Perry, M. A. Smith and X. Zhu (2010). "Abnormal mitochondrial dynamics and neurodegenerative diseases." Biochim Biophys Acta **1802**(1): 135-142.

Swerdlow, R. H. and S. M. Khan (2004). "A "mitochondrial cascade hypothesis" for sporadic Alzheimer's disease." Med Hypotheses **63**(1): 8-20.

Tong, B. C., C. S. Lee, W. H. Cheng, K. O. Lai, J. K. Foskett and K. H. Cheung (2016). "Familial Alzheimer's disease-associated presenilin 1 mutants promote gamma-secretase cleavage of STIM1 to impair store-operated Ca2+ entry." Sci Signal **9**(444): ra89.

Volgyi, K., G. Juhasz, Z. Kovacs and B. Penke (2015). "Dysfunction of Endoplasmic Reticulum (ER) and Mitochondria (MT) in Alzheimer's Disease: The Role of the ER-MT Cross-Talk." Curr Alzheimer Res **12**(7): 655-672.

Yao, J., R. W. Irwin, L. Zhao, J. Nilsen, R. T. Hamilton and R. D. Brinton (2009). "Mitochondrial bioenergetic deficit precedes Alzheimer's pathology in female mouse model of Alzheimer's disease." Proc Natl Acad Sci U S A **106**(34): 14670-14675.

Zampese, E., C. Fasolato, M. J. Kipanyula, M. Bortolozzi, T. Pozzan and P. Pizzo (2011). "Presenilin 2 modulates endoplasmic reticulum (ER)-mitochondria interactions and Ca2+ cross-talk." Proc Natl Acad Sci U S A **108**(7): 2777-2782.